2015

Engineered Surface Properties of Porous Tungsten from Cryogenic Machining

Julius M. Schoop
University of Kentucky, julius.schoop@uky.edu

STUDENT AGREEMENT:

I represent that my thesis or dissertation and abstract are my original work. Proper attribution has been given to all outside sources. I understand that I am solely responsible for obtaining any needed copyright permissions. I have obtained needed written permission statement(s) from the owner(s) of each third-party copyrighted matter to be included in my work, allowing electronic distribution (if such use is not permitted by the fair use doctrine) which will be submitted to UKnowledge as Additional File.

I hereby grant to The University of Kentucky and its agents the irrevocable, non-exclusive, and royalty-free license to archive and make accessible my work in whole or in part in all forms of media, now or hereafter known. I agree that the document mentioned above may be made available immediately for worldwide access unless an embargo applies.

I retain all other ownership rights to the copyright of my work. I also retain the right to use in future works (such as articles or books) all or part of my work. I understand that I am free to register the copyright to my work.

REVIEW, APPROVAL AND ACCEPTANCE

The document mentioned above has been reviewed and accepted by the student's advisor, on behalf of the advisory committee, and by the Director of Graduate Studies (DGS), on behalf of the program; we verify that this is the final, approved version of the student's thesis including all changes required by the advisory committee. The undersigned agree to abide by the statements above.

Julius M. Schoop, Student

Dr. T. John Balk, Major Professor

Dr. Thomas D. Dziubla, Director of Graduate Studies

ENGINEERED SURFACE PROPERTIES OF POROUS TUNGSTEN FROM CRYOGENIC MACHINING

DISSERTATION

A dissertation submitted in partial fulfillment of the requirements for the degree of Doctor of Philosophy in the College of Engineering at the University of Kentucky

By

Julius Malte Schoop

Lexington, Kentucky

Co-Directors: Dr. T. John Balk, Professor of Materials Engineering

and Dr. I. S. Jawahir, Professor of Mechanical Engineering

Lexington, Kentucky

2015

ABSTRACT OF DISSERTATION

ENGINEERED SURFACE PROPERTIES OF POROUS TUNGSTEN FROM CRYOGENIC MACHINING

Porous tungsten is used to manufacture dispenser cathodes due to it refractory properties. Surface porosity is critical to functional performance of dispenser cathodes because it allows for an impregnated ceramic compound to migrate to the emitting surface, lowering its work function. Likewise, surface roughness is important because it is necessary to ensure uniform wetting of the molten impregnate during high temperature service.

Current industry practice to achieve surface roughness and surface porosity requirements involves the use of a plastic infiltrant during machining. After machining, the infiltrant is baked and the cathode pellet is impregnated. In this context, cryogenic machining is investigated as a substitutionary process for the current plastic infiltration process. Along with significant reductions in cycle time and resource use, surface quality of cryogenically machined un-infiltrated (as-sintered) porous tungsten has been shown to significantly outperform dry machining.

The present study is focused on examining the relationship between machining parameters and cooling condition on the as-machined surface integrity of porous tungsten. The effects of cryogenic pre-cooling, rake angle, cutting speed, depth of cut and feed are all taken into consideration with respect to machining-induced surface morphology. Cermet and Polycrystalline diamond (PCD) cutting tools are used to develop high performance cryogenic machining of porous tungsten. Dry and pre-heated machining were investigated as a means to allow for ductile mode machining, yet severe tool-wear and undesirable smearing limited the feasibility of these approaches.

By using modified PCD cutting tools, high speed machining of porous tungsten at cutting speeds up to 400 m/min is achieved for the first time. Beyond a critical speed, brittle fracture and built-up edge are eliminated as the result of a brittle to ductile transition. A model of critical chip thickness (h_c) effects based on cutting force, temperature and surface roughness data is developed and used to study the deformation mechanisms of porous tungsten under different machining conditions. It is found that

when $h_{max} = h_c$, ductile mode machining of otherwise highly brittle porous tungsten is possible. The value of h_c is approximately the same as the average ligament size of the 80% density porous tungsten workpiece.

KEYWORDS: Cryogenic machining, porous tungsten, powdered metal, surface integrity, size effects

Julius Malte Schoop

August, 11th, 2015

ENGINEERED SURFACE PROPERTIES OF POROUS TUNGSTEN FROM CRYOGENIC MACHINING

By

Julius Malte Schoop

Dr. T. John Balk
Co-Director of Dissertation

Dr. I. S. Jawahir
Co-Director of Dissertation

Dr. T. D. Dziubla
Director of Graduate Studies

August, 11th, 2015

ACKNOWLEDGEMENTS

I would like to express my sincere gratitude to my advisor Professor Dr. T. John Balk and my co-advisor Professor Dr. I. S. Jawahir, without whose guidance I could not have completed this work. Both Dr. Balk and Dr. Jawahir have been tremendously helpful in developing both my technical and personal maturity. By patiently mentoring me to pursue increasingly complex answers to the phenomena of metal cutting from both a machining science and materials engineering point of view, both of my advisors have profoundly shaped my research approach. I am truly grateful for the time and effort that Dr. Balk and Dr. Jawahir have invested to help me achieve more than I would have thought myself capable of.

I would furthermore like to thank all of my committee members, Dr. Yang-Tse Cheng, Dr. Matthew Beck, and Dr. Jonathan Wenk for their time and valuable guidance. Special thanks to the very helpful support staff at the University of Kentucky, particularly Charles Arvin, Heather-Michelle Adkins and Floyd Taylor.

I have also been very fortunate to have had a fantastic group of friends and labmates in both Dr. Balk's and Dr. Jawahir's laboratories, including Nicolas Briot, Phillip Swartzentruber, Lei Wang, Xu Jiang, Tyler Vanover, Michael Detisch, Shu Yang, Zhengwen Pu, Tao Lu, Yusuf Kaynak, Dominico Umbrello, and Giovanna Rotella. I would especially like to thank Nicolas Briot for countless hours of helping me to perform mechanical testing experiments.

I have also been fortunate to have had to opportunity to be a visiting researcher at the wbk Institute of Production Science and the Karlsruhe Institute of Technology in Karlsruhe, Germany. Under the supervision of Prof. Dr.-Ing. habil. Volker Schulze, and with the helpful guidance of chief engineer Dr.-Ing. Frederik Zanger and the support of Florian Ambrosy, I was able to conduct a series of highly productive experiments that have resulted in two collaborative manuscripts.

Lastly I want to thank my family for sacrificially supporting me throughout this work. I am especially thankful for the support that my lovely wife Whitley has provided by always believing in me. I truly could not have completed this work without her.

TABLE OF CONTENTS

LIST OF TABLES

LIST OF FIGURES

CHAPTER 1.

INTRODUCTION

Porous tungsten is a refractory sintered powdered metal (PM) used to manufacture high current density dispenser cathodes [1]. While current industry practice is to machine sintered and pressed porous tungsten workpieces that have been infiltrated with a polymer compound, recent efforts have been focused on eliminating the use of plastic infiltrant [2-5]. Cryogenic machining of porous tungsten has been investigated as a means to improve consistency of surface quality since around 2005 [6]. While macroscopically brittle at room temperature, porous tungsten exhibits large amounts of plastic deformation during machining, where cutting temperatures may easily exceed the brittle to ductile transformation temperature ($T_{BDT} \approx 200^{o}C$) [7-9]. Therefore, surface pores are easily smeared during machining, which negates the benefits of using porous tungsten for the emitting surface of a cathode [1]. The reason for using porous tungsten rather than single crystal or polycrystalline tungsten is the ability of porous tungsten to be backfilled with a Ba based compound that reduces the work function of the emitting surface. Thus, porous tungsten operates much like a sponge that both holds and releases a secondary medium as needed.

In order to keep surface pores open to ensure functional performance of porous tungsten pellets after machining, a variety of processes were developed during the 1950s. Levi et al. [10] described a method of backfilling porous tungsten with a relatively low melting point, soft metal such as copper. After machining, the infiltrated porous tungsten matrix was heated to volatize the infiltrant, leaving just the bare porous tungsten pellet. Because of difficulties in removing all of the metal infiltrant and consequent contamination of the vacuum tube assembly during high temperature operation, the use of certain plastics as an alternative infiltrant became popular during the 1970s and has remained the industry practice until today. While requiring less energy and having less potential for contamination, plastic infiltration is nevertheless undesirable for a variety of reasons. Because of the low fracture toughness of porous tungsten, even slight mishandling of a workpiece during and after machining may introduce cracks. While infiltrated with plastic, the workpiece will appear to be intact, yet upon bake-out of the

infiltrant chips and cracks become apparent. Therefore, the scrap rate during infiltrant assisted machining is relatively high [11].

Cryogenic machining offers the possibility of achieving infiltrant-free machining of porous tungsten. By limiting ductility to prevent the smearing of pores, cryogenic machining is able to achieve excellent levels of surface porosity. While earlier studies were able to show that cryogenic machining improves the consistency of machined surfaces of plastic infiltrated porous tungsten, this current study demonstrates the even without the use of plastic infiltrant, excellent surface quality may be achieved [1, 6]. Therefore, the initial goal of improving surface quality of porous tungsten emitting surfaces has been met while a secondary benefit, the eliminating of the plastic infiltration process, is also realized. Cryogenic machining of porous tungsten relies on liquid nitrogen to cool both the cutting tool and workpiece. Lower cutting temperatures not only prevent excessive smearing but also reduce tool-wear, allowing for sustained machining performance and improved geometric tolerances. A uniquely low coefficient pf thermal expansion (4.5 $\mu m\ m^{-1}\ K^{-1}$), which is in fact the lowest value of any pure metal, along with its body-centered cubic (*BCC)* crystal structure make tungsten an ideal candidate for cryogenic machining. As a *BCC* metal, which have relatively few temperature activated slip systems, tungsten undergoes a brittle to ductile transition. Since this transition temperature is relatively high, cryogenic cooling allows for brittle fracture machining of porous tungsten.

This dissertation is focused on investigated the influence of machining parameters, cooling conditions and geometric relationships between the cutting edge and uncut chip in order to optimize both surface porosity and surface roughness of porous tungsten. A variety of characterization techniques are used to quantify the impact of each variable on as-machined surface integrity. By using chemically inert, low cost cermet cutting tools, a range of machining parameters for finish machining of porous tungsten is established. Acceptable levels of surface roughness and surface porosity are obtained at low cutting speeds. Residual stress measurements show increased compressive residual stress at the surface of cryogenically machined samples compared to dry machining, suggesting that cryogenic machining also strengthens the workpiece. In this way, chipping and undesirable fracture and cracking may be efficiently suppressed.

Due to the large amount of tool-wear experienced by cermet cutting tools, polycrystalline diamond (PCD) is explored as an alternative cutting tool material for porous tungsten. While most PCD grades tend to chip catastrophically, fine grained PCD is found to perform very well. Dry machining with PCD leads to cutting edge chipping regardless of tool material grade, likely due to excessive heat leading to graphitization of diamond. By modifying the cutting edge geometry of PCD tools to improve edge stability and reduce cutting edge notchedness, cryogenic high speed machining at cutting speeds up to v_c = 400 m/min is achieved. At the same time, tool-wear may be lowered significantly at high cutting speeds due to thermal softening in the primary deformation zone. Because of thermally activated severe plastic deformation, cryogenic high speed cutting does not allow for acceptable levels of surface porosity to be achieved. Using this novel method of machining porous tungsten should however be an efficient way of rough and semi-finish machining tungsten prior to a single finishing pass at lower cutting speeds.

Finally, the influence of uncut chip geometry on surface integrity of porous tungsten is studied for both dry and cryogenic machining. A critical chip thickness effect is found to have strong influence on the mode of machining. When the maximum uncut chip thickness exceeds a critical value, brittle fracture originates from the cutting tool and degrades the machined surface. This effect occurs during both dry and cryogenic machining. At very low value of uncut chip thickness, ploughing and spalling likewise lead to poor surface quality. When the maximum chip thickness is approximately equal to the critical chip thickness, which interestingly is approximately equal to the average ligament size of the porous tungsten workpiece material, ductile mode material removal is possible. Cryogenic machining results in significantly higher surface porosity from ductile mode machining by reducing the minimum uncut chip thickness and reducing the negative effects of tool-wear (i.e., ploughing due to increased edge radius). It is hypothesized that the manner in which cryogenic cooling reduces tool-wear is primarily due to the reduction of attrition wear, which occurs whenever an unsTable built-up edge is present. The formation of BUE is linked with brittle fracture machining, during which small brittle fracture chips are produced.

By correlating cutting force and cutting temperature data with the mode of machining, a qualitative model for cryogenic machining of porous tungsten is developed. It is hypothesized that both the workpiece microstructure (ligament size, pore morphology, mechanical properties) and shock compaction effects give rise to the critical chip thickness effect. By lowering the cutting temperature with liquid nitrogen, it is possible to sufficiently strengthen porous tungsten to greatly reduce smearing. Moreover, the negative effect of brittle fracture is effectively managed when cryogenic cooling is applied because complete compaction of the material in the primary deformation zone is achieved more readily, reducing the number of crack initiation sites.

Based on the results obtained during this current study, implementation of cryogenic machining of porous tungsten as an alternative to the current industry practice of plastic infiltrant assisted machining has become feasible. Superior surface quality, particularly reduced surface roughness and improved surface morphology as well as significantly larger compressive residual surface stress, can obtained with cryogenic machining. Cryogenic high speed machining and ductile mode machining of porous tungsten are two novel technologies that were developed as part of the present study. Both of these techniques allow for greatly increased productivity while simultaneously improving product quality.

CHAPTER 2.

BACKGROUND AND LITERATURE REVIEW

2.1 DISPENSER CATHODES

Dispenser cathodes are vacuum devices that operate by thermionic emission. Thermionic emission is the phenomenon of electron emission from a hot surface. If a given material can be heated to the point at which its lowest energy (outer shell) electrons gain sufficient kinetic (thermal) energy to leave the material's surface, thermionic emission takes place. Clearly, most materials are not capable of thermionic emission due to their relatively low melting points. Refractory metals, such as tungsten, are characterized by their very high melting points, i.e., high bond energy. Therefore, refractory metals are used in dispenser cathode assemblies.

In order to achieve thermionic emission, the emitting surface of a dispenser cathode needs to be heated to a high operating temperature ($800 - 1200\ °C$) [12]. Because of the very high melting point of tungsten (3,422 ºC), sustaining such temperatures does not significantly soften the emitting porous tungsten pellet. A vacuum seal around the cathode assembly prevents oxidation of the tungsten surface. Thermionic emission occurs in two regimes, namely temperature limited and space-charge limited. The former describes thermionic emission that is limited only by the temperature of the emitting surface and can be modeled with the Richardson-Dushman equation (Eq. (2-1)):

$$J = AT^2 e^{-\frac{\Phi}{kT}} \tag{2-1}$$

where J is the current density, A is the Richardson constant, T is temperature, k is the Boltzman constant and ϕ is the work function [13-15]. As can be seen from equation 1, temperature limited thermionic emission at a given temperature is controlled only by the work function of a material. Therefore, reducing the work function of the emitting surface of a cathode allows to either reduce the operating temperature or increase current density at the original operating temperature. Both of these improvements are desirable since lowering the operating temperature increases the life of the cathode while simultaneously reducing energy consumption. A schematic illustrating the construction

of a generic B-type cathode, which designates *Ba* impregnation, is shown in the following Figure.

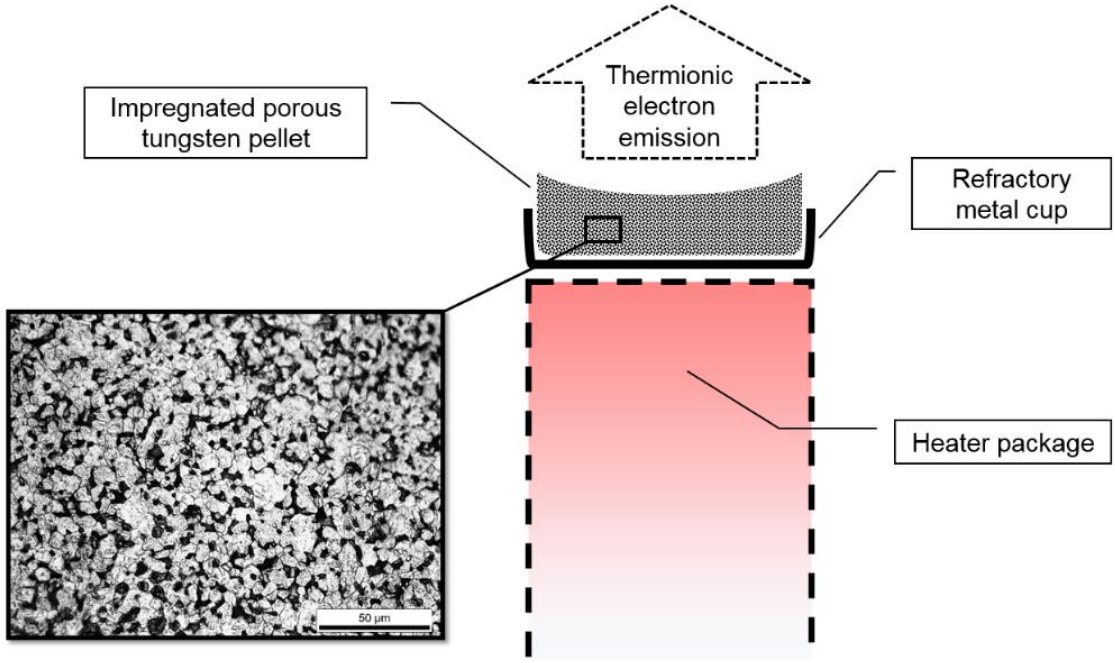

Figure 2-1. Schematic of B-type dispenser cathode with detail showing optical micrograph of 80% density porous tungsten microstructure (schematic based on technical drawing from Semicon Associates).

The work function of porous tungsten may be lowered by impregnating it with a *Ba* compound. Various ratios of Ba are used, the most common used ones being $Ba_4 \cdot Ca \cdot (Al_2O_3)$, $Ba_5 \cdot Ca_3 \cdot (Al_2O_3)_2$, and $Ba_6 \cdot Ca \cdot (Al_2O_3)_2$. Regardless of the composition of the impregnate, the key mechanism leading to a lowered work function of the emitting surface is *Ba* diffusion through the interconnected porous network of the emitting pellet towards the surface. At the surface, a monolayer of *Ba* interact with the tungsten substrate in such a way that the total work function of the surface is lowered significantly. Because of the high operating temperature necessary to let *Ba* diffuse to the surface, some *Ba* continuously evaporates [16]. In order to maintain a constant current density, the cathode needs to dispense additional *Ba*. Matching the rate of evaporation to the diffusion of additional *Ba* to the emitting surface is very difficult and usually achieved based on empirical observations [17, 18]. In addition to *Ba*, there are also other elements

that serve to lower the work function of dispenser cathode surface. Different sputtered overcoatings such as *Ir*, *Os*, and *Os-Ru* are used across the industry. Coated dispenser cathodes are denoted M-type cathodes. A schematic of an uncoated B-type dispenser cathode is shown in Figure 1.

2.2 MACHINING OF POROUS TUNGSTEN

The functional performance of dispenser cathodes is critically linked to the surface morphology of the porous tungsten pellet. To focus electrons at a specific point, many dispenser cathodes feature a concave radius on their emitting surface, as can be seen in Figure 1. Machining this radius, as well as the rest of the cathode body, requires the use of high-precision machine tools. Tolerances in the dispenser cathode industry are generally on the order of ± 10 μm, and may be as strict as ± 3 μm [19, 20]. To make matters more difficult, achieving geometric tolerances does not guarantee proper function of the final cathode assembly. A large enough number of surface pores must remain open to the emitting surface in order to guarantee consistent dispensing of Ba to counteract evaporation. Because conventional machining practices tends to smear surface pores shut, a variety of techniques have been developed to prevent smearing. All of the efforts to prevent or at least limit smearing are based on the use of some material as an infiltrant to stabilize pores during machining. As early as the 1950s Levi et al. [10] described the use of a metal infiltrant to allow acceptable surfaces to be machined on porous tungsten.

Nowadays, dispenser cathode pellets are vacuum infiltrated with a polymer compound that may be baked out at relatively low temperatures after machining [1, 5, 6]. While plastic infiltrated tungsten has a machinability rating similar to that of brass or cast iron, tool-wear is significantly larger due to the high strength of tungsten and the abrasive nature of the sharp-edged ligaments of porous tungsten [8, 21]. Un-infiltrated (as-sintered) porous tungsten is much more difficult to machine than infiltrated workpieces of the same material due to severe macroscopic brittleness of porous tungsten and highly abrasive fractured chips that resemble grinding dust [4]. While machining of infiltrated tungsten produces continuous curly chips which can be easily removed from the cutting

area, porous tungsten chips are small enough to become impinged between the cutting edge and the uncut chip, causing built-up-edge (BUE) and attrition wear [22].

2.2.1 Previous Studies

Because of the difficulties in machining un-infiltrated porous tungsten, previous studies have focused mostly on machining of infiltrated porous tungsten. Since Levi et al. first described the use of a metal infiltrant in the 1950s [10], no (published) efforts were made until recently to machine as-sintered porous tungsten. Anon et al. [21] performed some of the early experiments in the 1960s on machining of silver infiltrated tungsten and found that tool geometry had little effect on machining performance. Cutting speeds as high as v_c = 300 m/min were reached using positive rake angle carbide cutting tools, approaching speeds used for aluminum and brass alloys [21]. Due to the excellent machinability of infiltrated tungsten, little attention was given to improving machining performance for this composite material. As a result, very little early work from 1950-70 is available on machining of metal infiltrated tungsten.

Chen et al. [6] were the first to conduct an exploratory investigation to improve the surface quality of plastic infiltrated porous tungsten in 2005. By using sharped edge ($r_\beta \approx$ 6 μm) polycrystalline diamond (PCD) cutting tools with a variety of large corner radii ranging from 1.6 – 4 mm, Chen et al. were able to produce excellent surface finishes and high levels of surface porosity for at least 5 successive facing cuts.

Beginning in 2008, Tarter et al. [1] first studied the use of cryogenic cooling as a means to improve the sustainability of the dispenser cathode manufacturing process because of the potential to eliminate the use of infiltrant during machining. A more detailed version of the same results was published by Pusavec et al. [11] later in 2008, including a set of optimized machining parameters. While these initial results were indeed promising, no further advancements were made between 2008 and 2012, even though Pusavec did publish the same results from 2008 again on his own and in a different journal in 2012 [2, 11]. The initial machining parameter optimization results for

cryogenic machining of porous tungsten (of unspecified density, likely ≈ 90%) from the 2012 publication of Pusavec are included below.

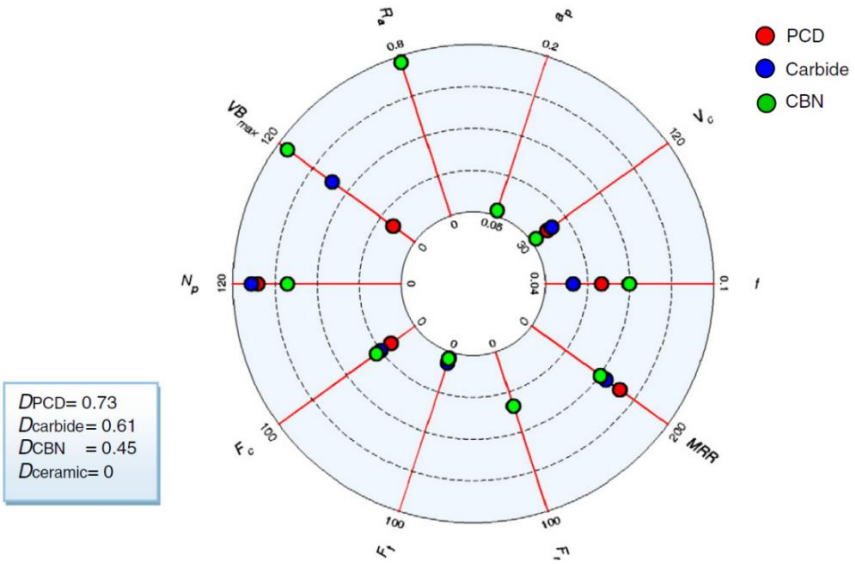

Figure 2-2. Optimization of machining parameters for cryogenic machining of porous tungsten for three different cutting tool materials (from [2] with permission of Elsevier Inc., license number 3630380501874).

It should be noted that during the course of the present study the early results of Pusavec et al. as shown in Figure 2 could not be verified, particularly the set of optimized machining parameters. A likely cause for this discrepancy is the use of different porosity levels of the porous tungsten workpieces during early studies, which did not document material properties, and the current study which exclusively used 82-80% density material. Nevertheless, the method developed by Pusavec et al. to quantify surface porosity was successfully used during this present study. More specific information on the experimental details of measuring surface porosity from scanning electron microscopy (SEM) micrographs using ImagePro software can be found in chapter 3, section 3.5.2. An example of a micrograph and the corresponding analyzed image from Pusavec's work is shown in Figure 2-3. It should be noticed that the both the pore size distribution and the minimum pore diameter considered for evaluation in Figure 2-3 are outside acceptable limits of the dispenser cathode industry and this present study.

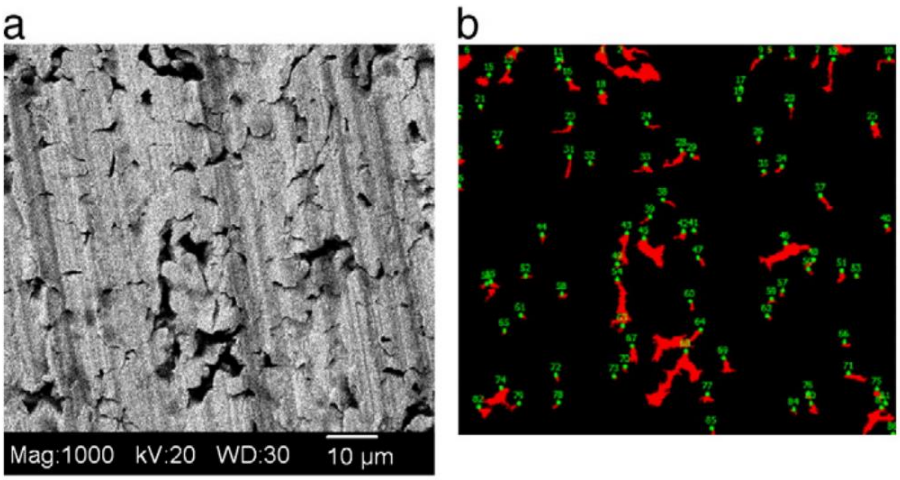

Figure 2-3. SEM micrograph of cryogenically machined porous tungsten surface (a) and surface pore analysis performed with ImagePro software (b) (from [2] with permission of Elsevier Inc., license number 3630380501874).

2.3 MACHINING OF OTHER POROUS MATERIALS

While there are only a small number of studies regarding machining characteristics of porous tungsten, a significant number of publications regarding machining of other porous materials exists. Two materials in particular, powder metallurgical *(PM)* steel and porous titanium foams, have been thoroughly investigated. Both of these materials are markedly different from porous tungsten yet they feature similar machining mechanisms and surface characteristics. The present study is expected to add additional insights that may likewise be extrapolated to other porous metals as well.

2.3.1 Powder Metallurgical Steel

Just as porous tungsten, powder metallurgical steel is produced by pressing and sintering of small particles into a bulk shape with relatively small residual porosity (generally 5-20 %) [23, 24]. *PM* parts are widely used in the automotive and general engineering industries to produce near-net shape parts that generally require only finish machining [25-27]. In 2006, over 20 billion USD were generated with *PM* components

in the United States alone [23]. Because sintered *PM* steels are highly abrasive due to the high hardness of individual powder particles (40-60 HRC), machinability is considered to be poor [28]. Nevertheless, significant advances in terms of productivity have been made due to the availability of highly wear resistant ceramic and cubic boron nitride (CBN) cutting tool materials [29, 30].

Surface quality and dimensional accuracy of machined *PM* parts are often problematic due to degrading surface quality with increasing cutting edge wear [23, 31]. Machining of green *PM* components (i.e., before final hardening) results in worse surface finish than machining of hardened component due to pull-out of weakly bonded particles. Because tool-wear is significantly lower when machining *PM* steel in a green state, Robert-Perron et al. [32] performed a set of optimization experiments to produce a surface finish better than $R_a < 1$ μm, a micrograph of which is shown in Figure 2-4 on the following page. Machining of green *PM* steel is quite similar to machining of un-infiltrated porous tungsten as both materials have a tendency towards undesirable fracture and tearing of ligaments.

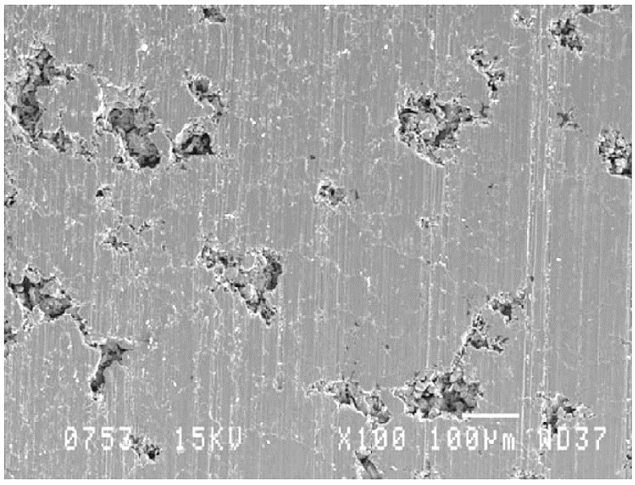

Figure 2-4. SEM micrograph of optimized surface finish of PM steel component machined in green state [v_c = 140 m/min, f = 0.025 mm/rev]. Surface pores are significantly larger than those observed for porous tungsten yet overall surface morphology is very similar (from [32] with permission of Elsevier Inc., license number 3632160620220).

Salak et al. [33] found that machinability and surface quality of *PM* steels are reduced as porosity increases due to BUE formation and decreased plasticity. Zurecki et al. [34] performed both flood cooled and cryogenic finish turning of *PM* steel. The researchers used both 7.7% porosity (high density) and 14.5% porosity (low density) *PM* steel in both the as-sintered and a hardened state. Zurecki et al. moreover reported reduced smearing for cryogenically cooled machining for both high and low density PM steel and surface densification of the hardened material due to a nanocrystalline 'white layer'. It should be noted that for the typical applications of *PM* steels surface porosity is not a desirable feature and therefore the term 'smearing' is used to describe irregularly 'ploughed' surfaces rather than shut pores as in the case of porous tungsten. Most applications for parts machined from *PM* steel require high geometric accuracy and low surface roughness to reduce wear and ensure proper fit [24, 27]. Therefore, densification (i.e., lack of surface porosity) is desirable to increase the strength of the as-machined parts, particularly the surface layer [23]. Densification is also associated with increased compressive residual stress, leading to improved functional performance of machined parts [34, 35].

There appears to be a consensus among researchers that harder and denser PM steels are more readily machinable than softer and more porous versions of the material because of increased plasticity and strength exhibited by the former [27, 31, 34, 36]. Because of significantly larger ligament sizes (0.1 – 1 mm) of *PM* steels than those of porous tungsten (5-15 μm), finish machining of porous tungsten is expected to be more dependent upon cutting edge geometry. Nevertheless, qualitative observations from machining of *PM* steel do suggest that cryogenic machining is capable of improving surface quality of porous materials by simultaneously reducing tool-wear and increasing surface hardness, both of which lead to improved surface roughness and reduced smearing [4, 34].

2.3.2 Porous Titanium Foams

Unlike the case of PM steel, open surface porosity is a desirable feature for as-machined porous titanium foams. Dense titanium is already widely used in biomedical applications such as bone screws and dental implants due to its high biocompatibility [37-41]. Because of the effect of implant induced bone loss, the use of porous titanium in biomedical implants has recently received significant attention [42-45]. By allowing for bone ingrowth, porous titanium allows for greatly improved mechanical strength of the joint between bone and implant [24, 39, 45]. However, fabrication of osteopathic implants from porous titanium with sufficient surface porosity to allow for proper bone ingrowth is exceedingly difficult due to the ease with which pores are smeared shut during machining [42, 46-48]. Moreover, the low thermal conductivity of high strength of titanium lead to accelerated tool-wear and high cutting forces [38, 49, 50]. An example of the morphology and microstructure of a typical titanium foam can be seen in the following Figure.

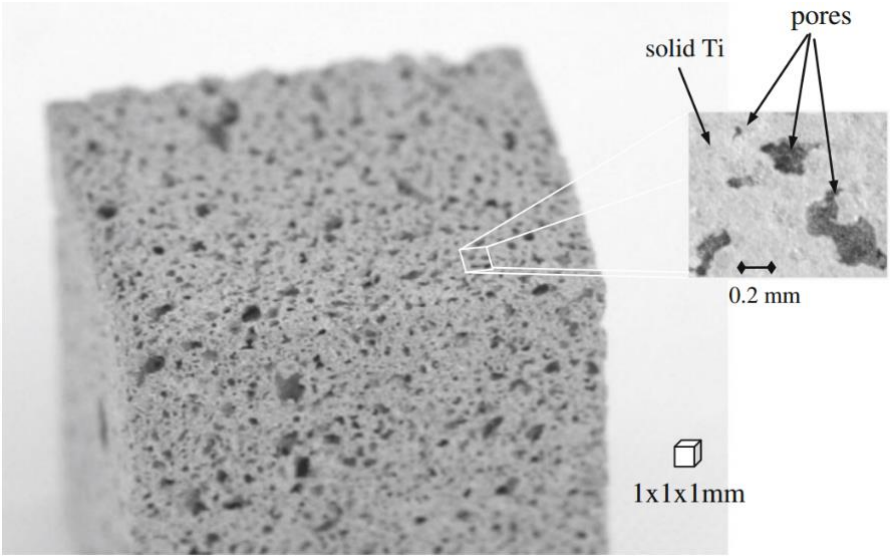

Figure 2-5. Morphology and complex 3D microstructure of a Ti-6Al-4V porous titanium foam sample (from [51] with permission of Springer, license number 3632110991906).

Fahkri et al. [46, 50, 51] found in multiple studies that cutting forces during micromachining (milling) of porous titanium foams (54% porosity) varied significantly

due to interactions between the cutting tool and pores within the material. The large size of pores within the titanium foam workpiece material (0.5 – 1.5 mm) and the small size of the cutters used for the micromachining operation (less than 1 mm) lead to interruptions within the cut [50]. The researchers pointed out that despite the widespread practice of machining porous metals, no appropriate model (i.e., other than modified materials for dense materials) for the cutting mechanisms of these materials has been proposed [51].

Tutuena-Fatan et al. [46] described two qualitative cutting mechanisms explaining the behavior of porous titanium foams, namely the "interrupted cutting mechanism" and the "deformation cutting mechanism," a schematic of which is shown in Figure 2-6. The latter mechanism is responsible for the smearing of surface pores due to micro-burr formation [46, 51]. Especially when the diameter of pores is large compared to the cutting edge radius, as is the case for titanium foams, there will be some material towards the beginning of each pore that is pushed into the pore, rather than removed with the rest of the chip [46]. Interestingly, the same mechanism is observed during machining of porous tungsten [4, 11].

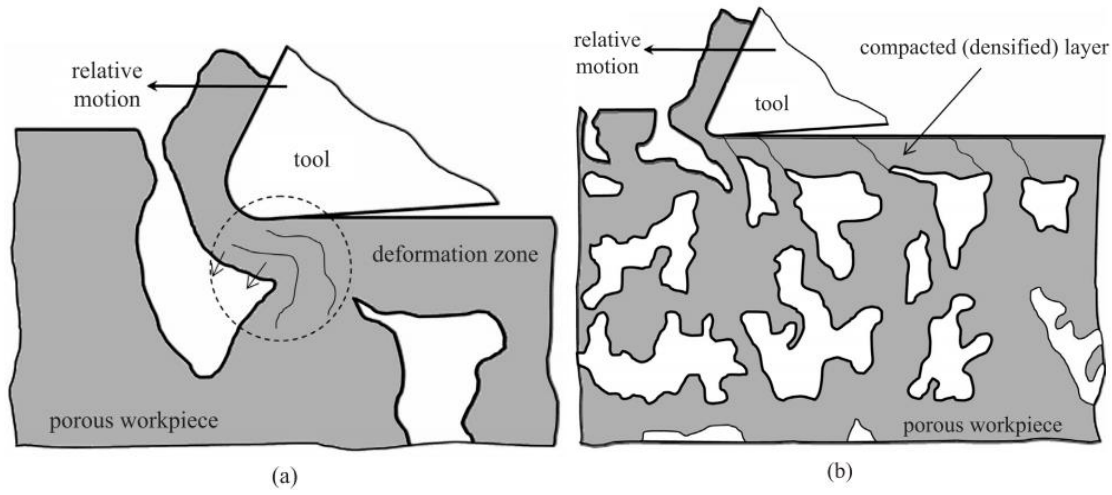

Figure 2-6. Detail of local pore smearing ahead of the cutting edge (a) and overview (b) of the deformation cutting mechanism of porous titanium foams hypothesized by Tutunea-Fatan et al. (adapted from [46] with permission of SAGE Publications).

2.4 MACHINING INDUCED SURFACE INTEGRITY AND FUNCTIONAL PERFORMANCE

Surface integrity is a collective term used to quantitatively describe the quality and properties of machined surfaces. Because of the broad definition of the term surface integrity, a variety of parameters may be employed to assess the surface integrity of a machined component [52-56]. An overview of the most commonly used levels of surface integrity data sets as first defined in a review by M'Saoubi et al. [55] in 2008 is included in the following Table.

Table 2-1. Levels of surface integrity data sets as outlined by M'Saoubi et al. [55].

Minimum data set	Standard data set	Extended data set
1. Surface finish 2. Macrostructure (10X or less) • Macrocracks • Macroetch indications 3. Microstructure • Grain size • Microcracks • Plastic deformation • Phase transformation • Intergranular attack • Pits, tears, laps, protrusions • Built-up edge • Melted and re-deposited layers • Selective etching 4. Microhardness	*1. Minimum SI data set* 2. Fatigue tests (screening) 3. Stress corrosion tests 4. Residual stress and distortion	*1. Standard SI data set* 2. Fatigue tests (extended to obtain design data) 3. Additional mechanical tests • Tensile • Stress rupture • Creep • Other specific tests (e.g., bearing performance, sliding friction evaluation, sealing properties of surfaces)

Because of the large number of possible surface integrity parameters, even the various data sets in Table 2-1 are not an exhaustive list. It is therefore very important to select and define a list of relevant parameters based on the specific machining process,

workpiece material and function of the finished component [52, 55, 57]. In the case of porous tungsten, surface roughness, surface porosity and residual stress are particularly relevant towards the functional performance of dispenser cathodes [1, 6]. Low surface roughness is necessary for proper wetting of the cathode emitting surface with Ba [15, 57]. A sufficient amount of surface porosity is required for the cathode to dispense additional Ba as evaporation takes place on the hot emitting surface [50]. Lastly, compressive residual stress at the surface has been hypothesized by the author to suppress chipping and fracture of the brittle porous tungsten workpiece during and after machining. Similar effects have been widely studied particularly for steel and aerospace alloys [58, 59].

In 2011, Jawahir et al. [60] published a three-year long study on the various characterization techniques used to measure surface integrity. Particularly the use of non-destructive techniques such as X-ray diffraction, Raman spectroscopy, scanning acoustic microscopy, laser ultrasonics and a variety of other methods is currently being developed to improve quantization of surface integrity [52, 60-64]. Destructive metallographic techniques to determine the stress states and depths of deformed layers as well as grain morphology and other microstructural parameters do however remain the most commonly used techniques [55]. Especially residual stress is often measured by selectively electropolishing a machined surface to obtain a depth profile of stress [65]. Because many researchers have described a strong correlation between the stress state of a component's sub-surface and functional performance such as wear resistance and fatigue resistance, residual stress is one of the most popular surface integrity parameters to be measured [57, 66, 67].

Functional performance may be increased by performing specialized machining operations to achieve surface modifications. Hard turning was developed by Tönshoff et al. [68] as an alternative to grinding. Because turning of hardened steel generally imparts compressive residually stresses and grinding has a tendency to produce tensile stress states in the sub-surface, fatigue life may be improved by using hard turning [67-71]. So-called 'white' and 'dark' layers resulting from machining processes have been invoked as having both beneficial and detrimental effects on functional performance,

though the majority of researchers report negative effects of severely work hardened or annealed layers that result from machining [56, 58, 64, 72].

Reducing the presence and/or influence of surface and sub-surface flaws, such as white/dark layers, is the most commonly invoked mechanism leading to improved functional performance [55, 71]. For example, Aspinwall et al. found that by reducing surface roughness of *Ti-6Al-4V* and *IN718* from wire electric discharge machining, surface integrity was improved simultaneously [59]. As early as 1978, DeVries et al. [73] showed that surface roughness was directly linked to both surface integrity and functional properties of machined steel parts. Since roughness is a type of flaw on the surface of a component, reducing surface roughness generally leads to improved functional performance. In certain cases, such as cylinder bores and dispenser cathode emitting surfaces, some imperfections are however desirable to allow for a secondary liquid medium to be retained. Achieving an optimum level of surface roughness while maintaining reasonable productivity is a complicated process involving all machining parameters, including the machine tool and cutting tool, to be chosen carefully [55, 63, 71, 74].

2.5 CUTTING EDGE EFFECTS

All cutting edges used for machining exhibit a finite amount of rounding or other deviation from a perfectly sharp wedge. Early metal cutting models such as the one developed by Merchant assumed a perfectly sharp cutting to estimate process forces [75-77]. While this approach works reasonably well at large feeds and speed when the ratio between uncut chip thickness h and the cutting edge radius r_β is relatively large (i.e., $h/ r_\beta >> 1$), size effects und phenomena such as built-up edge (BUE) lead to significant deviations for most realistic scenarios [78, 79]. The effect of cutting edge rounding is particularly pronounced in finish machining, when uncut chip thickness may become extremely small ($h < 10$ μm) [80].

In a recent review of cutting edge geometries and their influence on modern machining processes, Denkena et al. [81] discussed the various techniques used to

achieve precisely controlled cutting edge with defined geometric features. By altering cutting edge geometry, significant improvements of tool-life, surface finish and residual stresses may be achieved [82, 83]. Biermann et al. [84-86] performed several studies to both investigate and optimize cutting edge preparation for processes ranging from deep hole drilling to micromilling. Optimized cutting edge geometries of small micromilling cutters ($d < 1$ mm) allowed for elimination of chatter and tool vibration, leading to improved surface roughness [84]. In general, increasing cutting edge radius leads to improved cutting edge stability at the expense of surface finish [80, 87]. Because of the size effect, there is a certain minimum uncut chip thickness below which only elastic deformation occurs [88, 89]. The resultant ploughing area was termed the 'Spanzipfel' by Brammertz [90] in the 1960s.

Modifications to Brammertz's initial formulation such as side flow and scaling factors have been proposed by many researchers, particularly in the fields of micromachining and ultra-precision diamond turning [91-94]. Nevertheless, the physical principle of there being a portion of the uncut chip that cannot be removed by the cutting edge is now unanimously accepted [89]. As a result, the metal cutting process inevitably consists of both material removal in form of a chip as well as ploughing component that is likely responsible for the formation of commonly observed severely plastically deformed layers [88, 95, 96]. A schematic overview of the geometric relationship between the cutting edge, uncut chip and workpiece is shown in Figure 2-7 on the following page.

Thiele et al. [80] showed that an increase in ploughing with larger cutting edge radii when finish turning hardened *AISI 52100* bearing steel led to larger surface roughness and cutting forces. Interestingly, that same study also indicated that harder workpieces allow for improved surface finish, particularly when smaller edge hones are used [80]. Oishi [97] reported similar results and suggested that beyond a critical hardness, BUE formation is suppressed or at least stabilized to achieve very low surface roughness. Kummel et al. [98] studied the effect of laser micro-structuring of cutting tools to stabilize the BUE and reported improvements in both tool-life and workpiece surface finish.

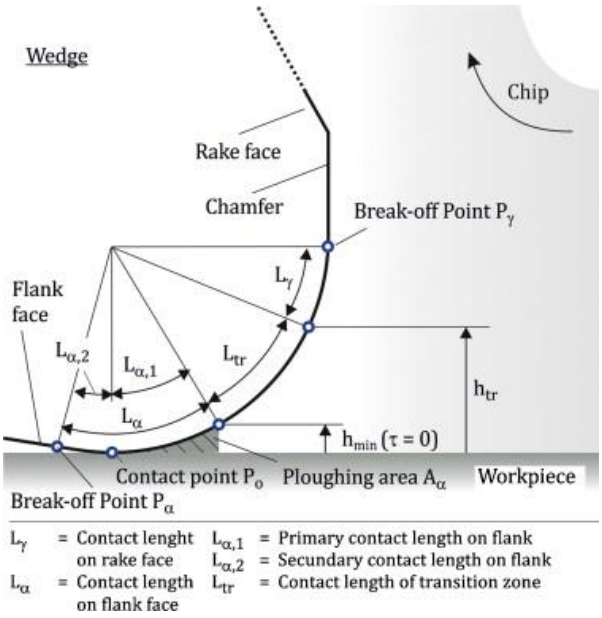

Figure 2-7. Schematic representation of the complex contact geometry of the cutting and uncut chip. The ploughing area A_α is of particular importance with respect to surface integrity as it influences surface roughness, hardness, residual stress and a variety of other surface integrity parameters (from [81] with permission of Elsevier Inc., license number 3633111297915).

Similar to BUE, material side flow and adhesion on the cutting tool also result from the size effect. Yousefi et al. [99] found that material side flow and adhesion on the secondary cutting edge lead to increased surface roughness at higher cutting speeds when machining an aluminum alloy. While BUE is generally more prevalent at low cutting speeds, Yousefi et al. suggested that increased cutting temperature allowed for some of the workpiece material to become welded onto the cutting tool and subsequently re-deposit onto the machined surface, much like an unstable BUE.

Moneim et al. [100] investigated the effect of tool roundness in high speed cutting of brass and zinc on the stability of BUE. The researchers determined that workpiece surface finish was optimal for a slightly rounded cutting edge rather than a perfectly sharp wedge or a large hone, especially at higher cutting speeds. Moreover, Moneim et al. remarked that occasional cracks observed on the machined surfaces are likely due to the tensile stress induced at the sharp apex of the stable BUE rather than the rounded

cutting edge which was found to impart compressive stress. Waldorf et al. [101] compared different analytical formulations of the ploughing effect for *AA-6061-T6*. They determined that for the negative rake angles and large cutting edge radii the assumption of a stable BUE, rather than ploughing below a specific stagnation point, was more appropriate when estimating cutting forces. Determining the chip formation mechanism and nature of the size effects remains a debated topic and is likely highly dependent upon the workpiece material and cutting edge geometry [81]. An illustration of the difference between cutting with a stagnation point and stable BUE is included in the following Figure.

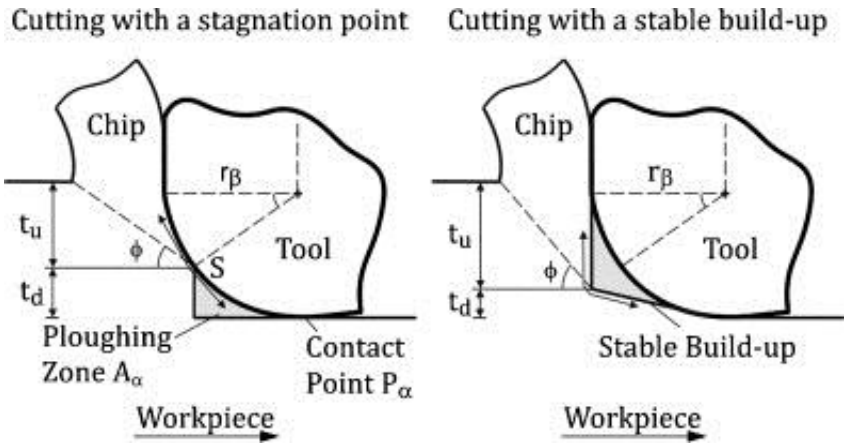

Figure 2-8. Comparison between two commonly proposed (from [81] with permission of Elsevier Inc., license number 3633111297915)

2.6 MINIMUM AND CRITICAL CHIP THICKNESS EFFECTS

Because of the finite size of the cutting edge and the very small uncut chip thickness values encountered in finish machining there is a size effect leading to increased cutting forces and limits in the attainable surface finish [102, 103]. As mentioned in the previous section, there is a minimum uncut chip thickness value below which only ploughing (elastic deformation) takes place. While not a concern for most rough machining and even conventional finish machining operations, some applications requiring extremely low surface roughness are strongly influenced by the minimum chip thickness effect

[104]. Micromachining in particular has motivated a large number of publications on the topic of minimum chip thickness [92, 105].

Several attempts have been made to calculate the value of minimum chip thickness. Kishawy et al. [95] performed orthogonal turning experiments to validate finite element based calculations of minimum chip thickness by finding the stagnation point for a variety of cutting edge radii. This same study found an increase in minimum chip thickness as a function of cutting edge radius. Liu et al. [93] developed an analytical model that was validated for two types of steel, *AISI 1020* and *1040* carbon steels, and *AA-6082-T6*. By taking into account both thermal softening and strain hardening effects with the Johnson cook material model excellent correlation between predicted and experimentally measured values was found. In order to measure the minimum uncut chip thickness, Liu et al. [93] performed side milling experiments and measured the height of the maximum peaks on the as-machined sidewall surface (the '*Spanzipfel*' proposed by Brammertz [90]) with an optical profiler. The mechanism of sidewall surface generation is shown in the Figure 2-9 on the following page. It should be noted that perfectly elastic behavior of the Spanzipfel as assumed by Liu et al. is rather unlikely, particularly in porous tungsten, where side-flow into adjacent pores is more likely than elastic spring-back.

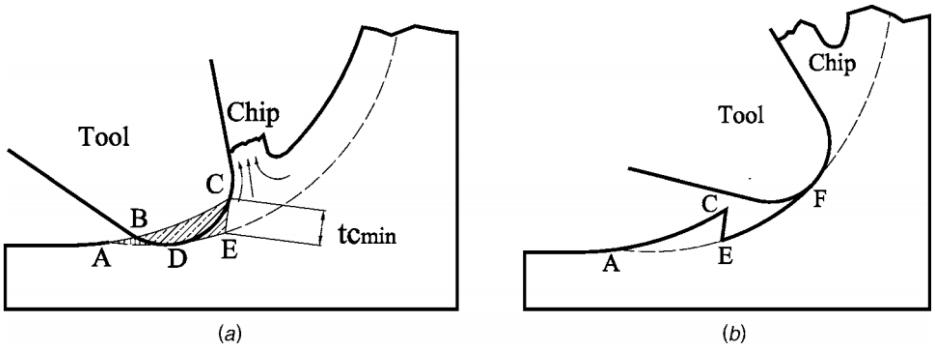

Figure 2-9. Mechanism of sidewall surface generation during upmilling, considering ploughing (a) due to the minimum chip thickness effect. After the cutting edge passes over the ploughing area (ACE), elastic recovery takes place, leaving a "Spanzipfel" (adapted from [93] with permission of ASME).

Because of the inherent surface roughness of porous tungsten resulting from surface pores, very low surface roughness values have to be achieved on the ligaments composing the dense portion of the surface. Therefore, the minimum chip thickness effect is highly relevant since it limits the minimum attainable surface roughness [5, 89]. Because minimum chip thickness is a function of both the material properties and the cutting edge radius, an optimum combination of machining parameters and cutting edge preparation will need to be determined in order to optimize surface roughness of porous tungsten. Wang et al. [105] performed a similar kind of analysis to optimize surface finish from micromachining of hardened tool steel using a version of the slip line model.

The very small value uncut chip thickness when using relatively sharp cutting tools ($r_\beta < 10$ μm), i.e., the kind of cutting tools used in finish machining, makes it very difficult to accurately measure h_{min}. No successful attempts have been published to date to directly measure h_{min} from turning experiments [89]. This is likely a result of the fact that the entire portion of the cutting edge involved in removing material is constantly engaged in turning, allowing for side flow of the ploughing area but making perfectly elastic recovery virtually impossible. Therefore, side milling using an up-cut configuration as the one shown in Figure 2-9 is much preferable when it comes to leaving an intact Spanzipfel to measure h_{min} directly [93, 106]. Since some amount of side flow should always be expected when encountering the minimum chip thickness effect, a modified version of the simple model of Brammertz that allows for measurement of h_{min} by simply determining the increase in surface roughness over the theoretical (kinematic) value is however more practical [107]. Schultheiss et al. [89] recently proposed one such model to estimate the increase in surface roughness in turning operations due the minimum chip thickness effect. Despite the difficulty of measuring the exact value of h_{min}, there is some consensus that the principle of the minimum chip thickness effect should motivate using the largest possible feed and nose radius with the smallest possible cutting edge radius in order to minimize the ploughing induced surface roughness increase [93, 103, 104].

For brittle materials, critical chip thickness is another factor strongly influencing machining induced surface roughness. In the late 1980s and early 1990s, ductile-regime grinding of brittle materials was developed by Bifano et al. [108, 109] to produce mirror

like surface finish. This technology improvement was made possible by controlling nanometrically small infeed per wheel revolution with modern grinding equipment, allowing for plastic flow rather than brittle fracture as the dominant machining mechanism [108]. Because of the very small cutting edge radii of typical grinding wheel grains ($r_\beta < 1$ μm), minimum uncut chip thickness is kept low enough to allow for material removal while at the same time the critical thickness h_c beyond which fracture occurs is not exceeded [110]. A commonly used equation (Eq. 2-2, which is based on the Griffith fracture criterion) to estimate the critical uncut chip thickness, sometimes referred to as the "critical-grinding-infeed-rate" d_c is given by:

$$d_c = \frac{ER}{H^2} = \alpha * \left(\frac{E}{H}\right)\left(\frac{K_{1c}}{H}\right)^2 \tag{2-2}$$

where E is Young's modulus, H is the hardness, R is the material's fracture energy, which may be estimated by the ratio of K_{1c}, the mode 1 fracture toughness, and hardness [108]. It should be noted that equation 2 only yields meaningful results for materials whose fracture toughness does not vary significantly with indentation depth [111]. Moreover, only materials exhibiting very low fracture toughness (i.e., brittle materials) have a critical chip thickness value relevant to machining. Because porous tungsten is macroscopically brittle, it is likely that there is a critical chip thickness effect, though no such results have been explicitly discussed to date [112, 113].

The most commonly studied materials with respect to the critical chip thickness effect are single crystal *Si*, glass and tungsten carbide. In addition to ductile-regime grinding, single point diamond turning is another technique used to machine brittle materials [114]. Diamond turning is generally used to produce ultra-high precision optical and semiconductor components [115, 116]. The cutting edge radius of single crystal diamond tools can be as low as several nanometers, enabling extremely small infeed values [117]. Ductile chip formation takes place below h_c, leaving a plastically deformed surface even in extremely brittle materials such as glass [110]. Because of the productivity limitations of using very slow feed values required to keep the maximum uncut chip thickness below the critical value, Yan et al. [117] developed a novel straight-nosed cutting tool to allow

for high feed ductile machining. By selecting a very shallow approaching angle the uncut chip thickness was effectively reduced while relatively large feed was attained.

The mechanism for ductile chip formation in single point diamond turning of brittle materials has been described by Liu et al. [118] as a combination of compressive stress induced by the cutting edge shielding the growth of pre-existing flaws to prevent fracture. Zhang et al. [119] developed a similar model for vibration-assisted machining of brittle materials, assuming a critical particle size necessary for fracture, much like Bifano et al. [108] did for the critical grinding infeed rate. Arif et al. [120-126] have published a large number of studies on ductile-mode machining of tungsten carbide and glass. Their approach was based on specific cutting energy to predict the transition from dislocation based ductile deformation to brittle fracture [121, 122, 126]. Experimentally, Arif et al. [120, 123-125] performed grooving, side milling and slot milling experiments. Grooving experiments, during which a single point cutting tool linearly moves across the surface of the workpiece while depth of cut increases steadily, have proved to be very effective in determining critical chip thickness [126]. A Figure illustrating a typical grooving study for both single crystal *Si* and *BK7* glass is included below.

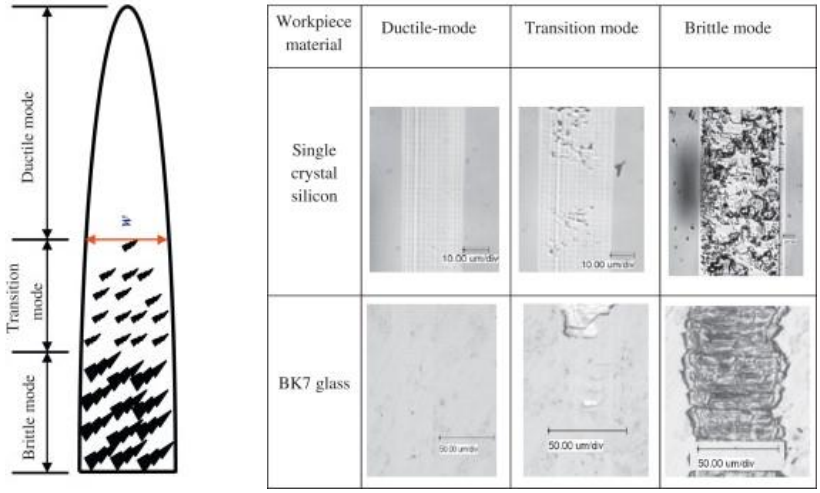

Figure 2-10. Ductile, transition and brittle mode machining of single crystal *Si* and *BK7* glass from varied depth of cut grooving experiments (adapted from [126] with permission from Elsevier Inc., license number 3633711130739).

Because grooving is unable to efficiently produce complex workpiece geometries, Arif et al. [121, 124] performed a series of milling experiments of brittle tungsten carbide. Realizing that completely avoiding fracture requires extremely low feed values and consequently large tool-wear and slow production time, Arif et al. [122] proposed a method of milling brittle materials in a 'up-cut' configuration to avoids cracks from reaching the machined surface. Because the goal the upmilling process described by Arif et al. [114, 123] is not to entirely prevent fracture as is the case in single point diamond turning, significantly higher material removal rates are possible. This is particularly relevant to the machining of porous tungsten, as single point diamond turning or grinding do not have sufficient productivity to replace the currently used infiltration process. Either milling or high feed turning with some fracture occurring near the top of the undeformed chip yet no fracture on the machined surface should allow for significant improvements in surface roughness. A schematic of the principle behind the limited fracture upmilling method described by Arif et al. is shown below.

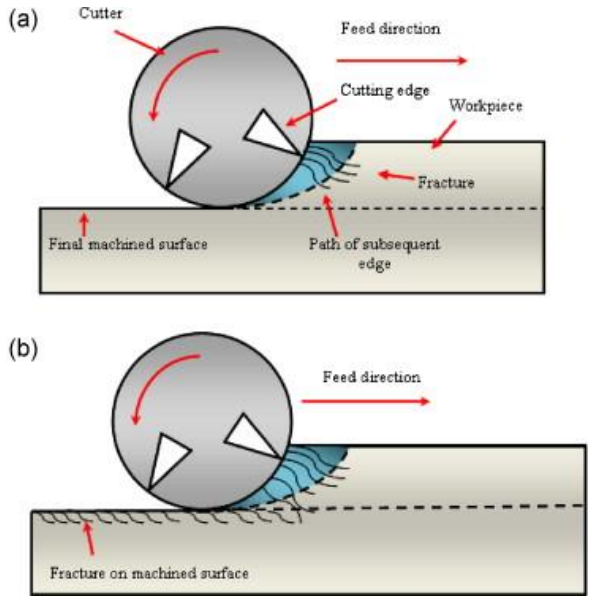

Figure 2-11. Upmilling process of brittle material with critical chip thickness induced fracture being removed by the subsequent path (a) and reaching the machined surface at high feed per tooth (b) (from [122] with permission of Elsevier Inc., license number 3633721035483).

2.7 CRYOGENIC COOLING IN MACHINING

Machining is a thermo-mechanical process during which most of the mechanical work done to cut the workpiece is converted into heat [127-130]. Because of the large temperatures that occur during machining, the cutting tool experiences significant wear, particularly when cutting high-strength materials at large cutting speeds [131]. Moreover, thermal damage may occur on the surface and in the sub-surface of the machined component, an effect most commonly referred to as 'white layer' generation [130, 132].

To control thermally induced tool-wear, cryogenic machining was first developed in the late 1960s and early 1970s [133-135]. Considered mostly a niche technology without broad application potential, little work was done on further developing cryogenic machining between 1970-1990. In 1989, Li et al. [136] first described the use of cryogenic cooling to use natural diamond cutting tools in ultra-precision machining of ferrous metals. By preventing thermally activated diffusion of the carbon in cutting tool towards the ferrous workpiece significant improvements in tool-life and thus geometric tolerance were achieved. Similar results were also reported by Lundin et al. [137] in 1992, who investigated the use of diamond tool for a variety of materials that chemically react with carbon. Evans et al. [138] performed cryogenic diamond turning experiments on stainless steel, achieving very low levels of surface roughness and exceptionally low tool-wear.

By the early 1990s, cryogenic machining was re-discovered as a means to not only control tool-wear but also offer improved sustainability and surface integrity [139-141]. Zhao et al. [141] discussed cryogenic cooling strategies for a variety of workpiece materials based on material properties. Hong et al. [131, 139, 142-149] published a large number of studies on the economic and ecological potential of cryogenic machining between 1995-2005. In an early study, Hong et al. [131] discussed the influence of material properties and thermal effects on the machinability of different materials in light of cryogenic cooling strategies. Most notably, Hong et al. [131] remarked that the brittle-to-ductile transition (BDT) of low carbon steel such as *AISI 1010* at low temperatures significantly improved machinability by suppressing built-up edge (BUE) formation and

improving chip breakability. For high strength materials such as *AISI 1070* high carbon steel and *AISI 52100* bearing steel, Hong et al. [131] hypothesized that lowered cutting temperatures are likely to improve tool-life but that increasing workpiece strength with cryogenic cooling is not desirable, which implies that cooling the cutting tool rather than the workpiece is to be preferred. For high-strength, low thermal conductivity materials such as titanium alloy 5 (*Ti-6Al-4V*), Hong et al. [145, 148, 149] performed a number of studies mainly focused on managing the very high temperatures on the rake face of the cutting tool. By developing a proprietary micro-nozzle to inject liquid nitrogen on the rake face to lift the chip and lubricate the tool/chip interface, Hong et al. [145] were able to improve tool-wear by up to five times.

The lubricating effect of liquid nitrogen in metal cutting has been studied by a number of researchers. Hong et al. [143, 145, 148] reported a reduction in friction for uncoated carbide inserts but an increase in friction for coated tools. Particularly for *Ti-6Al-4V*, Hong et al. [143, 147] measured significantly lower friction forces compared to both dry and emulsion flood cooled machining. Controversially, a recent study by Courbon et al. [150] reported no discernable lubricating effect of either liquid or gas phase cryogenic nitrogen coolant. Similar results were also obtained by Caudill et al. [151] when comparing cryogenic and dry burnishing of the same titanium alloy. Despite the current lack of consensus regarding the amount of lubrication provided by liquid nitrogen it is clear that the lubricating mechanisms of LN_2 is highly dependent upon the tribological properties of the workpiece, cutting tool as well as the state (gaseous/liquid) of the cryogenic coolant [143, 147, 148, 152]. Bassani et al. [152] studied hydrostatic lubrication with cryogenic fluids and did indeed find that the type of coating used (i.e., tribological properties of the sliding surfaces) had a strong effect of the lubricating effect of liquid nitrogen.

Beginning in the mid-2000s, increasing attention was given towards the influence of cryogenic cooling on surface integrity. Ghosh, Zurecki, Frey et al. [34, 153-156], all members of Air Products and Chemicals, Inc., published a number of studies on the beneficial effects of cryogenic cooling on processes ranging from hard turning of steels to cryogenic machining of polymeric biomaterials. In the case of polymeric materials, cryogenic cooling offers distinct advantages over conventional machining practices as

viscoelastic deflection is effectively reduced, allowing for improved geometric tolerances and reduced workpiece damage due to tearing [154, 157, 158]. The more common application of cryogenic hard turning has been studied by a number of researchers due to the ability to impart compressive residual stresses while reducing 'white layer' damage [155, 159]. Umbrello et al. [132, 160-162] published various studies on the topic of cryogenic machining of hardened steels. In an early one of these studies, Umbrello et al. [132] reported the ability of cryogenic machining to significantly reduce and in some cases completely suppress white layer formation. Umbrello et al. [160, 161] described the key mechanism responsible for the improved surface integrity from cryogenic machining as a lack of rapid heating and quenching as is the case during dry machining, which creates a white layer of untempered martensite. Moreover, by reducing thermal damage in the form of severely strained untampered martensite, cryogenic machining slightly decreases the amount of compressive residual stress in the machined surface, nevertheless offering significant compressive stress that stands in contrast to the tensile stress state resulting from hard grinding [161, 162]. Excerpts from the work of Umbrello et al. showing the reduction in white layer depth and compressive residual stress are included below.

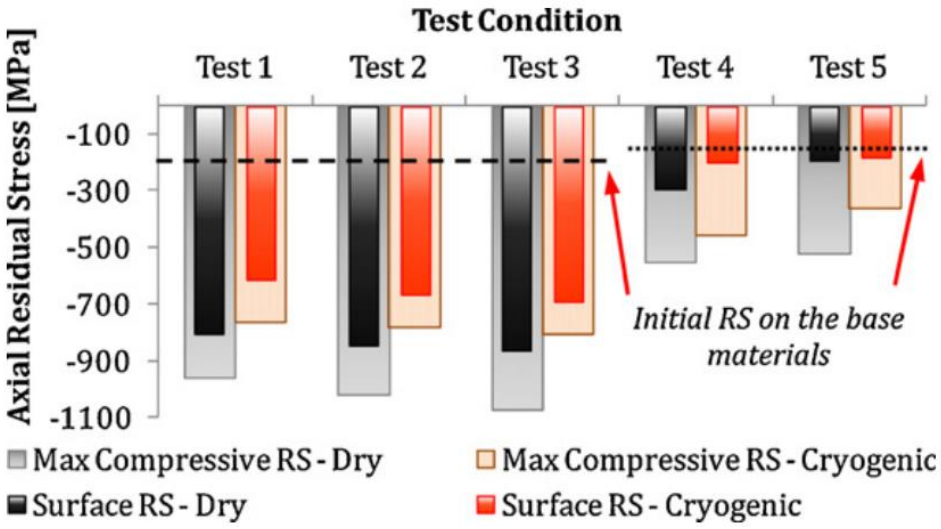

Figure 2-12. XRD Measurements of residual stress from both dry and cryogenic hard turning of AISI 52100 bearing steel, showing increased compressive residual stress for dry machining due to white layer damage (from [161] with permission from Elsevier Inc., license number 3636571309225).

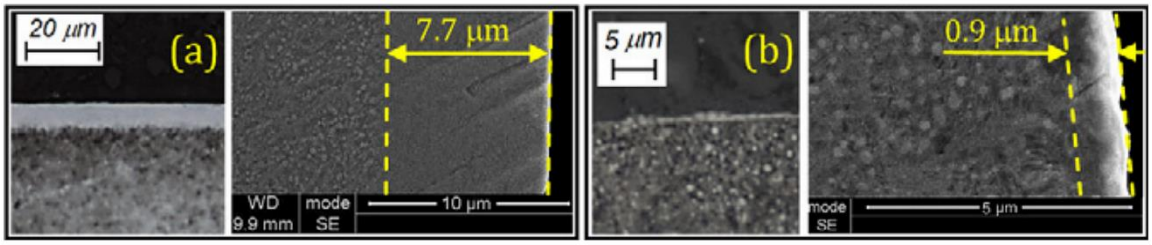

Figure 2-13. SEM micrographs of dry (a) and cryogenically (b) machined *AISI 52100* hardened bearing steel. The 'white layer' comprising the machined surface is considered detrimental to functional performance because it is comprised of untempered martensite (from [161] with permission from Elsevier Inc., license number 3636571309225).

In addition to steel, cryogenic cooling has also been applied to a number of other workpiece materials. Pu et al. [163-168] cryogenically machined and burnished *AZ31B Mg* alloy and found improved corrosion resistance as well as nanocrystalline surface layers. Since *AZ31B* is used to manufacture dissolving biomedical implants, altering the corrosion resistance of this material holds the promise of controlling the rate of *Mg* uptake into the body, i.e., the life of the implant [166, 168]. Pu et al. [164, 165] reported significantly increased compressive residual stresses in the sub-surface of cryogenically machined workpieces with an affected layer depth of more than 1 mm under certain conditions. The dominant mechanism for nanocrystalline surface layer generation in *AZ31B* was hypothesized to be dynamic re-crystallization by Pu et al. [163-165], though severe twinning was also observed, particularly for cryogenic burnishing.

Meyers et al. [169] provided a constitutive description for the phenomenon of twinning, which showed that twinning is a particularly relevant deformation mechanism at low temperatures and high strain rate. Moreover, due to a lack of thermally activated slip systems at low temperatures, twinning occurs most readily for metals with body centered cubic *(BCC)* and hexagonal close packed *(HCP)* crystal lattice structures, such as *Fe (BCC)*, *W (BCC)*, *Mg (HCP)* and *Ti (HCP)* [169, 170]. Interestingly, this same group of materials (*BCC* and *HCP*) also appears to respond most strongly to cryogenic cooling during machining [171-174]. Nevertheless, a small number of researchers have observed encouraging results for cryogenic machining of face centered cubic *(FCC)*

metals such as *Al* alloys, especially with regard to nancrystalline surface layers as reported by Rotella et al. [131, 175]. Because of the generally high machinability (chiefly low tool-wear) of *Al* alloys, only little work has been done on the impact of cryogenic machining on the group of *FCC* materials [173, 174, 176].

While surface integrity has increasingly provided the motivation for using cryogenic cooling in machining, tool-wear remains the dominant motivating factor for the majority of studies on cryogenic machining [34, 177-180]. This trend is not surprising since the development of modern engineering materials such as high strength titanium alloys, *NiT*i shape memory alloys, superalloys and a variety of other 'space-age' materials such as carbon fiber reinforced plastics (*CRFP*) has also presented the metal cutting community with a new group of 'difficult-to-machine' materials [150, 173, 181, 182]. Being designed for a specific engineering application, machinability is seldom considered when developing new materials [183-185]. As a result, certain properties of high performing materials such as Inconel and titanium alloys such as low thermal conductivity and high yield strength lead to severe abrasive and thermally activated diffusion wear [186-188]. Cryogenic cooling is an efficient means to lower both of these types of tool-wear by strengthening the cutting tool material and significantly reducing chemical activity that increases with the square of cutting temperature [148, 149, 177, 181, 189-191]. Kaynak et al. [171, 178, 181, 190] did however demonstrate that in the special case of *NiTi* shape memory alloys, cryogenic cooling increases tool-wear because of a phase transformation of the workpiece material, increasing its hardness and thus abrasive wear on the cutting tool. Hong et al. [131, 145] made similar arguments regarding the effect of cryogenic cooling on tool-wear for machining of high strength steels and titanium alloys.

Clearly, there is no "one size fits all" kind of solution in the case of cryogenic machining. Instead, as the wide range of results and proposed mechanisms motivating the use of cryogenic cooling has shown, each specialized application demands a careful attention to the combination of workpiece material characteristics, cutting tool material and coating, machine tool system as well as the manner in which the cryogenic coolant is applied. Determining these parameters for porous tungsten is the goal of this present study.

2.8 PHYSICAL PROPERTIES OF POROUS TUNGSTEN

Because porous tungsten is primarily used in refractory applications such as dispenser cathodes, heat exchangers and rocket nozzles, there is relatively little information on the mechanical properties of this material [192, 193]. Nevertheless, a limited number of data sets for flexural, compressive and tensile strength of porous tungsten close to and above room temperature is available [113, 194-199]. In order to better understand machining of porous tungsten, some high strain rate data for polycrystalline tungsten will be discussed as well.

The term 'porous tungsten' covers a wide range of possible microstructures and porosity levels. Each kind of porous tungsten is fabricated by pressing and sintering of micron-size powder [200]. The physical shape and chemical composition of this powder, i.e., sphericity, diameter, purity, etc. as well as the sintering and pressing parameters all influence the properties of porous tungsten [201-203]. For dispenser cathode applications, porosity distribution in generally considered the most crucial parameter [194, 203, 204]. Selcuk et al. [194] developed a method of using microhardness to evaluate porosity distribution and found excellent correlation between the two measures. In separate studies, Selcuk et al. [205-207] also studied the correlation between tungsten particle morphology and the effectiveness of low temperature sintering with a reactive sintering aid (Al) for increased control over as-sintered porosity. Current industry practice involves the use of very high sintering temperatures of approximately 2000 °C and a reductive hydrogen atmosphere which offer little control over the exact level of porosity [202, 206]. With the currently used process, which was also used to fabricate the material used during this present study, porosity levels ranging from 5-40 % can be achieved [113, 198]. However, determining the exact as-sintered porosity requires careful measurement of each individual workpiece with a *Hg* porosimeter.

As a result of the wide range of possible microstructures resulting from different processing parameters, the mechanical properties of porous tungsten vary as a function of porosity [113, 198, 199, 203, 208-210]. The majority of these studies were performed during the 1970s. In 1972, Francois et al. [198] published an extensive study on the influence of porosity on electrical and thermal conductivities as well as elastic properties

and flexural strength. The most relevant results from this study have been summarized in the following Figures.

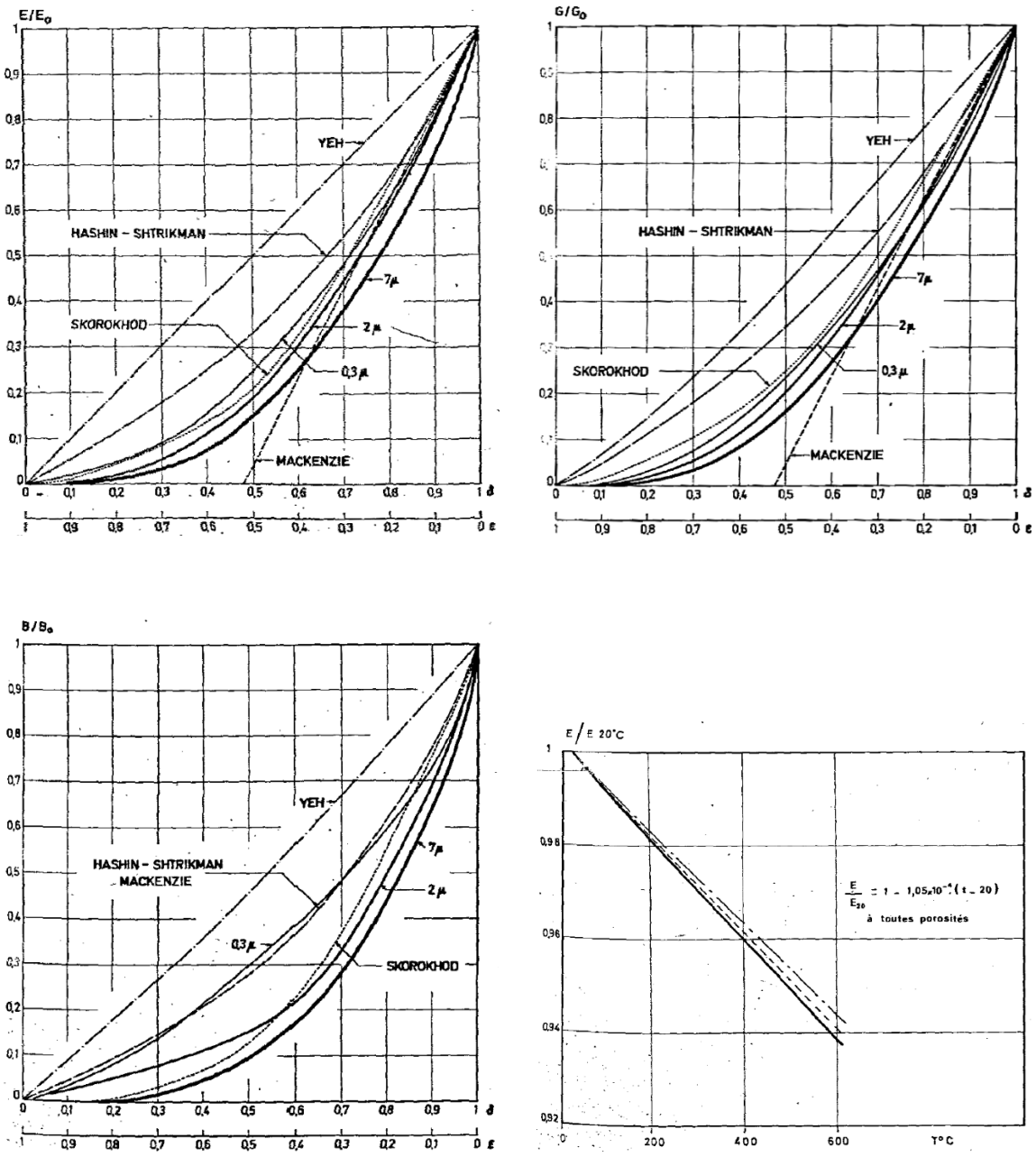

Figure 2-14. Elastic properties of porous tungsten as a function of porosity for three different grain sizes. Reduction in Young's modulus as a function of temperature is included in the bottom right hand Figure (from [198]).

The elastic property data as measured by Francois et al. [198] shown in Figure 2-14 illustrate the strong influence of porosity on the various elastic moduli of porous tungsten. All three moduli, i.e., E, G, and B are strongly affected by porosity, reaching approximately 50% of the value of dense tungsten at a density of 80% (i.e., the material used during this study). Interestingly, Young's modulus is reduced by only 6% when porous tungsten of 80% density is heated from room temperature to 600 °C (i.e., the range of temperatures relevant to machining). Based on these results, porosity would be expected to have a much more significant effect on the machinability of porous tungsten than cutting temperature. This is of course a gross oversimplification considering the significant effects of cutting speed and tool/workpiece interactions. Nevertheless, the data provided by Francois et al. should prove helpful in extrapolating the results from this present study to a wider range of density levels of porous tungsten.

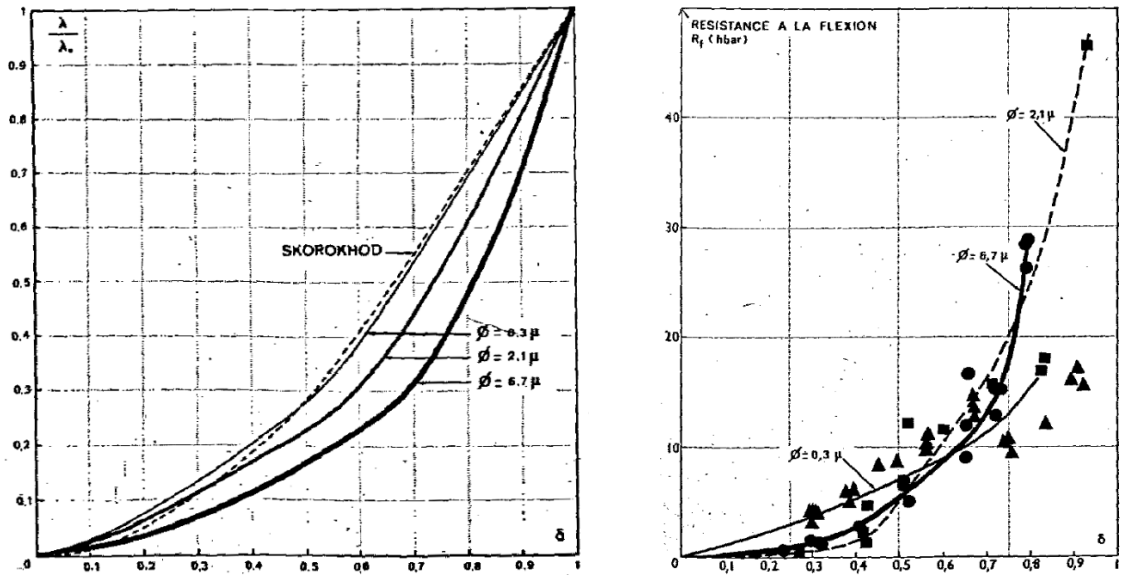

Figure 2-15. Relative coefficient of thermal conductivity $\frac{\lambda}{\lambda_0}$ of porous tungsten (left hand Figure) and flexural strength (right hand image), both as a function of relative density. Results for three grain sizes are included (adapted from [198]).

The reduction in thermal conductivity λ as a function of porosity as measured by Francois et al. shown in Figure 2-15 offers some explanations regarding the poor

machinability of porous tungsten. Namely, the fact that thermal conductivity is reduced by approximately 50% for porous tungsten of 80% density and an average grain size of 6.7 μm suggests that heat generated during the cutting process will tend to stay near the cutting edge, causing accelerated wear [87, 88, 198]. Flexural strength data also shown in Figure 2-15 will be compared with four point bend testing results obtained as part of this present study. In addition to the work of Francois et al. discussed in the above paragraphs, there is a small number of other relevant studies regarding the mechanical properties of porous tungsten.

Bell et al. [113] measured the compressive and tensile yield strength of porous tungsten over an average grain size range of 3 – 6.7 μm. Compressive yield strength varied from 930 MPa for the smallest grain size to 670 MPa for the largest grain size. Bell et al. also remarked that compressive yield strength did strength did not vary with pore morphology and suggested that deformation is primarily controlled by the matrix of ligaments. Likewise, the researchers observed little variation in tensile strength with either grain size or pore morphology and reported an average value of approximately 130 MPa. Weihong et al. [195] measured the tensile yield strength and elastic modulus of porous tungsten of 80% density between room temperature and 2500 °C. They observed nearly linear reduction in tensile strength from 150 MPa (RT) to 20 MPa at 2500 °C. Young's modulus decreased linearly between 20 °C and 1400 °C from 2.21 GPa to 1.78 GPa (19% reduction), following by a steep decrease to 970 MPa between 1400 -1800 °C.

Aside from quasistatic mechanical property data, only one study has been performed on high strain rate properties of porous tungsten. In 1977, Dandekar et al. [211] published a detailed study on the behavior of 79% density porous tungsten under shock compression at room temperature. The average grain and pore sizes of the material were 2 μm and the researcher used sound-wave speed measurements to determine Poisson's ratio to be 0.256 ± 0.014. The values bulk, shear, and Young's moduli of porous tungsten as measured by Dadekar et al. were 156.1 ±8.9, 91.0±2.4, and 228.6 ± 6.9 GPa, respectively. By shock loading thin (t = 0.5 – 2 mm) samples of porous tungsten at a strain rate of approximately 10^6 s^{-1}, Dadekar et al. identified several distinct Hugoniots. For stresses up to 1.43 GPa, a linear-elastic response occurs, yielding the principal Hugoniot. Between 1.43 and 4.5 GPa some softening occurred due to splitting of the

shock into an elastic and an unstable component. Above 6.4 GPa, the elastic precursor shock was followed by a steady shock wave, leading to a strengthened material response. The researchers remarked that while plastic deformation (pore collapse) takes place beyond the elastic limit of 1.43 GPa, complete collapse of all pores, i.e., full compaction, occurs at a stress of 4.9 GPa [211]. This behavior should be particularly relevant in understanding the deformation behavior of porous tungsten during machining, as compaction effects are clearly to be expected according to the deformation cutting theory [46, 50]. The data obtained by Dadekar et al. are included in the form of one of the Figures from their 1977 publication as shown below.

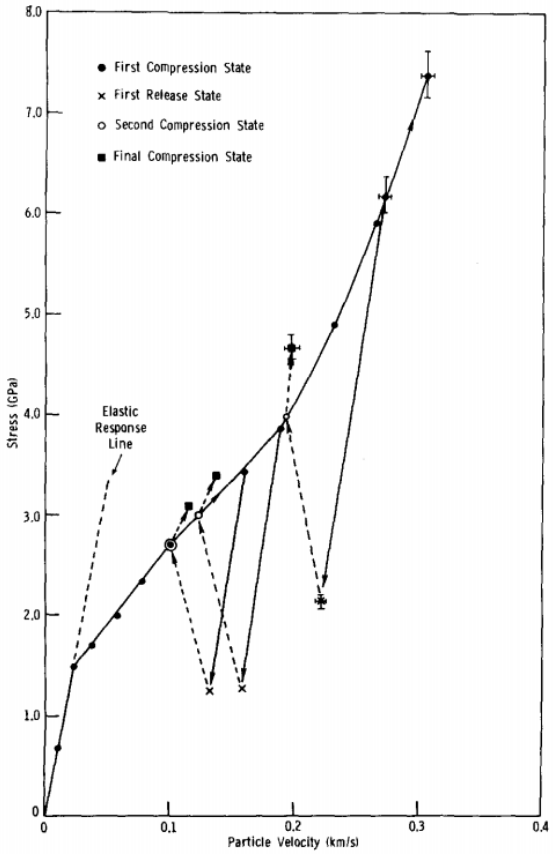

Figure 2-16. Shock compression behavior of 79% density porous tungsten. Pores begin to be irreversible collapsed when shock stress exceeds 1.43 GPa (i.e., the elastic limit). Beyond 4.9 GPa the material becomes completely compacted (from [211] with permission of AIP Publishing LLC, license number 3637210475585).

CHAPTER 3.

MATERIALS AND EXPERIMENTAL METHODS

3.1 CRYOGENIC MACHINING

Cryogenic cooling was used as a means to reduce cutting temperature during machining of porous tungsten. The cryogenic coolant employed for this purpose was liquid nitrogen, which had an approximate temperature of -180 °C. In addition to cooling the workpiece and cutting tool, applying pressurized liquid nitrogen also aids in clearing chips from the cutting area. The flow rate of liquid nitrogen was kept constant at 0.5 kg/min which was driven by a pressurized tank of liquid nitrogen at a pressure of 150 MPa. A simple system of cryogenic hoses and valves was used to avoid any expansion chambers within the delivery system between the liquid nitrogen tank and the nozzle near the cutting region. The majority of cryogenic machining was performed as part of a face turning operation. By taking advantage of the limited range of motion of a fixed tool post cryogenic delivery was simplified significantly compared to through-spindle delivery that has been implement by some as part of cryogenic milling. A limited number of cryogenic side milling experiments were performed as well, however delivery of liquid nitrogen was performed externally, i.e., not through the spindle or the cutting tool. While this approach does not provide the same kind of flow penetration and cooling ability as internal cryogenic delivery would, it is significantly easier to implement and avoids the need for expensive thermal insulation inside of the spindle.

In general, cryogenic machining is most readily implemented on fixed tool post and gang-tooling type lathes, particularly vertical lathes. Whenever it is possible to deliver liquid nitrogen through a closed system of hoses and valves and when bending and pulling forces on this delivery system can be kept small, cryogenic machining may be implemented on a given machine tool or for a specialized process. The dispenser cathode machining process of porous tungsten, which consists most importantly of a concave face machining operation, lends itself well to the implementation of cryogenic cooling. An example of liquid nitrogen being applied on a simple horizontal lathe with a single tool post (HAAS TL-2) as part of a face turning operation can be seen in the following Figure.

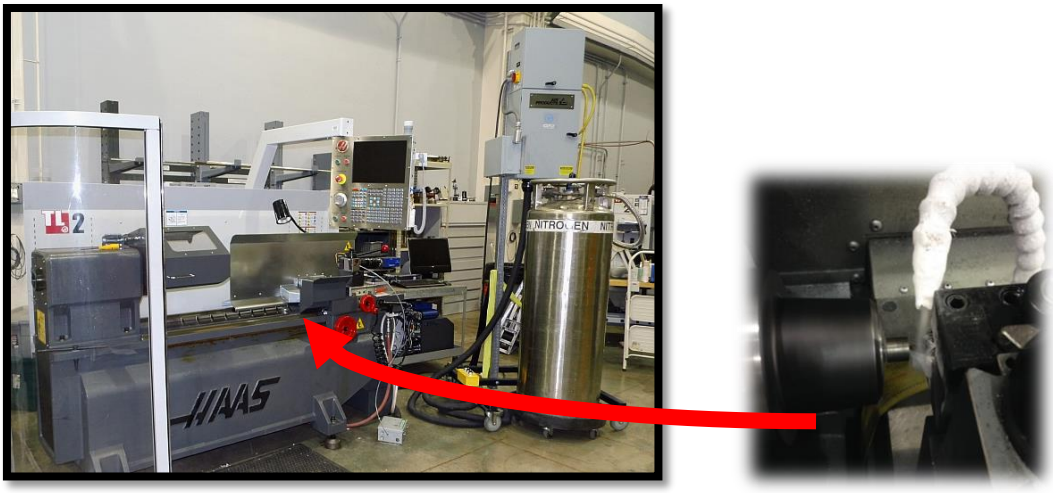

Figure 3-1. Experimental setup for cryogenic machining on HAAS TL-2 CNC lathe. Right hand side detail of cryogenic cooling during a facing cut shows how liquid nitrogen is applied onto the rake face of the cutting tool through a 3mm diameter nozzle. The process displayed is face turning, during which the cutting tool traverses radially inward.

3.1.1 Cryogenic Pre-Cooling

A variety a cryogenic pre-cooling conditions were tested for their influence on surface quality in porous tungsten. The most straightforward manner of achieving different pre-cooling conditions is altering the time of pre-cooling while keeping other variables such as flow rate and pressure constant. Because the actual workpiece and cutting temperatures depend on a variety of other factors such as thermal conduction and convection on the workpiece and cutting tool a separate approach to determining pre-cooling temperature was pursued.

By first drilling a variety of small holes (d = 1 mm) into a porous tungsten workpiece at 50% of the workpiece radius and 0.75 and 1.5 mm axial distance from the machined face, a simple set of calibration experiments was carried out. The probe tip ($d \approx 0.9$ mm) of an E-type thermocouple, attached to an OMEGA© MWTC wireless transmitter fixed to the lathe's chuck, was inserted into each hole along with a small amount of thermal paste. The workpiece temperature was recorded as a function of time and the influence of rotating

speed, nozzle size and flow rate were empirically correlated with steady-state bulk workpiece temperature. An additional thermocouple was place in a 0.5 mm deep notch on the flank face of the cutting tool, 0.5 mm below the primary cutting edge. LN_2 flow rates were correlated to as-pre-cooled workpiece and cutting tool temperatures of -90 °C and -180 °C, respectively. It is worth noting that steady-state bulk workpiece pre-cooling temperature is by no means the same as cutting temperature. The heat generated even during cryogenically cooled machining operations may easily exceed several hundred degrees Celsius. A schematic of the experimental setup can be seen in the Figure below.

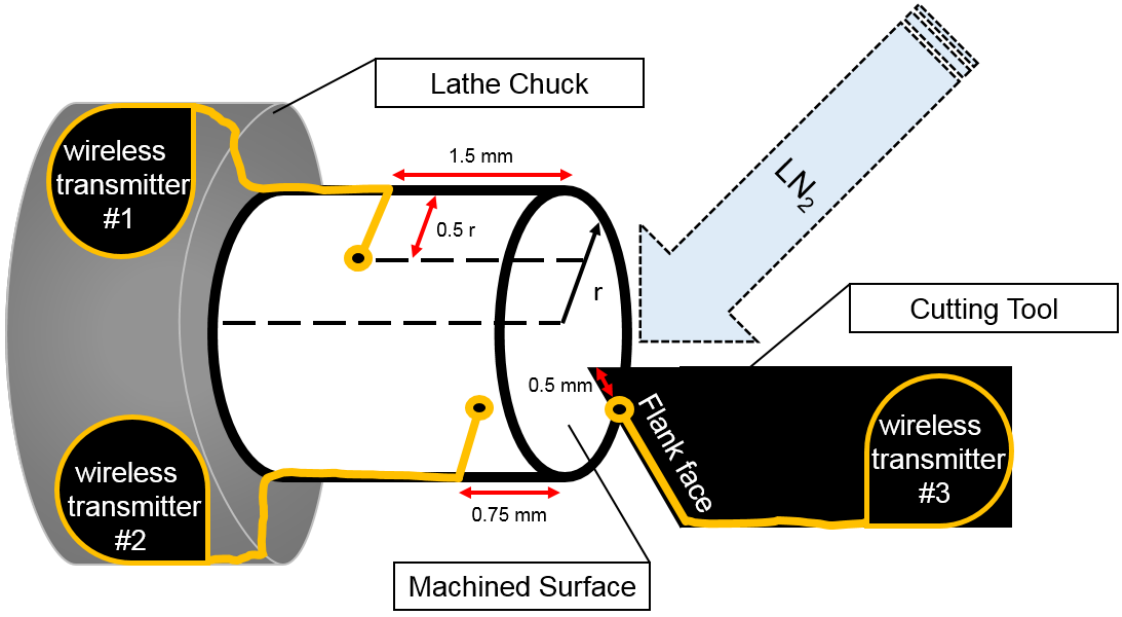

Figure 3-2. Schematic of experimental setup for temperature measurement of cryogenic pre-cooling temperatures of both workpiece and cutting tool by means of wireless thermocouple transmitters. The process illustrated here is face turning, during which liquid nitrogen is applied onto both the rake face of the tool and the workpiece front surface simultaneously with a single nozzle. By altering flow rate of liquid nitrogen pre-cooling temperature may be controlled (Figure not to scale).

3.1.2 Cryogenic Side Milling

In addition to face turning, which was used as a model for the dispenser cathode manufacturing process, side milling experiments were performed as well. Because in side

milling the cutting tool both rotates around its own axis and traverses in either the x or y direction of the milling machine Table, cryogenic delivery is more difficult to implement than in face turning. To achieve both chip clearance and workpiece/tool cooling, the cryogenic delivery nozzle was affixed to the milling machine's head. Because side milling cuts were performed using 'conventional' up-cut milling, liquid nitrogen was applied from the rake face in order to clear chips. An illustration of the experimental setup for cryogenic side milling experiments is provided in Figure 3-3 below.

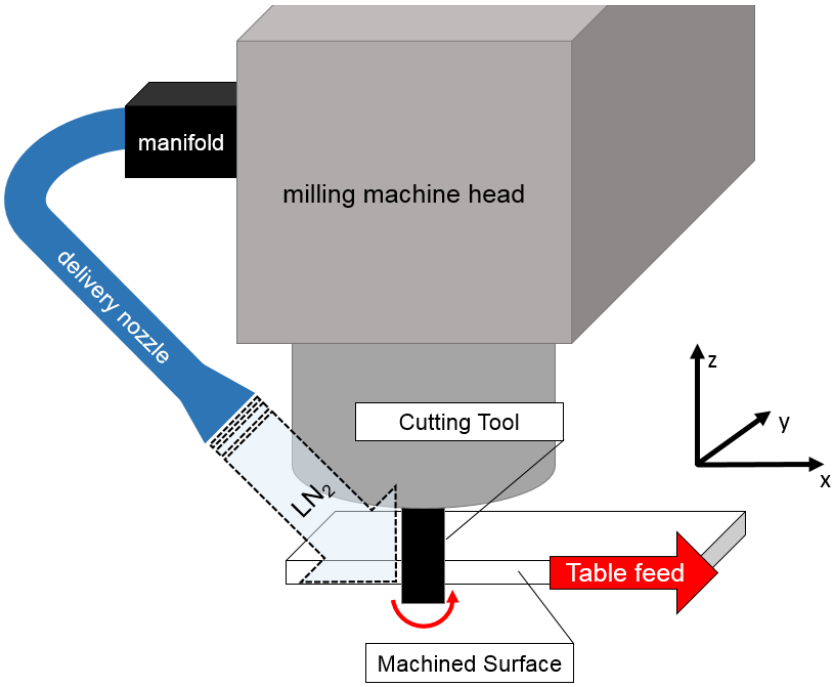

Figure 3-3. Schematic of cryogenic delivery method for side milling experiments. Liquid nitrogen is applied at an angle from the rake side of a milling cutter performing a conventional up-cut. In this manner, the tool and workpiece are kept cool while chips are effectively cleared away from the cut (Figure not to scale).

3.2 Infrared Temperature Measurements

In order to estimate cutting temperatures during cryogenic machining, a FLIR SC7000 infrared thermal camera was used. Because applying liquid nitrogen as a coolant resulted in a cloud of frozen water vapor surrounding both the cutting tool and

workpiece, no accurate temperature measurements were possible using infrared technology for cryogenic experiments. For this reason, infrared temperature measurements were only performed for dry machining of porous tungsten using the same machining parameters as analogous cryogenic machining experiments. In this manner, temperature data was collected to validate a material model that will be presented in the ensuing discussion. Thermal images were acquired at a rate of 100 Hz with a resolution of 640 x 512 pixels. Three wavelength range channels were used simultaneously in order to cover a broad range of temperatures. Each experimental condition was repeated 5 times to provide a meaningful average of the maximum cutting temperature.

To convert infrared measurements into meaningful temperature data, it is necessary to specific the emissivity of the material being observed. Different materials may have a wide range of emmisivities, ranging anywhere from 1.0 to almost zero. The total hemispherical emissivity ε of tungsten in the infrared spectrum may range from 0.03 up to 0.4 depending on the surface roughness, temperature, and oxidation state of the sample surface [212-215]. Machined porous tungsten samples were calibrated by controlled heating monitored with a calibrated E-type thermocouple thermally connected to the sample. By varying emissivity to match thermocouple data with infrared temperature output, an empirical emissivity constant of $\varepsilon = 0.12$ was determined and used for subsequent infrared thermal measurements. Because there remains some uncertainty in this empirical emissivity value for porous tungsten, infrared temperature measurements were assigned an additional uncertainty of ± 4% over the experimental scatter, which was less than ± 1% between subsequent experiments of the same machining condition. Cutting temperature was measured by recording the maximum temperature occurring in the primary deformation zone at the cutting edge. For each temperature measurement, the experimental condition was repeated five times to ensure that the maximum temperature value recorded was repeatable. By properly timing the beginning of the machining process and the infrared temperature acquisition, the measured value of maximum cutting temperature varied very little (±1%). An overview of the experimental setup for the FLIR SC7000 thermal camera is shown in Figure 3-4 on the following page.

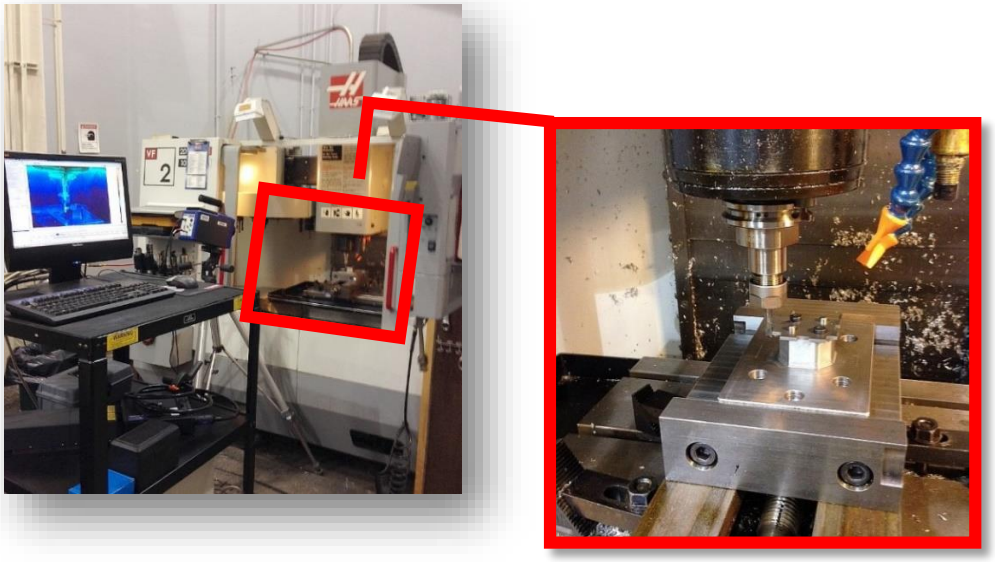

Figure 3-4. Overview of experimental setup of infrared cutting temperature measurements for side milling experiments in porous tungsten using a FLIR SC7000 thermal camera. An inlet of the fixture used to hold samples during side milling cuts is outlined in red. The infrared camera and corresponding software can be seen on the left hand side in the main image.

3.3 CUTTING FORCE DATA ACQUISITION

Cutting forces were recorded with a KISTLER type 9257B three-channel dynamometer. Because uncut chip thickness varies along the cutting edge during turning, side milling was selected for force acquisition experiments. In up-cut side milling the uncut chip thickness changes from zero to a maximum value, as does the cutting force. Therefore, it is possible to calculate the specific cutting force k_c at a given maximum chip thickness by measuring the maximum cutting force during a chip formation cycle. For each force measurement, 10 values were recorded and averaged to obtain a meaningful number. Reported scatter is comprised of the spread between the maximum and minimum of the 10 force values as well as an uncertainty of ±5% representing the inherent inaccuracy of the dynamometer itself. To determine the specific cutting force from side milling force data, it is first necessary to determine the cutting force F_c from

the two relevant force channels. For a side milling cut along either the x or y direction of the dynamometer coordinate system, the magnitude of the cutting force at the maximum chip thickness may be calculated using Eq. (3-1):

$$|F_c(h_{max})| = \sqrt{F^2_{x(h_{max})} + F^2_{y(h_{max})}} \tag{3-1}$$

To facilitate repeatable sample preparation for subsequent processes such as EDM cutting of micro bend-testing or SEM samples, a fixture with two dowel pins and two low profile socket cap screws was developed. Each 2.75 mm thick porous tungsten plate featured 8 protrusions, each of which was machined with a different set of machining parameters. In this way 8 samples were machined quickly in one setup, allowing for a large number of experimental conditions to be tested. Repeatability of each porous tungsten plate on the fixture was ± 10 μm. To ensure accuracy of the depth of cut beyond this value (± 5 μm), each sample plate was pre-machined on the fixture prior to performing force acquisition experiments. Both the dynamometer and the fixture with a porous tungsten workpiece mounted are shown in the following Figure.

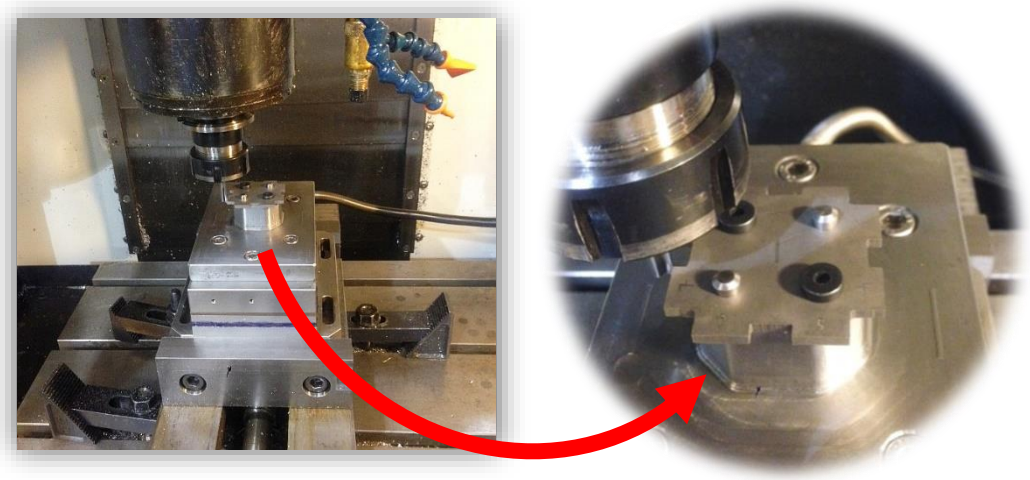

Figure 3-5. Experimental setup for force acquisition during side milling of porous tungsten. A specialized fixture, shown in the right hand image, was developed to hold a plate of porous tungsten containing 8 samples.

3.4 CUTTING EDGE RADIUS MODIFICATION

Because cutting edge radius has a significant effect on both tool-life and attainable surface finish, a number of cutting tools were modified (honed) to alter the cutting edge radius to a specific value. Denkena et al. [81] have proposed a comprehensive terminology for the various possible kinds of cutting edge geometries. Since the commonly used measure r_β is inadequate to describe the majority of cutting edge geometries due to non-symmetry of the cutting with respect to the rake and flank faces, the following parameters were introduced:

Table 3-1. Summary of parameters of form-factor method for cutting edge characterization.

S_α	Cutting edge segment on flank face
S_γ	Cutting edge segment on rake face
$\bar{S} = \frac{S_\alpha + S_\gamma}{2}$	Average Cutting edge rounding
$K = \frac{S_\gamma}{S_\alpha}$	Form factor
Δr	Profile flattening
φ	Apex angle

While it should certainly be advocated that the form-factor method Denkena et al. be used to properly characterize cutting edge geometries, care was taken to prepare cutting edges with a form factor of $K = 1$, i.e., a perfectly symmetrical radius. Therefore, the use of a single parameter r_β remains appropriate for the cutting edge geometries discussed in the context of this present work. To better illustrate both the appropriateness of the form-factor method and the more simplistic r_β description for different cutting edges the following Figure was prepared.

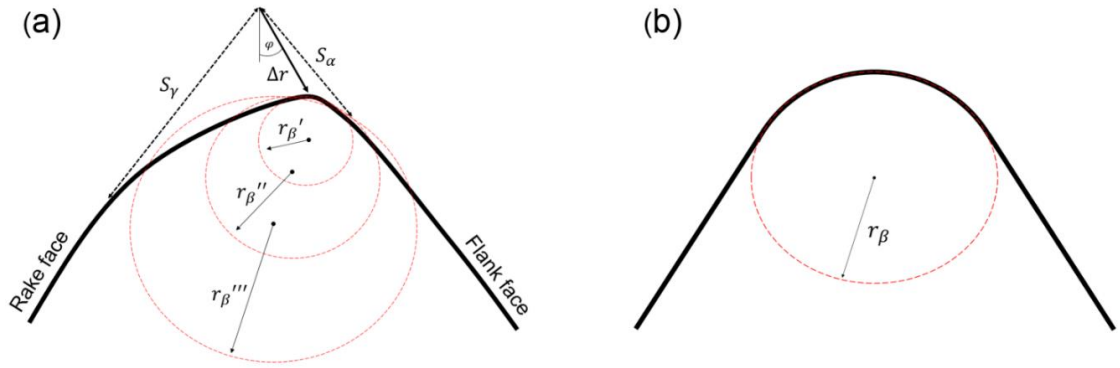

Figure 3-6. Comparison between a non-symmetrical cutting without a single unambiguous cutting edge radius (a) and a symmetrically rounded cutting edge with radius r_β. Because (b) is a special case of (a) for $S_\alpha = S_\gamma$, i.e., $K = 1$, it cannot be normative yet remains appropriate for special cases. Both the figure and terminology for the form-factor method shown in (a) are adapted from Denkena et al. [81].

In addition to cross-sectional cutting edge geometry, there are also surface properties of cutting edges. Of particular importance in finish machining is cutting edge notchedness, which is generally described by the surface roughness R_z. Grinding and lapping of the cutting edge may lead to chipping which increases notchedness. As a result, the chipped cutting edge will generally not be able to produce surface roughness better than its own inherent notchedness. Chips on the cutting edge also lead to exposed peaks which may break off as well. Therefore, tool-life will be reduced if notchedness becomes too large. In the particularly case of polycrystalline diamond (PCD) tools, notchedness is hypothesized to have a significant impact on both tool-life and attainable surface finish due to the composite nature of the diamond/binder matrix of this tool material. Therefore, reducing notchedness was considered as well as cutting edge radius.

While there is a variety of technologies available to alter cutting edge geometries, drag (stream) finishing was chosen for its ability to produce uniformly rounded cutting edges. Other methods such as abrasive brushing, abrasive blasting, grinding and magneto abrasive machining are all biased towards producing a (slightly) non-symmetrical cutting edge geometry because material is only removed from one direction at a time. The

OTEC SF2 steam-finishing machine used to increase cutting edge radii of PCD tools with an as-supplied cutting edge radius of $r_\beta \approx 6$ µm to 10 and 14 µm, respectively. This was achieved by rotating each cutting tool at a speed of 10 rpm with an inclination angle of 30º relative to the surface of the abrasive media consisting of silicon carbide and crushed walnut shells. The rotating speed of the drum containing the abrasive media was kept constant at 60 rpm. The average time to achieve a radius of 10 µm was 40 minutes while the processing time to obtain a cutting edge radius of 14 µm was 630 minutes. Therefore, a cutting edge radius of 10 µm was selected for more detailed investigation. An overview of the processing setup for stream finishing of PCD cutting tools is shown in the following Figure.

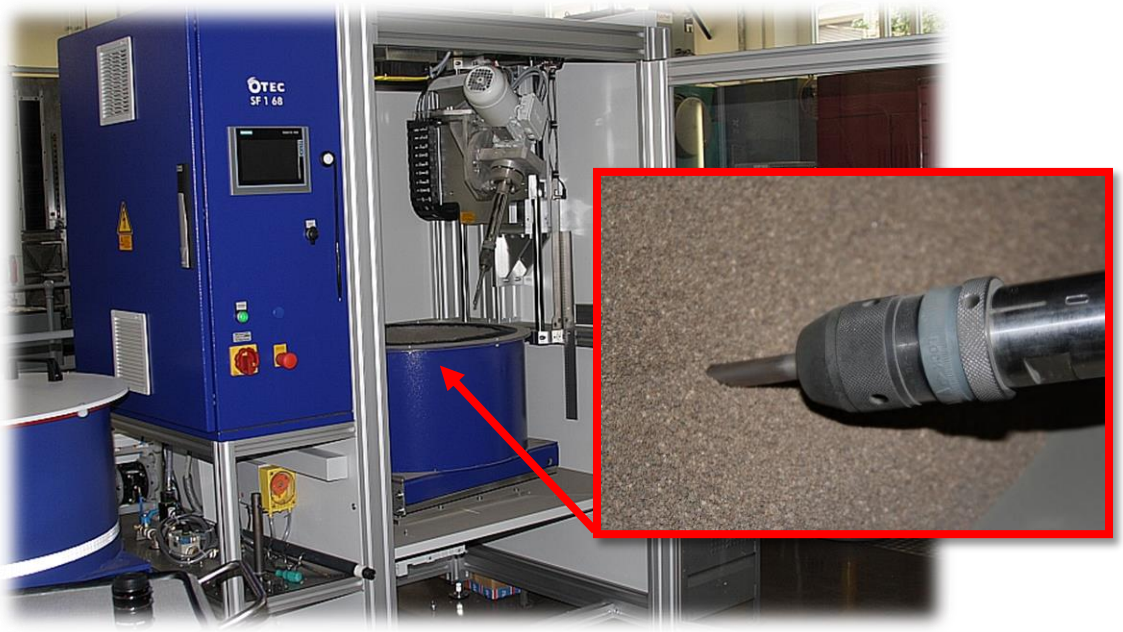

Figure 3-7. Processing setup for abrasive stream finishing of PCD cutting tools for cutting edge modification. The cutting tool is mounted in a custom made tool holder which is held in a keyless chuck, highlighted in the right hand side inlet. By rotating both the tool holder and the drum containing the abrasive media of *SiC* and crushed walnut shells a highly uniform cutting edge radius with low cutting edge notchedness may be achieved.

3.5 CHARACTERIZATION

Because of this study's focus on improving surface characteristics of porous tungsten by means of cryogenic machining, quantifying the 'quality' of a given surface was very important. Current industry practice for the manufacture of dispenser cathodes relies on little data and surface quality is graded on a subjective scale from 'acceptable,' 'marginal,' to 'unacceptable.' Determining which category a given surface falls into is the responsibility of experienced operators and technicians. In order to study the effects of various machining parameters such as cutting speed, feed, depth of cut, etc. and the influence of cooling conditions a range of advanced characterization techniques were employed during this study. While the majority of these techniques were focused on analyzing surface properties, some characterization of mechanical properties of these surfaces was performed as well by means of 4 point micro-specimen bending, which will also be discussed in this section.

3.5.1 Electron Microscopy

Scanning electron microscopy of machined porous tungsten surfaces was carried out on a Hitachi S-4300 microscope. The electron source of this microscope was a field emission gun. In addition to porous tungsten surfaces, a number of cutting edges were also analyzed using SEM to study both tool-wear and cutting edge geometries. The majority of SEM work was however focused on characterizing surface morphology and surface porosity of machined porous tungsten. To improve image quality by reducing charge buildup in the sample a custom holder was fabricated from copper. Three setscrews hold the sample in place while the entire backside of the parted-off sample disc is electrically connected to the sample holder. Both the electron microscope and the holder are shown in Figure 3-8 on the following page.

Figure 3-8. Hitachi S4300 scanning electron microscope and custom copper sample holder for machined porous tungsten samples. The holder substantially improved image quality by draining electrical charge efficiently.

3.5.2 Surface Porosity Evaluation

The current dispenser cathode industry acceptability standard states that:

"There shall be a minimum of 30 open pores uniformly distributed and visible in a 0.075 mm 0.125 mm area photographed (or equivalent digital image) at 1000x magnification. When required, representative photographs shall be taken from two locations on the cathode at approximately 10% and 90% of the radius. The typical pore size range shall be between approximately 3–7 µm [216]".

Therefore, SEM micrographs where taken at a magnification of 1000x over an area of 10,000 μm^2 for each machined porous tungsten surface. To better characterize the uniformity of a given surface, three micrographs were taken at 10%, 50%, and 90% of the radius of each sample for a total of 9 micrographs per machined surface. Each micrograph was analyzed using ImagePro software. By increasing the contrast of a high quality SEM micrograph by approximately 50%, the software defines a pore as a 'dark' area. To define the range of pore diameters to be considered, ten micrographs of 80% density porous tungsten that had been fractured after being submerged in liquid nitrogen

were analyzed. The resulting inherent pore size distribution for 80% density porous tungsten can be seen in Figure 3-9.

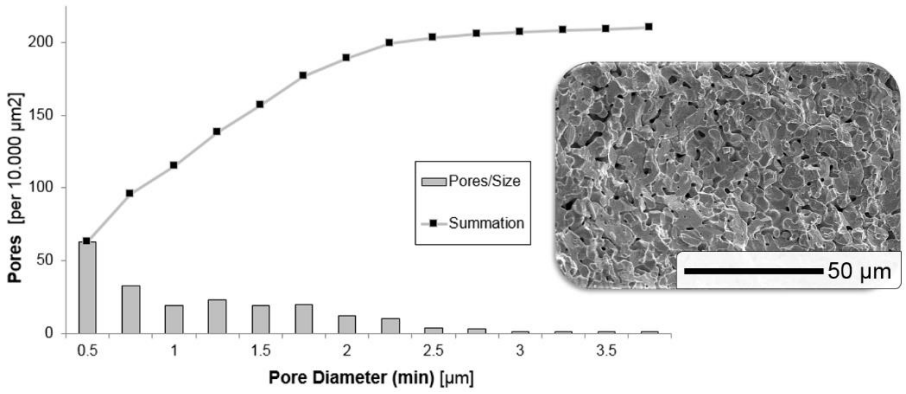

Figure 3-9. Pore size distribution of 80% density porous tungsten as determined by ImagePro software.

As evident in Figure 3-9, the inherent pore diameter distribution of 80% density porous tungsten does not allow for the industry standard of 30 pores in the 3-7 µm diameter range to be met; there are less than 10 such pores per 10,000 μm^2 in any given sample's microstructure. Therefore, the fact that such large pores are routinely found on machined surfaces of porous tungsten implies that not all 'pores' present on machined surfaces are the result of the underlying microstructure. To include all true pores in the analysis of as-machined surface porosity, the diameter range from 0.5 – 7 µm was used. Because there are approximately 200 such pores in a 10,000 μm^2 area, 200 pores is considered the maximum possible number of pores. Therefore, the range of acceptable porous surfaces shall be defined as "30-200 visible surface pores with a diameter of 0.5 – 7 µm" in the context of this study. A typical SEM micrograph with the corresponding analysis is shown in the Figure 3-10.

It should be noted that while digital means of accessing surface porosity, such as ImagePro software used during the present study, are certainly an accurate technique, there are several limitations to this approach. First, image quality is very important when using software to analyze images. Both the quality of the SEM micrograph and the post-

processing steps performed to improve contrast may alter the final pore count. In order to reduce the effect of image quality as much as possible, a consistent procedure was used to acquire SEM micrographs (constant working distance, acceleration voltage, etc.). Moreover, post-processing to enhance contrast was only performed within ImagePro.

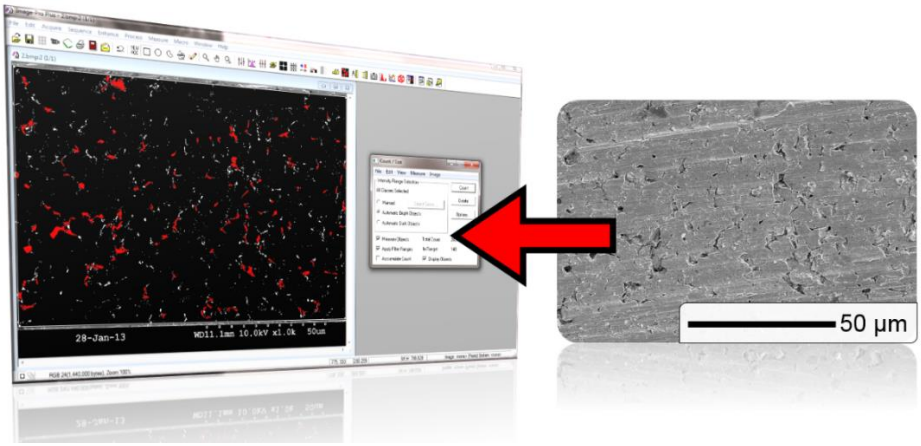

Figure 3-10. Example of surface porosity evaluation with ImagePro software. Inside the software, the SEM micrograph shown on the right hand side was slightly altered by increasing contrast so pores were recognized as 'dark areas'. The diameter range considered for analysis was 0.5–7 µm.

3.5.3 Optical microscopy

While surface porosity micrographs were recorded using SEM, optical microscopy was also used to analyze the microstructure of porous tungsten. A Leica DFC425 digital camera was used in conjunction with a Nikon EPIPHOT 300 optical microscope equipped with 2.5x, 5x, 10x, 20x, and 50x objectives. Because the depth of field with a 50x light objective is significantly worse than that of an electron microscope at similar magnification, optical microscopy was mainly used at smaller magnification to detect features in the range of 0.05 – 1.0 mm. For cross-sectional microscopy of porous tungsten, samples were embedded in a high strength epoxy to prevent edge rounding and final polishing was carried out using 1 micron diamond slurry. Tool-wear (flank and nose wear) was mainly measured optically, using an appropriate fixture.

3.5.4 Scanning White Light Interferometry

In addition to surface porosity, surface roughness is another key parameter describing the quality of a machined surface of porous tungsten. Current industry standard requires an average surface roughness value of 32 μin, which is equivalent to R_a = 0.8 μm. There are several ways to measure surface roughness, the most commonly used ones being optical comparison using a set of standardized samples and Profilometry. The latter technique uses a stylus with a small radius tip to probe the machined sample's surface. Because no feature smaller than the diameter of the stylus tip radius can be detected and considering the wear an initially 'sharp' stylus will experience, Profilometry does not yield very reliable surface roughness data for finely finished surfaces (R_a < 1 μm). Therefore, a non-contact technique was used to measure R_a of machined porous tungsten samples. A Zygo NewView 7300 scanning white light interferometer (SWLI) equipped with 20x and 50x objectives was used for this purpose. By scanning the sample vertically and recording interference fringes to assembly a point cloud of data, SWLI allows nanometrically accurate (±5 nm) 3D surfaces to be digitized.

Similar to surface porosity measurements, measurements of surface roughness of machined porous tungsten were taken at 10%, 50%, and 90% of each sample's radius. From each of the three measured areas, ten equally spaced measurement lines were taken to obtain a statistically significant average value for R_a and the scatter across a given surface. Due to the porosity of the workpiece material, surface roughness cannot be directly correlated with a similar dense material. Nevertheless, qualitative comparison between samples machined with different parameters can be made. Because of the large number of measurements taken from each sample (30 measurements) the repeatability of the average roughness measured for a given sample was better than ± 0.05 μm. Cutting edge radii measurements were measured in a similar manner as surface roughness. Three areas along the primary cutting edge were recorded at a magnification of 50x. From each 3D profile of the cutting edge ten radius measurements were conducted using MetroPro edge radius analysis software. A Figure summarizing the most common uses of SWLI during the course of this study is shown on the following page.

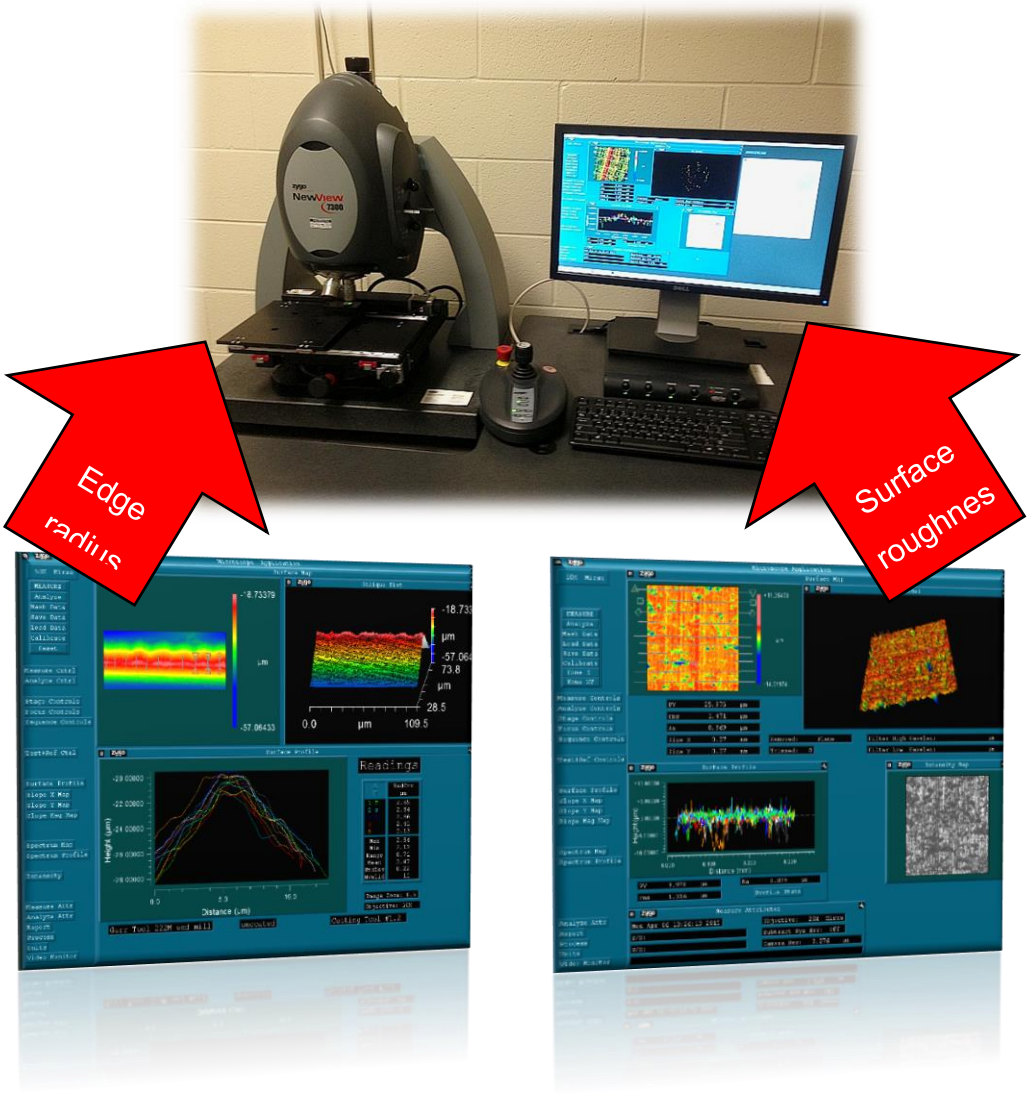

Figure 3-11. Overview of most commonly used applications of Zygo NewView 7300 3D profiler. Top image shows the instrument, which uses a laser to create nanometrically accurate point clouds of interference fringe data. Edge radius and surface roughness measurements were performed on the same instrument yet analyzed with specialized applications, shown in the bottom two images.

3.5.5 Residual Stress Measurement

A small number of residual stress measurements were taken on the surface of cryogenically and dry machined samples of both porous and dense polycrystalline

tungsten. The measurements were performed during the course of a visiting research stay at the Karlsruhe Institute for Technology (KIT) in Karlsruhe, Germany. The institute for applied materials (iam) carried out the measurements on an X-ray diffractometer using the $\sin^2\psi$ –method. For this analysis method plane stress is assumed, i.e., the stress component normal to the surface is defined to be zero [65]. Plane stress does however not mean that strain is zero in the vertical direction, because there will be some Poisson's ratio contraction due to the principal stresses σ_1 and σ_2 in the surface plane. This strain can be measured by characterizing the contraction of the lattice spacing. While the unstressed lattice constant d_0 is often unknown, it may be approximated by $d_{\phi 0}$ (Eq. (3-2)) to an accuracy of ± 1% because $E \gg (\sigma_1 + \sigma_2)$. Practically, $d_{\phi 0}$ is the value of $d_{\phi\psi}(hkl)$ at $\sin^2\psi = 0$.

$$d_{\phi 0} = d_0 \left\{1 - \left(\frac{\nu}{E}\right)_{hkl} (\sigma_1 + \sigma_2)\right\} \approx d_0 \tag{3-2}$$

By measuring the lattice spacing $d_{\phi\psi}$ across a range of angles relative to the sample surface, the surface residual stress σ_ϕ can be calculated from the slop of a linear fit of $d_{\phi\psi}$ against $\sin^2\psi$ by Eq. (3-3):

$$\sigma_\phi = \left(\frac{E}{1+\nu}\right)_{hkl} \frac{1}{d_{\phi 0}} \left(\frac{\partial d_{\phi\psi}}{\partial \sin^2\psi}\right) \tag{3-3}$$

Residual stress measurement with XRD is a surface-sensitive characterization technique with an approximate depth of penetration of less than 25 μm in most metals. To compile a depth profile of residual stress, electro polishing is often used to remove a small amount of material without introducing additional stress [57]. While it was initially planned to create such a depth profile for both dense and porous tungsten samples, the very low intensity of the signal during analysis of porous tungsten did not allow for a large number of total measurements to be taken. Therefore, only a single data point was taken on the surface of each sample. To better illustrate the manner in which residual stress is determine with the $\sin^2\psi$ method, the Figure 3-12 was prepared.

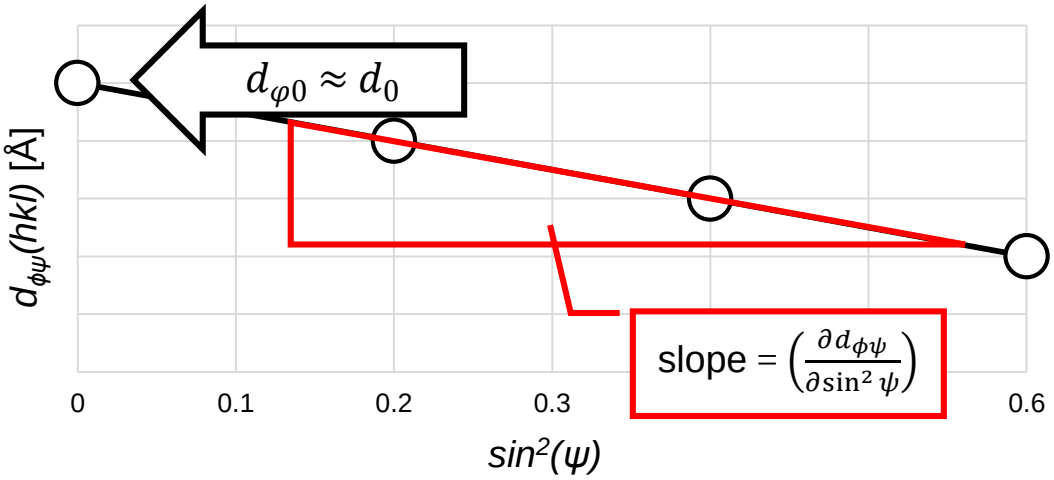

Figure 3-12. Example of typical chart used to determine residual surface stress with the $sin^2\,\psi$ method. Extrapolating to $sin^2\,0$ allows for the unstressed lattice spacing d_0 to be approximated to within ± 1%. By further calculating the slope of the best fit line from a chart such as this one it is possible to determine residual stress.

3.5.6 Micro-Specimen Four Point Bend Testing

In order to assess the influence of cryogenic and dry machining with different machining parameters on the mechanical properties of porous tungsten of 80% density, micro-specimen (millimeter size) bend testing experiments were conducted for a small number of samples. Rather than three point bending, four point loading results in a constant stress state (constant bending moment) between the central (moving) supports. In this way, effects of localized flaws, such as pores, are reduced and a representative average flexural strength value may be obtained from the machined surface.

Each sample was machined either dry or cryogenically by side milling as described in section 3.1.2. The geometric shape of the workpiece used for the side milling process, namely a 2.5 mm thick sheet rough cut by wire EDM from a round bar of porous tungsten and finished on a cast iron lapping plate using 3 micron diamond abrasive to remove the heat affected layer from the EDM process, allowed for bend testing samples to be easily cut following the machining experiment. Each flat sheet of porous tungsten featured two 10 mm long tabs, the sides of which were machined. Therefore, each sheet held a total of

8 experimental conditions/samples. The repeatability of the four precision bored holes in the flat sheet of porous tungsten on a custom made fixture to cut off 0.4 mm thick samples for bend testing was better than ± 0.01 mm. An example of a machined sample being cut off using wire EDM can be seen in the Figure below.

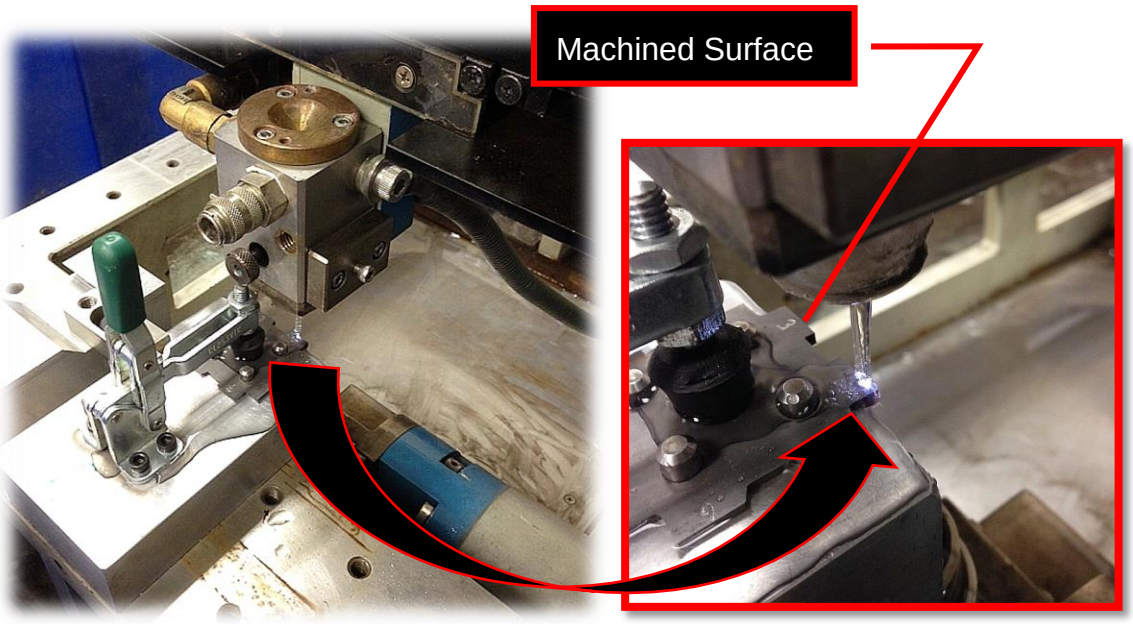

Figure 3-13. Millimeter size bend testing sample preparation using wire EDM and a custom fixture with four precisely located dowel pins. The sides of the flat sheet of porous tungsten was dry or cryogenically machined with different machining parameters on each tab prior to cutting off a 0.4 mm thin sample for bend testing.

Following wire EDM cutoff, each 10 x 2.5 x 0.4 mm sample was carefully lapped on the EDM cut side (i.e., opposing the machined surface) to remove any potential thermally damaged layer and to achieve a flatness and parallelism tolerance better than ± 5 μm across each sample. Great care was taken to process all samples equally in order to minimize sample preparation induced variations in flexural strength. The final dimensions of samples for four point bend testing were a length of 8 mm, width of 2.5 mm and thickness of 0.35 mm. The basic geometry of the four point bending setup used during this present study is shown in the following Figure.

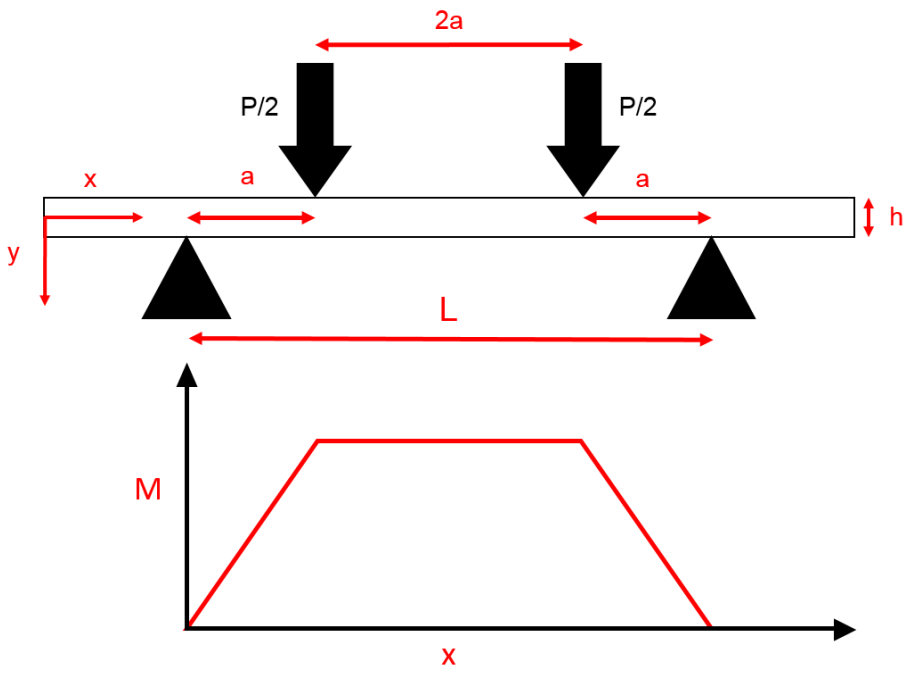

Figure 3-14. Schematic of four point bend testing of machined porous tungsten samples. The dimensions use for millimeter size specimen testing were L = 6 mm, a =1.5 mm (a = $L/4$), h = 0.35 mm, b = 2.5 mm. Both the fixed supports and the load points were comprised of polished tungsten carbide pins with a diameter of 1.5875 mm.

A quarter-point load distribution scheme was chosen in order to maximize to area of constant bending moment to avoid local stress concentration effects that may introduce large scatter. From classical beam theory, it is possible to calculate the relationship between deflection and bending moment and/or stress for this configuration. Assuming plane strain, differential equation governing the elastic deflection of a simple beam is given by Eq. (3-4):

$$\frac{\partial^2 y}{\partial x^2} = \frac{M}{EI} = \frac{1}{\rho} \tag{3-4}$$

where M is the bending moment, E is Young's modulus, $1/\rho$ is the curvature, and I is the moment of inertia, which is $I = \frac{bh^3}{12}$ for a rectangular beam, where b the width and h is the thickness of the beam. Between the two central loads, the bending moment is

constant and given by $M = \frac{PL}{8}$. By integrating Eq. (3-4) and applying the appropriate boundary conditions, the normal axial strain ε_x as a function of deflection y in the central load span of a rectangular beam under four point bending as shown in Figure 3-14 becomes:

$$\varepsilon_x = \frac{M}{EI}\Delta y = \frac{3PL}{2Ebh^3}\Delta y \tag{3-5}$$

where Δy is the deviation from the neutral axis of the beam, i.e., $-h/2 < \Delta y < h/2$. The deflection at the loading points (i.e., the displacement of the moving grip) can be calculated by Eq. (3-6):

$$y_a = \frac{Pa^2}{6EI}(3L - 4a) = \frac{PL^3}{4Ebh^3} \tag{3-6}$$

The maximum deflection, occurring between the central loading points is:

$$y_{max} = \frac{Pa}{24EI}(3L^2 - 4a^2) = \frac{11PL^3}{15Ebh^3} \tag{3-7}$$

The (constant curvature) deflection at any point between the two loading points, located a distance Δx from the middle of the beam is described by:

$$y_{center} = \frac{PL}{2Ebh^3}\left(3\Delta x(L - \Delta x) - \frac{L^2}{4}\right) \tag{3-8}$$

Finally, the flexural strength of a rectangular beam in four point bending with a load span of $L/2$ can be obtained by inserting $\Delta y = h/2$ into Eq. (3-5) and is thus:

$$\sigma_f = \frac{3PL}{4bh^2} \tag{3-9}$$

The microspecimen sample testing apparatus used for this present study was constructed by Nicholas Briot, a fellow researcher in Prof. Dr. John Balk's research group. The construction of the system at the University of Kentucky was modeled after a similar setup in the laboratory of Prof. Dr. Chris Eberl at the Karlsruhe Institute of Technology (KIT) in Germany. Nevertheless, several significant difference exist between the two microspecimen testing setups. Both systems operate on the principle of

digital image correlation (DIC), which has also been described for the use in microspecimen bend testing by Eberl et al. [217] in 2010.

The minimum strain resolution of the UK system is 3.3 x 10^{-5}, which provides excellent resolution even for very small or brittle samples. Rapid position of the moving grip is performed by a precise linear actuator (stepper motor) with a range of 25 mm and resolution better than 1 μm. Controlled displacement of the moving grip (the central loading points) is achieved with a piezoelectric actuator with a range of 100 μm and 25 nm resolution. Load is measured using a miniature load cell mounted between the moving grip and piezoelectric actuator. The load range of the FUTEK© LSB200 load cell used during this study is ± 200 N, with a resolution of better than 0.5 % of the signal amplitude. An overview of the experimental setup can be seen in the Figure 3-15.

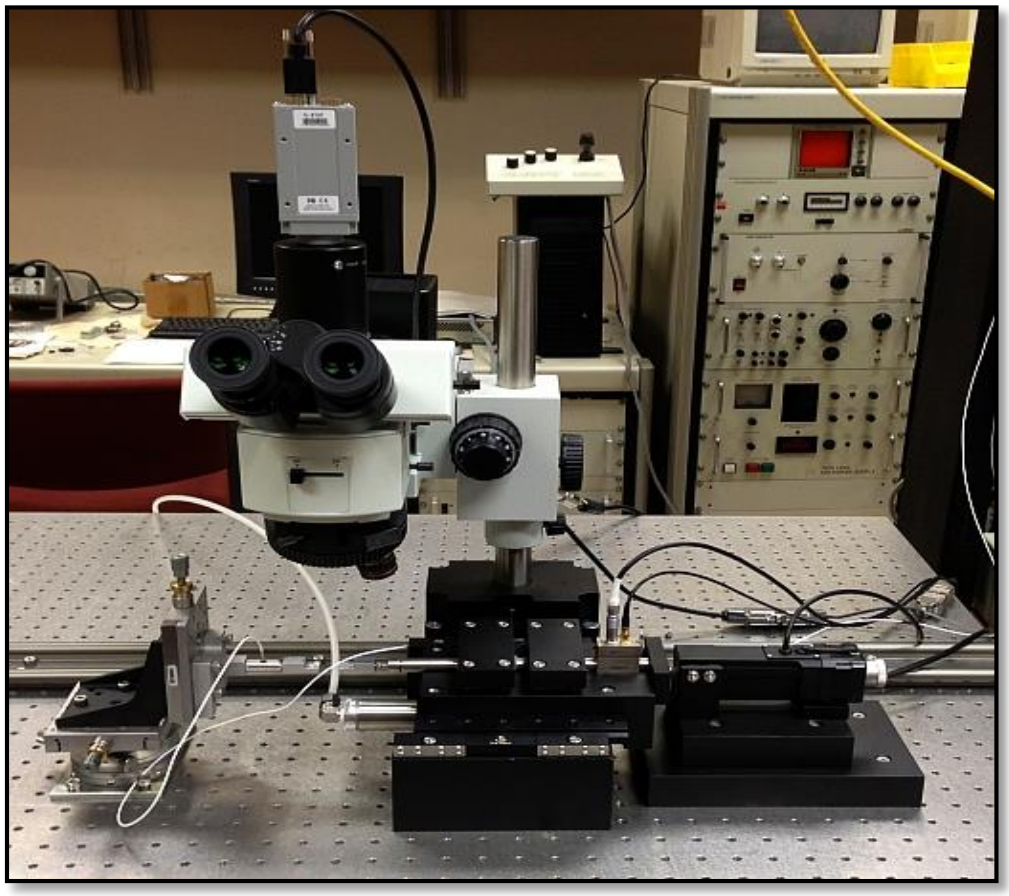

Figure 3-15. Experimental setup for microspecimen four point bend testing of machined porous tungsten samples. Custom grips were used to facilitate accurate and repeatable measurement of flexural strength.

Special care was taken to firmly mount all components flush with one another in order to optimize alignment and stiffness. A signal amplifier is used in conjunction with the load cell prior to data acquisition. Both force data and DIC displacement measurements are collected using MATLAB© software and custom code. A programmable logical controller (PLC) operated by Unity Pro M software is used to minimize lag during data acquisition. A set of custom grips was machined to accommodate the unique sample size and to ensure maximum rigidity. The grips were CNC machined from hardened *AISI 4140* steel (45 HRC). Bearing pins were fabricated from highly polished, precision ground tungsten carbide rods with a diameter of 1.588 mm (1/16”).

CHAPTER 4.

ESTABLISHING A SET OF MACHINING PARAMETERS FOR CRYOGENIC MACHINING OF POROUS TUNGSTEN WITH SINGLE POINT CERMET CUTTING TOOLS

4.1 INTRODUCTION

Cryogenic machining of porous tungsten was first investigated by Tarter et al. [1] in 2008. These initial results suggested that cryogenic machining is able to eliminate the use of the plastic infiltrant which is currently use during the dispenser cathode manufacturing process. Pusavec et al. [2, 11] further developed the initial results from Tarter et al. and first published a set of optimized machining parameters in 2008, as well as a re-published version of the same results in 2012. While all of the early studies on cryogenic machining of porous tungsten provided strong evidence regarding the feasibility of cryogenic machining of porous tungsten, this present study is focused on further improving the surface quality from this novel process. Initial results by the author documented the difficulties in repeated the work of Pusavec et al. [1, 3, 4], particularly with regard to the machining parameters from Pusavec et al.'s 2008 report. A likely explanation for this apparent discrepancy is the fact that Pusavec et al. did not document the porosity of the material used during their study. Moreover, both the machine tool and the cutting tool material (a MAZAK CNC lathe and polycrystalline diamond tools) used by Pusavec et al. [11] were different from the materials used during the course of this present work.

As part of the effort to establish an initial set of machining parameters for cryogenic machining of porous tungsten, a variety of cutting tool materials were investigated. Due to the very high cost of PCD cutting tools (≈ \$100 / cutting edge) compared to more commonly used 'carbide' (*WC* + *Co* binder) and 'cermet' (*TiC/TiN* + *Co* binder) tools (≈ \$5 / cutting edge), the latter class of cutting tool materials was used for initial investigations. Preliminary results quickly revealed that tungsten carbide (*WC*) based carbide tools show high affinity for porous tungsten, leading to severe built-up edge (BUE) and rapid tool-wear. Only uncoated tool grades were considered due to the excessively large cutting edge radius of coated tools (r_β > 20 μm). It should be noted that recent advancements in physical vapor deposition coating technology has led to the

development of extremely thin coatings, allowing for relatively sharp coated tools. Because cutting tool manufacturers generally do not disclose information regarding the precise chemical composition of coatings or the tolerance for cutting edge radii, no such coated yet sharp (r_β < 10 μm) tools were available to the author at the time these initial results were obtained.

As an alternative, wear resistant uncoated cermet cutting tools were selected (Kyocera grade TN60). These titanium carbide/nitride based tools are widely used in Japan due to the limited supply of tungsten and the higher hardness of *TiC* and *TiN* compared to *WC*. Cermet tools have been shown to offer reduced wear compared to carbide, allowing for high-speed finishing of steel and cast iron [218-220]. Preliminary results also showed that cermet cutting tools are able to produce excellent surface quality in porous tungsten [3, 4]. Unlike other high-temperature materials such as titanium, Inconel and even dense tungsten, uninfiltrated porous tungsten cannot be effectively machined with positive rake angle tools [4]. The extremely abrasive chips generated when machining as-sintered porous tungsten result in rapid tool-wear, especially for positive rake angle tools whose small wedge angle makes them vulnerable to abrasive wear. Therefore, negative rake angle tools are used during this study. To achieve a negative rake angle along with low cutting edge radius, precision ground cermet cutting tools (CNGA geometry) were used in a dedicated tool holder to achieve a rake angle of γ = -5°. The effect of various rake angles on surface integrity of porous tungsten will be further studied in chapter 5.

In this chapter, a precise range of machining parameters will be developed for cryogenic machining of porous tungsten with cermet cutting tools. Moreover, the effects of cryogenic pre-cooling and cutting edge radius will be studied, particularly as to the relationship with as-machine surface morphology. Lastly, the impact of rake angle on the stress state of the machined surfaces of both fully dense (polycrystalline) and 80% density porous tungsten is investigated. Achieving compressive residual stress is of particularly importance in porous tungsten due to the very low fracture toughness (brittleness) of this workpiece material. As a result of the forces encountered during machining process and improper handling, the scrap rate of porous tungsten dispenser cathode pellets is high [1, 3]. Suppressing undesirable chipping would consequently improve the sustainability of the dispenser cathodes manufacturing process.

4.2 EXPERIMENTAL DETAILS

Face turning experiments were carried out on a HAAS TL-2 CNC lathe. Liquid nitrogen was applied onto both the rake face and un-machined surface simultaneously at a flow rate of 0.5 l/min. Prior to machining, cryogenic pre-cooling was applied with the workpiece rotating at 90 rpm over intervals of 60, 90, and 120 seconds. A single cutting edge was used for each experimental condition and each machined surface was parted off carefully to obtain 2 mm thick discs. The cutting tool material was cermet grade TN60 by Kyocera©. The geometry of the turning inserts was TPGA, i.e., neutral rake angle (90º wedge angle). To obtain the desired rake angle, a tool holder was used to create a rake angle of -5º.

Surface roughness measurements were taken on a ZYGO© NewView 7300 scanning white light interferometer (SWLI). Using a 20x objective, a set of three 150 μm downward scans were carried out at 10%, 50%, and 90% of the radius of each machined surface. Likewise, SEM micrographs were taken at corresponding locations at a magnification of 1000x to comply with the dispenser cathode industry standard for determining as-machined surface porosity. In accordance with the same standard, an area of 10,000 μm^2 (0.003" x 0.005") was subsequently analyzed using ImagePro software. Scatter for both surface roughness and surface porosity corresponds to the maximum and minimum measured values, within a statistically relevant confidence interval of 95%.

Cutting edge radius modification (honing) was achieved via drag/stream finishing on an OTEC SF-1 machine. Uniformly rounded cutting edges with r_β = 5 μm, 30 μm, and 60 μm were obtained, while the starting condition of the as-delivered tools was r_β = 2 μm (i.e., upsharp ground). Both dry and cryogenic machining experiments were carried out for 80% density porous tungsten and fully dense polycrystalline tungsten. Residual (tangential) surface stress was measured using the $sin^2(\psi)$ method, except for dry machined dense tungsten, where excessive tool-wear resulted in too little relevant (machined) surface area to be analyzed.

4.3 RESULTS AND DISCUSSION

4.3.1 Tool-wear Effects in Porous Tungsten Machining

To assess tool-wear in finish machining of porous tungsten, nose wear was selected as the most relevant measure. Geometric tolerances of dispenser cathode pellets machined from porous tungsten are often on the order of ± 10 μm. Considering the inherent inaccuracies of the machine tool, workpiece thermal expansion/contraction and operator error, achieving such tolerances requires tool-wear to be extremely low. The tool-wear parameter *KS* is defined as the wear retract of the cutting edge in the nose region of the cutting tool [221]. Nose wear *N* is proportional to the wear retract *KS* by the cosine of rake angle. Because the cosine of small number (such as the 5 degrees of rake angle used in this context) is very close to unity, *KS* is practically equal to *N*. Therefore, nose wear directly impacts the geometric tolerances of the machined component. Measuring nose wear directly, i.e., in plan view of the rake face, requires extrapolation of the unworn portion of the corner radius (nose). This method is prone to large scatter because of parallax and similar optical and processing errors. For the purposes of this study, the geometric relationship between easily measured flank wear in the nose region VB_C and nose wear *N* was used to reliable measure the latter in an indirect fashion.

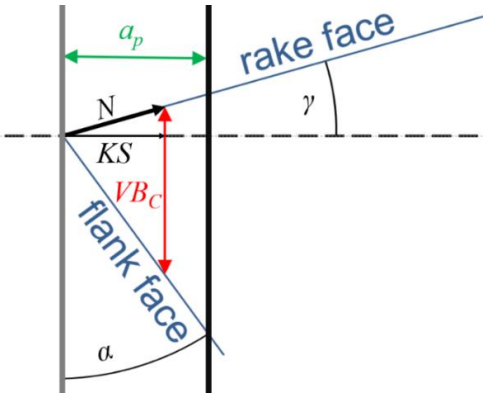

Figure 4-1. Schematic illustrating the geometric relationship between nose and flank wear for a negative rake angle cutting tool. By measuring flank wear, a relatively simple task, nose wear can be calculated analytically to great precision
(from the author's published work [22], with permission of Taylor and Francis).

As can be seen in Figure 4-1, flank wear VB_C, is related to nose wear as a function of both the clearance angle α and the (negative) rake angle γ. By using simple trigonometry, the following relationship (Eq. (4-1)) can be derived:

$$N = VB_C * \left(\frac{tan(\alpha)}{cos(\gamma)+sin(\gamma)*tan(\alpha)}\right) \quad (4\text{-}1)$$

From Eq. (4-1) it is evident that N is related to VB_C by a constant as long as clearance and rake angle are kept constant, as was the case during this study. Practically, this meant that flank wear was measured for each cutting tool and converted using a factor of 0.28 (α = 16º, γ = -5º). In other words, nose wear of the cermet cutting tools used for the experiments discussed here was 28 % of flank wear. An experimental error of ± 5 µm in the measurement of VB_C resulted in an error of only ± 1.4 µm in N. To ensure that nose wear did not impede the achievable tolerances of porous tungsten components, an acceptability limit of N < 10 µm shall be used in the ensuing discussion. The experimental results for the effects of depth of cut and cryogenic pre-cooling on nose wear are shown in the following Figure.

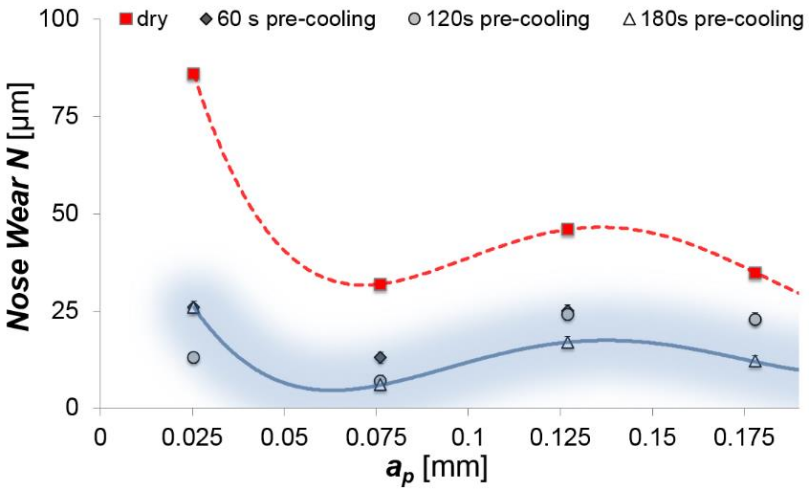

Figure 4-2. The effects of cryogenic pre-cooling and depth of cut on nose wear of cermet cutting tools (from the author's published work [22], with permission of Taylor and Francis).

[v_c = 15 m/min, f = 0.025 mm/rev]

The most immediate observation from Figure 4-2 is the significant reduction on nose wear with cryogenic pre-cooling compared to dry machining. An average reduction of approximately 50% is achieved by means of cryogenic cooling. The length of pre-cooling had little effect on the amount of nose wear, though extended pre-cooling (180 s) led to slightly lower nose wear at larger depths of cut. This effect is likely due to the depth of penetration of the cooling effect of liquid nitrogen, which increases as a function of pre-cooling time. Cutting temperature obviously has a significant effect on tool-wear in machining of porous tungsten. This result is not surprising, as metal cutting is known to generate significant heat between at cutting tool/chip interface [222, 223].

Especially at low depth of cut, when uncut chip thickness becomes equal to or smaller than the cutting edge radius, ploughing leads to significant buildup of heat. This effect has been document by many researchers in the field of micromachining, where very small values of uncut chip thickness are commonly encountered [7, 92, 105]. In the context of porous tungsten, the ploughing effect clearly has an effect on tool-wear and is likewise expected to affect surface roughness and surface porosity as well.

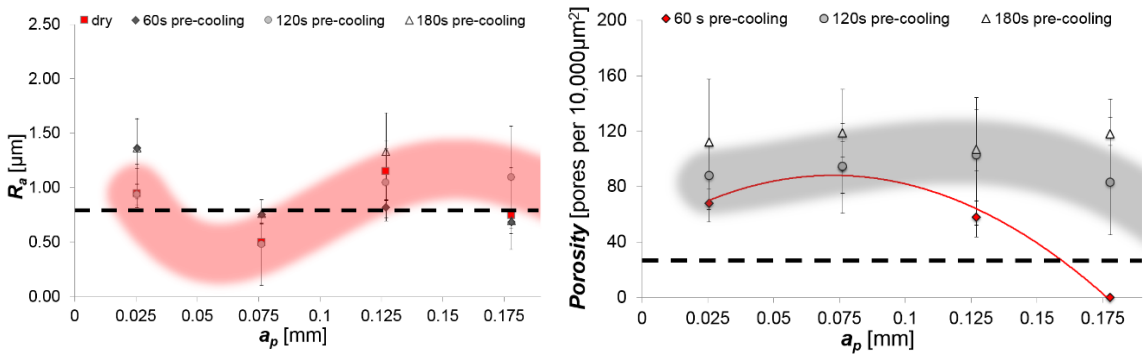

Figure 4-3. Surface roughness and surface porosity as a function depth of cut for a variety for cryogenic pre-cooling conditions. Both ploughing at low depth of cut and fracture and larger depth of cut negatively affect surface quality. Only a small range of depth of cut yields an acceptable surface finish (from the author's published work [22], with permission of Taylor and Francis).

[v_c = 15 m/min, f = 0.025 mm/rev]

According to the acceptability criteria of the dispenser cathode industry (*EIA-941*), both surface roughness in excess of $R_a < 0.8$ μm at any representative area on the machined surface and surface porosity of less than 30 pores per 10,000 μm^2 are cause for rejection [224]. These acceptability limits are included in Figure 4-3 in the form of dashed lines. Achieving acceptable surface roughness is only possible in the range between $a_p = 0.05 – 0.1$ mm. Lower depth of cut leads to ploughing, where the minimum chip thickness effects causes an increase in surface roughness. Larger depth of cut increases the cutting temperature as well as the likelihood of fracture, likewise increasing surface roughness. The duration of cryogenic pre-cooling had relatively little effect on surface roughness. In fact, dry machining resulted in practically identical levels of surface roughness as cryogenic machining. A likely explanation for this phenomenon is temperature induced plasticity of the porous tungsten workpiece material during dry machining. Severe smearing occurring during dry machining did result in no discernable surface porosity. For this reason, no dry machining results are shown in the right hand graph of Figure 4-3.

Surface porosity is affected most strongly by the duration of cryogenic pre-cooling. As can be seen in Figure 4-3, limited pre-cooling (60 s, red line) led to significant reductions in surface porosity with increasing depth of cut. At $a_p = 0.175$ mm, complete smearing left no visible pores. However, both 120 s and 180 s of pre-cooling allowed for highly porous surfaces to be obtained even at larger depths of cut. Based on this observation it is hypothesized that cutting temperatures at depths of cut in excess of $a_p = 0.15$ mm when only 60 s of pre-cooling are applied are sufficient to exceed the brittle to ductile transition temperature of tungsten, which is approximately 200 ºC [225-227]. The simultaneous reduction in surface porosity and increase in surface roughness observed to some degree for all three pre-cooling conditions furthermore may be explained by adhesion and re-deposition of machined chips.

While negative rake angles stabilize the cutting edge and lead to reduced tool-wear and temperature buildup at the tool tip, chip evacuation can be problematic [81, 82, 97]. Because the chips generated during cryogenic machining of porous tungsten are generally very small, they may become trapped between the cutting tool and the workpiece, forming a built-up edge (BUE). Evidence for BUE when cryogenically machining

porous tungsten with negative rake angle cermet cutting tools was observed via SEM. The morphology of the resultant surface also explains the large scatter of both surface porosity and roughness in Figure 4-3.

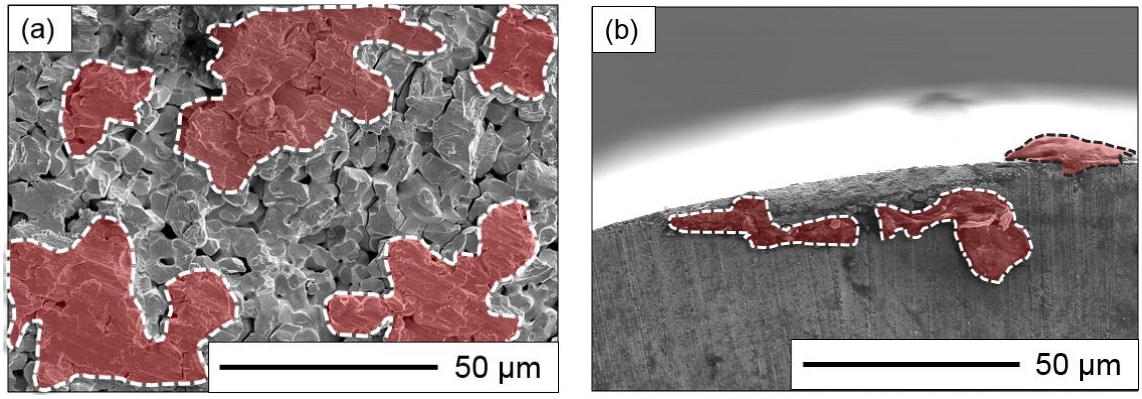

Figure 4-4. Scanning electron micrographs of surface morphology of cryogenically machined porous tungsten (a) with re-deposited chips highlighted in red, as well as the corresponding cutting edge (b) with evidence of built-up edge (from the author's published work [22], with permission of Taylor and Francis).
[v_c = 15 m/min, a_p = 0.075 mm, f = 0.025 mm/rev, $t_{pre\text{-}cooling}$ = 180 s]

The evidence for the hypothesized mechanism of unstable BUE re-deposition onto the machined surface during cryogenic machining of porous tungsten shown in Figure 4-4 also provides clues regarding the machining mechanism. The large fracture pits seen in Figure 4-4a suggest that brittle fracture occurred during machining. Nevertheless, the smeared islands on the same surface are also evidence of high yet localized cutting temperature. The burnishing action of the cutting edge moving across the pre-fractured workpiece surface likely generates significant heat, allowing individual tungsten ligaments to be welded to the cutting edge and randomly be smeared across the surface.

4.3.2 Chip Morphology

The occurrence of both brittle fracture and severe plastic deformation may also explain the tool-wear trend seen in Figure 4-2, where increasing depth of cut led to a slight increase in nose wear. At increased depth of cut, larger pieces/chips are generated as a result of brittle fracture. When these larger fragments of porous tungsten adhere to the cutting edge and are subsequently sloughed off, significant heat is generated, leading to the formation of smeared islands and accelerated tool-wear. Likewise, smaller chips may act much like an abrasive, quickly 'grinding' down the cutting edge by both abrasion and attrition wear. Evidence for brittle fracture chips as well as shear machining chips from both dry and cryogenic machining is shown in the following Figure.

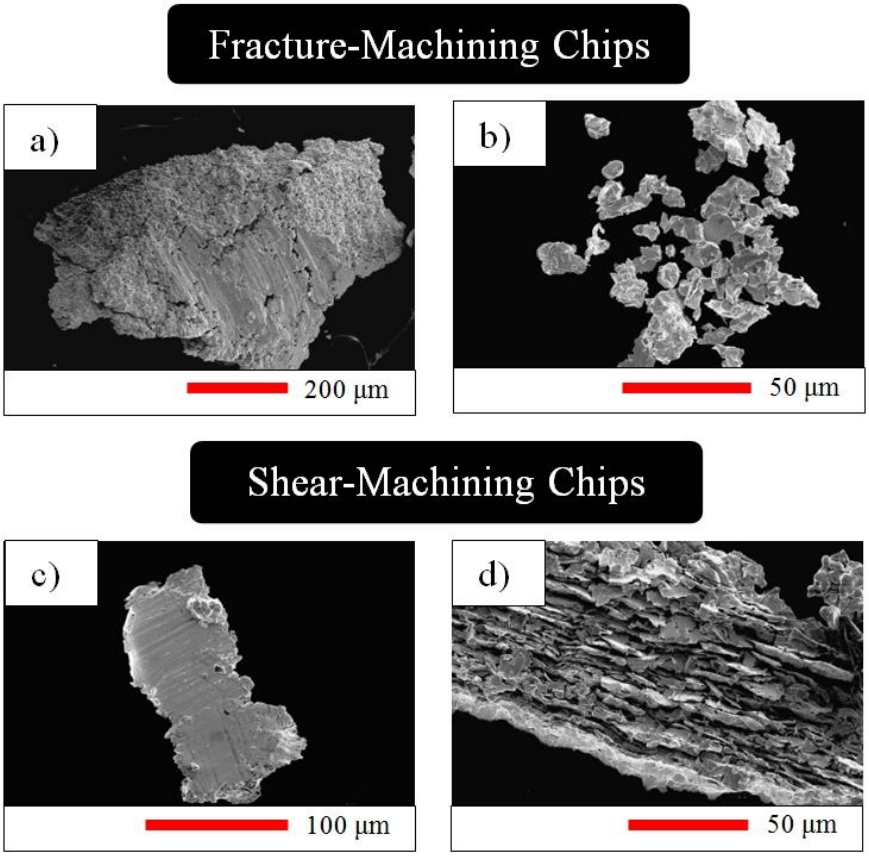

Figure 4-5. SEM micrographs of chips generated dry and cryogenic machining of porous tungsten with negative rake angle cermet cutting tools (from the author's published work [4], with permission of Elsevier, Inc., license number 3660870523804).

Based on the SEM micrographs shown in Figure 4-5, two general categories of chips generated during machining of porous tungsten, i.e., shear and fracture machining chips, are defined. Fracture machining chips occur when $a_p > 0.05$ mm, due to the relative 'sharpness' of the cutting edge in relation to the uncut chip thickness. The large fracture machining chips in Figure 4-5a are evidence of undesirable brittle fracture of the workpiece ahead of the cutting edge, as the size of this type of chip is significantly larger than would be expected from the geometry of the uncut chip.

Small fracture chips, shown in Figure 4-5b, occur under almost all conditions when machining porous tungsten. Often, small fracture machining chips are comprised of just 2-3 ligaments/particles of tungsten. Because of their small size, these chips are hypothesized to be primarily responsible for the formation of BUE and associated attrition wear of the cutting tool. Because negative rake angle cutting tools have a tendency to increase the amount of brittle fracture during cryogenic machining of porous tungsten, small fracture chips are more commonly observed with such tools.

Shear machining chips, as shown in Figures 4-5c-d, occur during dry machining and at all small depths of cut when cryogenic pre-cooling is applied. The completely compacted and severely plastically deformed small shear machining chip in Figure 4-5c documents the very high temperature and stress encountered when machining porous tungsten at low depths of cut ($a_p < 0.05$ mm). All ligaments have been crushed to yield a very thin chip that is essentially extruded ahead of the cutting edge via ploughing. When $a_p > 0.1$ mm, large shear machining chips become dominant. These chips are very complex and contain three distinct zones, as can be seen in Figure 4-6. While the top surface (Figure 4-6, zone "a") remains essentially undeformed, most of the porous tungsten ligaments within the chip (zone "b") are crushed to near full compaction. Lastly, severe plastic deformation on the cleaved/machined surface (zone "c") is evidence of high localized cutting temperature. Clearly, the forces and temperatures generated during cryogenic machining of porous tungsten place tremendous stress on both the chip and the cutting tool.

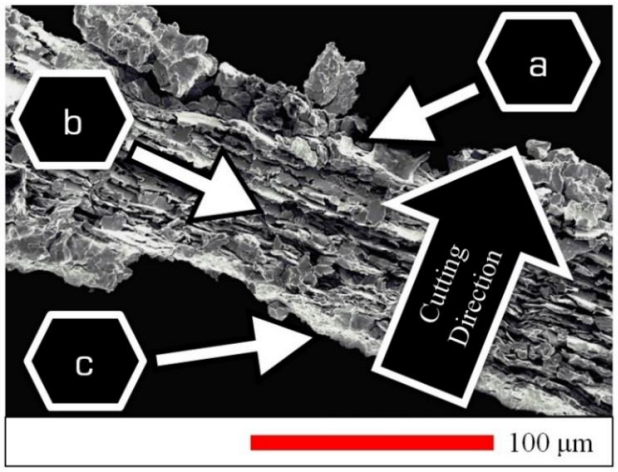

Figure 4-6. SEM micrograph of large shear machining chip with three zones (a,b,c) as well as the cutting direction highlighted (from the author's published work [4], with permission of Elsevier, Inc., license number 3660870523804).
[v_c = 15 m/min, a_p = 0.127 mm, f = 0.025 mm/rev, $t_{pre\text{-}cooling}$ = 60 s]

4.3.3 Cutting Speed Effects

Because the problem of re-deposited chips and BUE in cryogenic machining of porous tungsten leads to inconsistent surface quality, several possible solutions were considered. Ideally, a cutting tool material with very low affinity for tungsten would allow for the elimination of BUE. Both the chemical composition of the tool as well as its surface structure (i.e., tribological properties) would need to be optimize to achieve this goal. Improving chip evacuation with a combination of low-friction surface preparation of the cutting tool and properly positioned cryogenic delivery nozzle may also help prevent BUE. Likewise, eliminating undesirable and uncontrolled brittle fracture ahead of the cutting edge would lead to improved surface quality.

Since brittle fracture increases with extended cryogenic pre-cooling, a limited approach to pre-cooling to allow for some plasticity may reduce brittle fracture. However, even dry machining resulted in fracture machining chips, suggesting that porous tungsten's response to machining is inherently brittle. This does of course not mean that no plastic deformation takes place, as has clearly been shown in the previous discussion. Rather, some portions of the uncut chip will be subject to brittle fracture

while others will experience severe plastic deformation and/or ploughing; all of these effects will be considered in the following chapters. The most immediate solution to BUE in machining is to increase the cutting speed to reduce flow stress as well as the friction at the tool/chip interface due to thermal softening, [79, 97, 98].

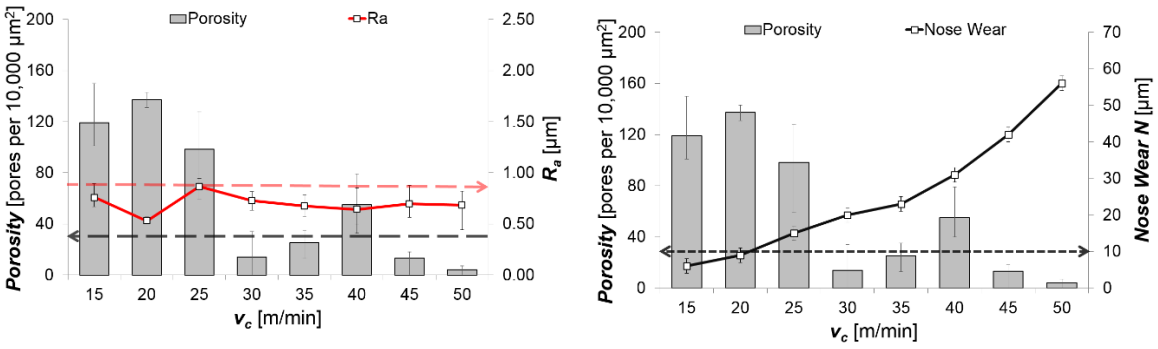

Figure 4-7. The effect of cutting speed on cryogenic machining of porous tungsten. Due to excessive tool-wear, cutting speed may not exceed 20 m/min when using cermet tools (from the author's published work [22], with permission of Taylor and Francis).
[a_p = 0.075 mm, f = 0.025 mm/rev, $t_{pre\text{-}cooling}$ = 180 s]

To explore the effect of cutting speed on cryogenic machining performance of porous tungsten, a set of experiments summarized in Figure 4-7 was carried out. The depth of cut chosen for these experiments was fixed at a_p = 0.075 mm, based on observations from Figure 4-3. Significantly lower scatter in surface roughness occurred at cutting speeds between v_c = 20-35 m/min. Surface porosity, which is shown in both graphs of Figure 4-7 to help interpret both roughness and tool-wear data, reached a maximum of 145 pores at a cutting speed of 20 m/min. This value is close to the theoretical maximum of 200 pores per 10,000 µm^2, which implies that only 27.5% of all available pores were smeared shut. Considering the acceptability limit of 30 pores (85% smearing), the level of surface porosity achieved at cutting speeds between v_c = 15 – 25 m/min is excellent. However, due to the surface roughness requirement of R_a < 0.8 µm, only a cutting speed of 20 m/min yields sufficiently low surface roughness while also fulfilling the porosity requirement. The reason for the significant decrease in surface porosity beyond v_c = 25 m/min can be seen in the right hand graph of Figure 4-7.

Tool-wear increases steadily with cutting speed when cryogenically machining porous tungsten with cermet cutting tools. Beyond a cutting speed of v_c = 20 m/min, nose wear exceeds the acceptable limit of N < 10 µm. At v_c = 40 m/min, nose wear tripled to N = 30 µm and at v_c = 50 m/min nose wear reached almost 60 µm, which is close to the maximum possible amount of $N_{max} = a_p$ = 75 µm. The reason for the severe tool-wear at increasing cutting speeds is hypothesized to be increased cutting temperature, which is further aggravated by rubbing of the worn flank area of the cutting tool on the machined surface. Therefore, as tool-wear increases, so does cutting temperature due to rubbing which in turn further accelerates tool-wear, leading to a run-away effect. This phenomenon further emphasizes the importance of controlling tool-wear and maintaining nose wear of less than 10 µm to prevent rubbing and ploughing of the tool.

Moreover, the rubbing action of a worn cutting tool also causes severe smearing, as can be seen in the trend of surface porosity in Figure 4-7. Practically, tool-wear in excess of N = 30 µm, which occurred under all dry machining conditions in Figure 4-2 and at v_c = 40 m/min in Figure 4-7 with 180 s of cryogenic pre-cooling, leads to severe smearing and ploughing with unacceptable surface porosity. The fact that v_c = 40 m/min yielded an average of 60 surface pores is due to random tears/fracture pits in the surface that are caused by the worn cutting edge. Therefore, the resulting surface could not be used to manufacture dispenser cathodes since the scatter in both surface roughness and porosity is too large.

Excessive tool-wear of cermet cutting tools even at low cutting speeds prevents sustained machining performance of porous tungsten. Even though cryogenic pre-cooling reduces tool-wear by more than 50%, nose wear of close to 10 µm after a single facing cut at an ‘optimum’ cutting speed of 20 m/min would require frequent tool changes to maintain both surface quality and dimensional tolerances. The surface quality obtained at v_c = 20 m/min and a_p = 0.075 mm is however very good and would certainly allow for porous tungsten to be machined without the use of plastic infiltrant. A summary of the different kinds of surface morphologies from cryogenic machining can be seen below.

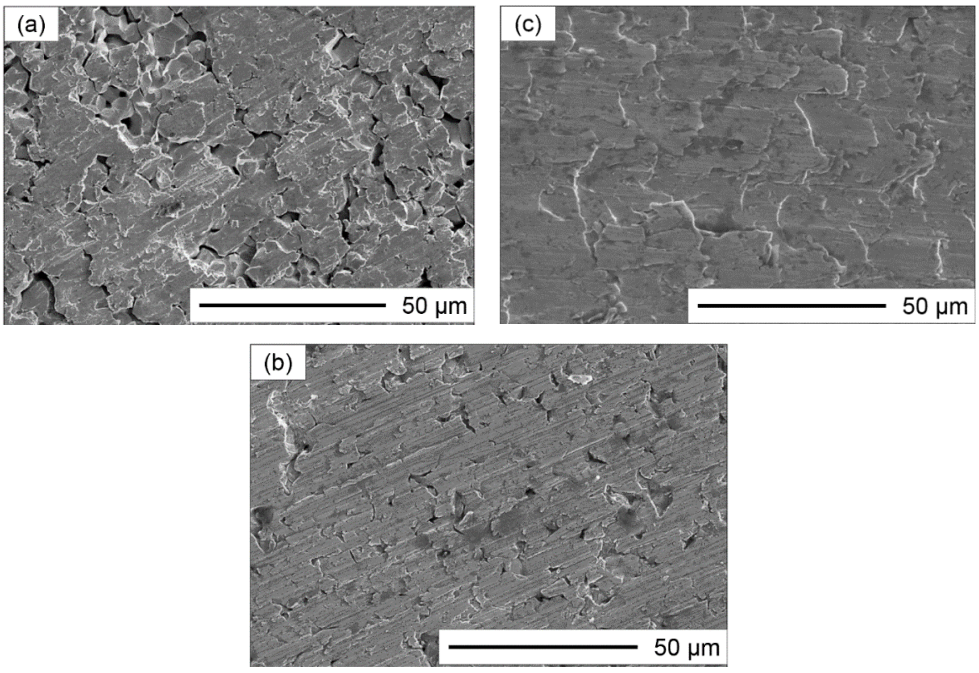

Figure 4-8. SEM micrographs of surface morphology obtained from cryogenic machining of 80% density porous tungsten at cutting speeds of 15 m/min (a), 20 m/min (b), and 40 m/min (c). The bottom micrograph (b) represents the best surface quality obtained with negative rake angle cermet tools (from the author's published work [22], with permission of Taylor and Francis).

[a_p = 0.075 mm, f = 0.025 mm/rev, $t_{pre\text{-}cooling}$ = 180 s]

Three distinct types of surfaces were obtained from cryogenic machining of porous tungsten at different cutting speeds. At low cutting speeds, deep fracture pits and re-deposited chips leave a mixed surface with good porosity yet poor surface roughness as can be seen in Figure 4-8a. When cutting speed is increased, severe tool-wear leads to rubbing and ploughing of the workpiece surface. The surface shown in Figure 4-8c corresponds to a cutting speed of v_c = 40 m/min, towards the end of the cut. While the initially unworn tool produces acceptable surface porosity, rapid dulling of the cutting edge due to tool-wear leads to severe smearing. Plastic flow of individual ligaments can be seen in Figure 4-8c, supporting the hypothesis of large cutting temperatures at increased cutting speeds. When tool-wear is kept sufficiently low by limiting cutting speed to v_c = 20 m/min, a good combination of shear machining and limited fracture is

achieved. The resulting surface is shown in Figure 4-8b, and represents the optimum surface morphology attainable with the negative rake angle cermet cutting tools used for this study. It is hypothesized that by limiting tool-wear, higher cutting speeds may still allow for excellent surface morphologies to be obtained. For this purpose, PCD cutting tools will be explored in later chapters.

4.3.4 Observations on Cutting Edge Radius Effects

In order to maximize the performance of both the cermet tool grade used during this initial study of cryogenic machining of porous tungsten as well as that of more wear resistant PCD and PCBN tool grades used in future studies, the effect of cutting edge preparation was explored. Only uniformly rounded cutting edges were employed to limit the amount of possible variables. Two corner/nose radii were used, namely 0.2 mm and 0.4 mm. In addition to tool-wear and surface roughness, the residual stress state of the machined surface was assessed for both dense and 80% density porous tungsten.

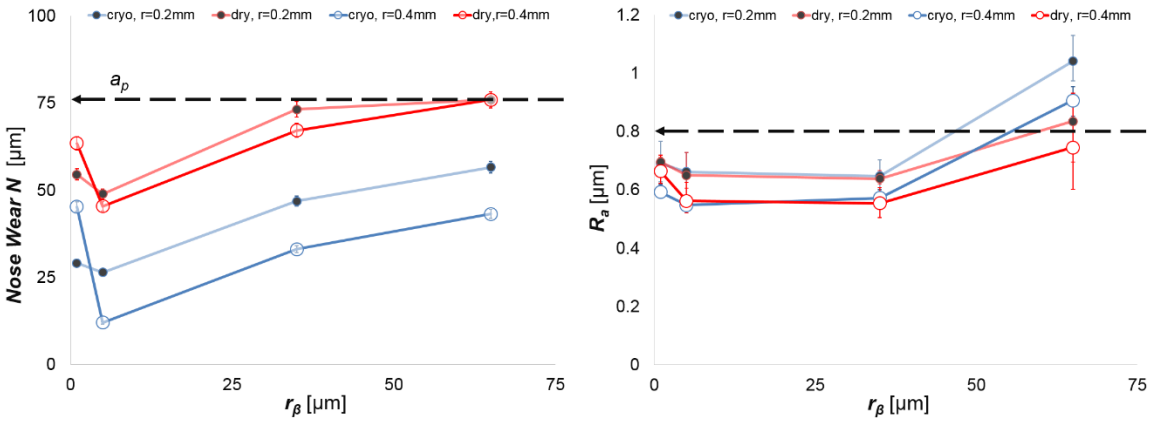

Figure 4-9. Nose wear and surface roughness data from cryogenic and dry machining of porous tungsten as a function of r_β for two different nose radii r_c. The maximum possible nose wear ($N_{max} = a_p = 75$ µm) and the acceptability limit for surface roughness ($R_a < 0.8$ µm) are highlighted by dashed arrows (from the author's published work [22], with permission of Taylor and Francis).

[$v_c = 20$ m/min, $a_p = 0.075$ mm, $f = 0.025$ mm/rev, $t_{pre\text{-}cooling} = 180$ s]

The experimental results for nose wear in Figure 4-9 show that cryogenic cooling reduces wear by as much as 75% compared to dry machining. While the overall trend of tool-wear is the same for both cryogenic and dry machining, the wear under all experimental conditions, with one exception, was well in excess of the acceptable limit of $N < 10$ μm. The only condition with acceptable nose wear occurred for a nose radius of $r_\beta = 5$ μm along with a corner radius of 0.8 mm. An upsharp cutting edge ($r_\beta = 2$ μm) resulted in much larger tool-wear than a light hone. This observation is consistent with that of many other researchers and hypothesized to be due to a lack of mechanical strength of very sharp cutting edges along with the effect of grinding induced defects such as chips and tool marks on the cutting edge [81, 86, 96]. Cutting edge radii beyond 5 μm did however also lead to increased wear. Because the uncut chip thickness for the finish turning operation carried out for the experiments discussed here was very small, larger cutting edge radii resulted in significant ploughing. As a result, tool-wear for these cutting edges, though mechanically strong, was accelerated because of significant heat buildup.

For both dry and cryogenic machining, a larger corner radius of $r_{c.} = 0.8$ mm delivered consistently lower nose wear, which is hypothesized to be due to an increased length of engagement compared to the smaller corner radius of 0.4 mm. Therefore, the largest possible nose radius should be used when cryogenically machining porous tungsten in order to limit tool-wear. However, there clearly is some physical limitation to how large a cutting edge radius may become before uncut chip thickness in the vicinity of the machined surface becomes so small that severe ploughing ensues. In other words, very large corner radii effectively 'dull' the cutting edge relative to the uncut chip. More details on this phenomenon will be given in ongoing chapters.

Surface roughness showed relatively little dependence on both corner and cutting edge radius, as can be seen in the right hand graph of Figure 4-9. Only the very largest cutting edge radius of $r_\beta = 60$ μm led to unacceptable surface roughness of $R_a > 0.8$ μm. Again, the reason for this observation is ploughing due to the minimum chip thickness effect. When the cutting edge radius is significantly larger than the uncut chip thickness, chip formation near the final machined surface becomes impossible and ploughing ensues. The resulting surface morphology is similar to that shown in Figure 4-8c.

Because most commercially available cermet and carbide cutting tools are prepared with cutting edge radii on the order of r_β = 20 – 120 μm, it is clear that efficient machining of porous tungsten requires careful selection of both the tool material grade and corresponding cutting edge preparation.

The cermet grade used for the experiments discussed in this context clearly lacked sufficient wear resistance to allow for high-volume production of dispenser cathodes from porous tungsten. As a result, the following chapter (#5) will explore cryogenic machining of porous tungsten with highly wear resistant polycrystalline diamond (PCD) tools. Nevertheless, qualitative observations regarding the effects of both corner and cutting edge radii should certainly be valid for more wear resistant tool materials as well. The much lower cost of cermet tools when compared to PCD allowed for a much larger range of experimental conditions to be tested with cermet tools. As part of this effort, the effect of cutting edge radius on the stress state of the machined surface and near sub-surface was investigated.

4.3.5 Residual Stress

Because one of the problems associated with the current industry practice of plastic infiltrant assisted machining is a high scrap rate due to hidden defects such as chipping and fracture of the workpiece, the effect of cryogenic cooling on residual stress was explored. Tangential residual stress was measured on the surfaces of dry and cryogenically machine porous tungsten with a density of 80% as well as for cryogenically machined fully dense tungsten. Dry machining of dense tungsten with the parameters used for porous tungsten resulted in such large tool-wear that only a few millimeters were machined before failure of the tool, leaving insufficient relevant surface area to be analyzed. Therefore, residual stress was only measured on cryogenically machined samples of dense tungsten. Figure 4-10 summarizes residual stress measurements for both 80% density porous and fully dense tungsten.

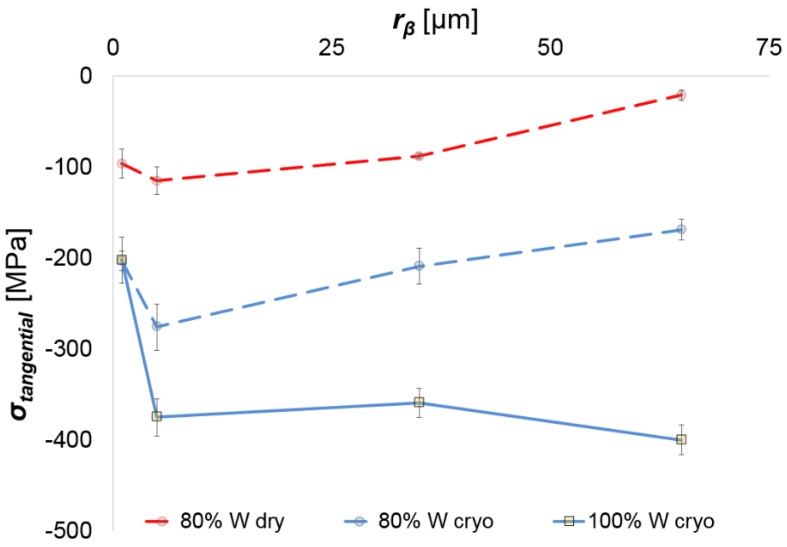

Figure 4-10. Tangential residual surface stress of dry and cryogenically machined 80% density porous tungsten (dashed lines) and cryogenically machined dense polycrystalline tungsten (solid line) (from the author's published work [22], with permission of Taylor and Francis).

[v_c = 20 m/min, a_p = 0.075 mm, f = 0.025 mm/rev, $t_{pre\text{-}cooling}$ =180 s]

The trend in residual for cryogenically machined polycrystalline tungsten shown in Figure 4-10 is consistent with similar studies on steel and magnesium. Caruso et al. [228] found increased residual stress when cryogenically machining *AISI 52100* bearing steel with larger cutting edge radii. Likewise, Pu et al. [165, 167, 168] reported increased depth of the affected layer and increased compressive residual stress when cryogenically machining *AZ31B Mg* alloy with larger cutting edge radius tools. The increase in compressive residual stress with larger cutting edge radii is hypothesized to be due to an increase in unit cutting pressure and more negative effective rake angle. As effective rake angle decreases, the surface beneath the cutting edge is compressed more, leading to compressive residual stress to be retained. Cryogenic cooling furthermore prevents thermal softening/annealing of this compressive stress state.

The trend in residual stress for both dry can cryogenic machining of porous tungsten suggests a different machining mechanism compared to dense tungsten. Rather than

dense tungsten, porous tungsten exhibited the largest amount of compressive stress from machining with sharp cutting edges. The difference in residual stress between dry and cryogenic machining of porous tungsten was about 60%, i.e., cryogenic cooling led to more than twice the amount of compressive residual stress. Clearly, thermal softening is the most likely mechanism responsible for this difference. When porous tungsten is cryogenically cooled during machining, its yield strength is hypothesized to increase analogous to the mechanical properties of polycrystalline tungsten [225, 226, 229, 230]. As a result of increased strength at low temperature, porous tungsten will store more elastic energy when cryogenically cooled. Moreover, dry machining results in high cutting temperatures, as evidenced by the amount of severe plastic deformation observed in micrographs such as Figure 4-8c. Thermal softening and the resultant plastic flow reduce the amount of compressive residual stress, which is why dry machining of porous tungsten results in less than half the compressive residual stress compared to cryogenic machining.

However, the decrease in compressive residual stress of porous tungsten as cutting edge radius is increased demands a more nuanced explanation. While cryogenic machining of dense tungsten did not lead to brittle fracture, cryogenic machining of porous tungsten certainly had this effect. As evidenced by discontinuous chips and large scatter in surface roughness, porous tungsten responds quite differently to cryogenic cooling than fully dense tungsten. Because of the inherent defects within its microstructure (i.e., pores), porous tungsten is prone to intergranular brittle fracture. Increasing the cutting pressure will therefore no necessarily increase the elastic energy stored within the ligaments (i.e., residual stress), but may lead to the collapse of pores and/or fracture along grain boundaries. As a result, more negative rake angles are expected to increase the amount of brittle fracture in porous tungsten. When the material ahead of the cutting edge is fractured, less residual stress will be stores because of discontinuities within the sub-surface of the workpiece. Brittle fracture will therefore limit the amount of residual stress than can be imparted by the cutting edge.

However, increasing tool-wear due to the minimum chip thickness effect further complicates the machining mechanism of porous tungsten with relatively large cutting edge radii ($r_\beta > 10$ μm). Ploughing and re-deposition of machined chips result in high

temperatures near the cutting edge, thermally softening the workpiece and increasing wear of the cutting edge. As the cutting edge wears, ploughing becomes more pronounced. When the surface of the porous tungsten workpiece is ploughed and smeared, a tensile stress state is induced. Therefore, larger cutting edge radii, which wear more rapidly when machining porous tungsten, will lead to a decrease in compressive residual stress in this material.

4.4 CHAPTER CONCLUDING REMARKS

By using cermet cutting tools, an initial set of machining parameters for cryogenic machining of porous tungsten was established. Obtaining the surface morphology required for dispenser cathode emitting pellets requires balancing various effects. Both brittle fracture, which occurs primarily at low cutting speeds and large depth of cut and with extended cryogenic pre-cooling, as well as ductile shear and ploughing, which increase at higher cutting speeds and low depth of cut, can be observed to some degree under call conditions. Surface quality was best when applying cryogenic pre-cooling for at least 180 s and using a lightly honed cutting tool (r_β = 10 μm) at a cutting speed of v_c = 20 m/min and depth of cut of a_p = 0.075 mm and feed of f = 0.025 mm/rev. Cryogenic cooling furthermore resulted in more than twice the amount of compressive residual compared to dry machining which may reduce the likelihood of undesirable workpiece fracture due to increased compressive residual surface stress. While the cermet cutting tools used during this initial study did not possess sufficient wear resistance to machine a large number of workpieces, more wear resistant tool materials should further improve the viability of cryogenic machining as an alternative to conventional machining practices for porous tungsten.

CHAPTER 5.

CRYOGENIC MACHINING OF POROUS TUNGSTEN WITH PCD CUTTING TOOLS

5.1 INTRODUCTION

Most cutting tool materials are unable to produce more than a few acceptable surface when machining porous tungsten because of large (abrasive) tool-wear. Negative rake angle cermet tools do provide significant improvements compared to more commonly used carbide tool grades. However, even wear resistant cermet tools can only be used at relatively low cutting speeds (v_c < 30 m/min). To achieve more productivity and improve the sustainability of cryogenic machining of porous tungsten, more wear resistant polycrystalline diamond (PCD) tools were explored.

Because of the large variety of PCD tool grades, an initial exploration of the most wear resistant grade for porous tungsten machining was carried out. In addition to cryogenic machining, pre-heated machining was used as a possible means to improve surface roughness. However, because of the chemical affinity between carbon and tungsten, catastrophic tool failure occurred when pre-heating the workpiece. Using the 'optimum' PCD tool material, a set of cryogenic machining experiments on the effects of as-pre-cooled workpiece temperature and rake angle were carried out. It was hypothesized that by selection an optimum rake angle, surface morphology may be fine-tuned. Moreover, by controlling bulk workpiece temperature rather than pre-cooling time, more control over the machining mechanism of porous tungsten was achieved.

Despite the significantly higher wear resistance of PCD compared to cermet, as-received PCD tools were unable to machine porous tungsten at cutting speeds beyond 60 m/min due to catastrophic edge chipping. To allow for higher cutting speeds to be attained, drag finishing was used to increase edge radii and reduce notchedness of PCD tools. Using modified cutting edge radius PCD cutting tools, cryogenic high speed machining with was investigated and shown to offer dramatic productivity improvements for rough and pre-finish machining of porous tungsten.

5.2 EXPERIMENTAL DETAILS

Face turning experiments for preliminary PCD tool material optimization were carried out on a HAAS TL-2 CNC lathe. Four different PCD tool grades were investigated, namely Diamond Innovations© Compax 1200, 1300, 1500, and 1800. Each of these grades corresponds to a different average diamond grain size, with the exception of Compax 1800, which is comprised of two different grain sizes, as can be seen in the following Table.

Table 5-1. Overview of PCD grades and corresponding average grain size.

PCD Grade	Diamond Particle Grain Size
1200	1.7 μm
1300	6 μm
1500	25 μm
1800	25, 4 μm

Cryogenic pre-cooling temperature was measured using wireless OMEGA© MWTC transmitters and E-type thermocouples embedded in 1 mm diameter holes drilled into the workpiece. For more details on cryogenic pre-cooling temperature measurements and sample geometry section 3.1.1 may be consulted. For all experimental conditions, cryogenic cooling was applied using a proprietary system comprised of a set of conventional cryogenic hoses and valves. Liquid nitrogen flow rate and pressure were kept constant at 0.5 l/min and 150 psi, respectively.

Three custom tool holders were fabricated to assess the effect of rake angle. By using flat rake face CCGW geometry turning inserts, effective rake angles of 0º, -5º, and -10º were achieved. Cutting edge radius modifications were carried out by drag finishing in a mixture of walnut shell and *SiC* abrasives on an OTEC SF-1 stream finishing machine. Edge radii of 10 μm and 14 μm were produced by drag finishing, while the as-received condition of Compax 1200 PCD tools was r_β = 6 μm. High speed cryogenic machining was conducted on an INDEX G200 CNC lathe with a maximum spindle speed of 5000

rpm. Surface roughness measurements were taken on a ZYGO NewView 7300 non-contact SWLI. SEM micrographs were taken with a Hitachi S4300 microscope.

5.3 RESULTS AND DISCUSSION

5.3.1 Determination of a Suitable PCD Cutting Tool Material for Porous Tungsten Machining

While previous studies by Chen, Tarter and Pusavec et al. had demonstrated the ability of PCD cutting tools to generate excellent surface quality in both infiltrant-assisted and cryogenic machining of porous tungsten, no information regarding the relative performance of different PCD grades was available at the beginning of this present study [1, 2, 6, 11]. Because there is a wide variety of different PCD grades with different binders, grain sizes and edge preparations that are commercially available, choosing an appropriate grade for cryogenic machining of porous tungsten requires that careful consideration be given to all features of various PCD grades. First, the binder material used to bond together the millions of polycrystalline diamond particles which perform the cutting action has a strong impact on wear resistance [231-234]. While *Co* remains the most commonly used metallic binder for both carbide and PCD tools, *Ni*, *Nb* and a variety of other materials have been investigated for improved wear resistance and thermal conductivity [231-234].

For cryogenic machining of porous tungsten, Diamond Innovations© provided four highly wear-resistant grades from the Compax product line. Table 5-1 summarizes the average grain sizes of each of the four grades used for the purposes of this study. In simple terms, Compax 1200 is a fine-grained PCD grade with low cutting edge radius for fine finishing of *Al* and *Ti* alloys. As grain size increases from 1.7 μm in Compax 1200 to 25 μm in Compax 1500 and 1800, wear resistance increases when machining Al alloys (information based on correspondence with Diamond Innovations engineers). Notably, transverse rupture strength, a measure of the toughness of brittle tool materials, decreases from 2 GPa for Compax 1200 to 0.85 GPa for Compax 1500. In other words, finer grain

PCD tools are expected to be more resistant to both microscopic and macroscopic (i.e., catastrophic) cutting edge chipping.

All grades of PCD exhibited some degree of inherent brittleness, which is why PCD is commonly only used for continuous machining. Because machining porous materials such as porous tungsten results in a kind of interrupted cut, cutting tool material toughness and resistance to chipping is very important for sustained machining performance. Experimental results for the four PCD materials investigated for cryogenic machining of porous tungsten are summarized below.

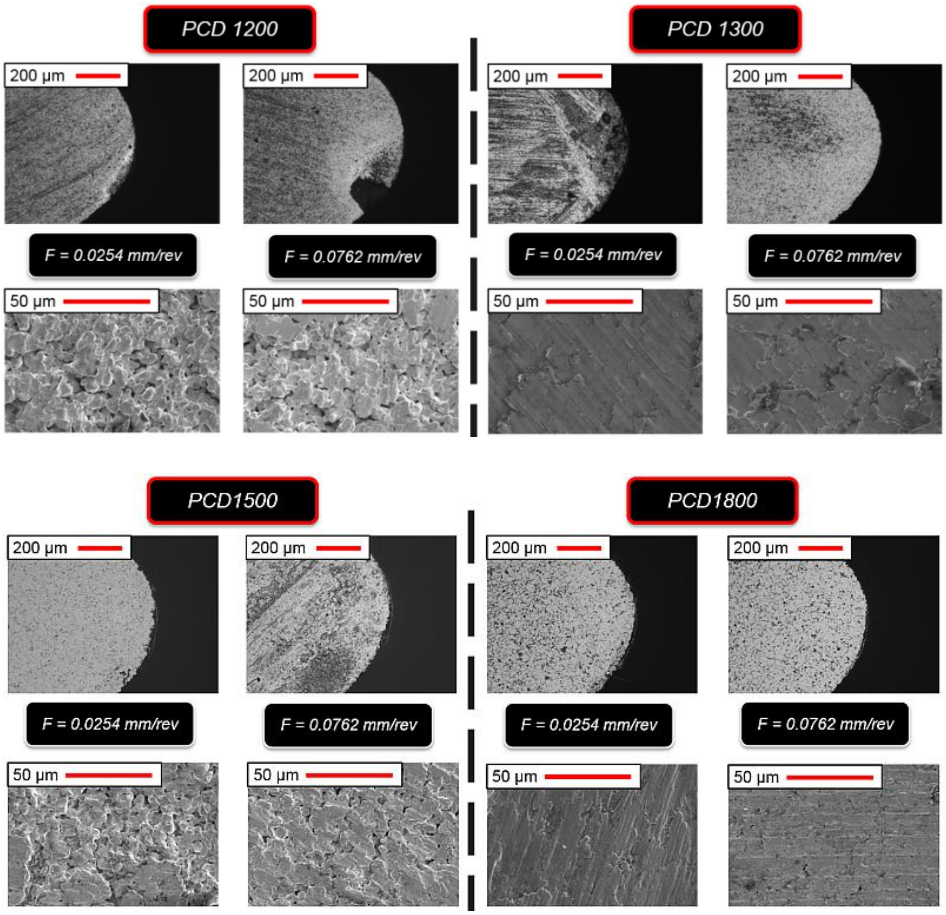

Figure 5-1. Summary of tool-wear and surface morphology for four different PCD tool material grades at two different feeds. Based on these results, PCD 1200 was chosen for its ability to generate excellent surface porosity with low tool-wear.

[v_c = 20 m/min, a_p = 0.127 mm, $t_{pre\text{-}cooling}$ = 180 s]

Based on the results shown in Figure 5-1, Compax 1200 was selected as the most appropriate PCD tool grade for cryogenic machining of porous tungsten. The excellent edge quality of grade 1200 resulted in a highly porous surface with little to no smearing. Because the larger feed of f = 0.076 mm/rev led to both catastrophic edge chipping of the tool and random smearing of the workpiece surface, a lower feed of f = 0.025 mm/rev will be used for further optimization. Interestingly, both Compax 1300 and 1800 exhibited very little tool-wear yet were unable to produce a porous surface. The reason for this effect is likely the relatively large cutting edge radius of both of these grades, which was measured as larger than 10 μm via non-contact white light Profilometry.

A close competitor with Compax 1200, grade 1500 produced excellent surface porosity. However, the relatively large grain size of Compax 1500 resulted in pronounced edge chipping and grain pullout. While the sharp edges of exposed diamond grains likely helped increase surface porosity, tool-life was so poor that e second facing cut could not be completed without catastrophic edge chipping. In contrast to this, Compax 1200 completed 5 facing cuts with very little wear (N < 5 μm). It is hypothesized that the small grain size and higher toughness of Compax 1200 make it well suited for quasi-interrupted finish machining of porous tungsten. Nevertheless, higher cutting speeds that the very low value of v_c = 15 m/min used for this initial investigation (based on cermet optimization results) led to catastrophic edge chipping of all four grades tested. Dealing with the low cutting edge strength of PCD tools will be the subject of subsequent chapters.

5.3.2 Pre-Heated and Dry Machining of Porous Tungsten with PCD Tools

Because porous tungsten is machined primarily by controlled brittle fracture under cryogenic cooling conditions it was hypothesized that pre-heated machining may allow for ductile mode machining. By thermally softening the workpiece material by means of a laser or very high cutting speeds, tool-wear and cutting forces can be reduced in a variety of workpiece materials, ranging from hardened steels to Inconel and titanium alloys [82, 235-239]. Pre-heated machining of porous tungsten was hypothesized to allow for quasi-dense machining due to thermally activated plastic flow. While such

behavior would certainly lead to significant smeared, tool-wear may be reduced by eliminating undesirable cyclical loading of the cutting edge of highly brittle PCD tools.

Unfortunately, pre-heated machining of porous tungsten was shown to not be feasible with cermet, coated carbide and PCD cutting tools. The former tool materials led to complete smearing and severe abrasive wear, more than 300% larger than under comparable dry conditions. The most obvious difference between cryogenic and pre-heated machining of porous tungsten with PCD tools is the presence of uniformly distributed surface cracks across the machined surface. These cracks measure 50-100μm in length and span a width of approximately 10-20 μm. Moreover, the cracks, which indicate that ligaments have been pulled out of the surface, are consistently oriented perpendicular to the direction of machining. Figure 5-2 shows such a surface, along with the corresponding PCD tool-wear image.

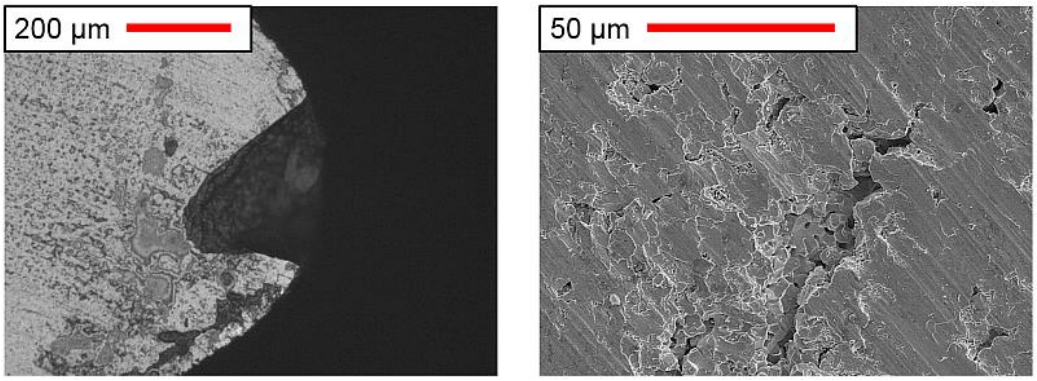

Figure 5-2. SEM micrographs of PCD cutting edge (left hand image) and corresponding machined porous tungsten surface (right hand image). In order to improve the ductility of the porous tungsten workpiece, pre-heating to approximately 200 °C was used. Rather than an improvement in surface quality, large cracks perpendicular to the cutting direction occurred on the machined surface (from the author's published work [3], with permission of Springer, license number 3660871100855).

As Figure 5-2 clearly shows, pre-heated machining of porous tungsten led to catastrophic failure of PCD tools. Such severe edge chipping indicates a unique tool-wear mechanism, most likely due to strong chemical adhesion between the heated tungsten

workpiece and the PCD tool. Similar observations have been made when dry machining *Co*, *Al* and *Ti* alloys with PCD inserts [240-242]. Tanaka et al. [241] proposed that the chipping of PCD tools commonly observed when machining copper occurs via micro-fracture along the grain boundaries of the tool due to thermo-chemical erosion of oxygen at these crack tips. It seems that a similar mechanism may cause the excessive tool-wear during pre-heated machining of porous tungsten. A possible means of avoiding such failure would be to conduct machining in an oxygen-deprived atmosphere. However, this is already the case for cryogenic machining since the strong flow of liquid nitrogen onto the workpiece locally displaces the oxygen from the air.

Since cryogenic machining has already been shown to be an efficient method for machining porous tungsten without the use of a plastic infiltrant, there seems to be no reason to further pursue pre-heated machining. We will therefore focus on the proper use of cryogenic machining rather than pre-heating in the ensuing discussion; dry machining will be used in some cases (for non-PCD tools) to provide a comparative base line. Both dry and pre-heated machining with PCD tools is not possible because of the chemical interactions between tungsten and carbon at elevated temperatures.

5.3.3 The Effects of Rake Angle and Cryogenic Pre-Cooling Temperature

Because of the much higher wear resistance of PCD compared to practically all other tool materials (with the exception of single crystal diamond), it was hypothesized that PCD tools would allow for the effect of tool-wear to be neglected when short cutting distances are used. This turned out to be a valid assumption, as the tool-wear for a single facing cut across a 12 mm diameter porous tungsten was so small that not even SEM microscopy could detect any meaningful tool-wear ($VB_C < 10$ μm). Part of the reason for the very low tool-wear was the short cutting length as well as the low cutting speed of $v_c = 20$ m/min, which was adopted from previous experiments with negative rake angle cermet tools.

In order to gain a more nuanced understanding of the effect of rake angle and cryogenic pre-cooling on as-machined surface integrity of porous tungsten, three different rake angles and two different pre-cooling conditions were investigated. Rather

than using pre-cooling time, as was the case during cryogenic machining experiments with cermet tools, bulk workpiece temperature was measured. Temperature measurement was achieved by means of wireless thermocouple emitters attached to the lathe's chuck. The results obtained from this experiment is shown in the following Figure.

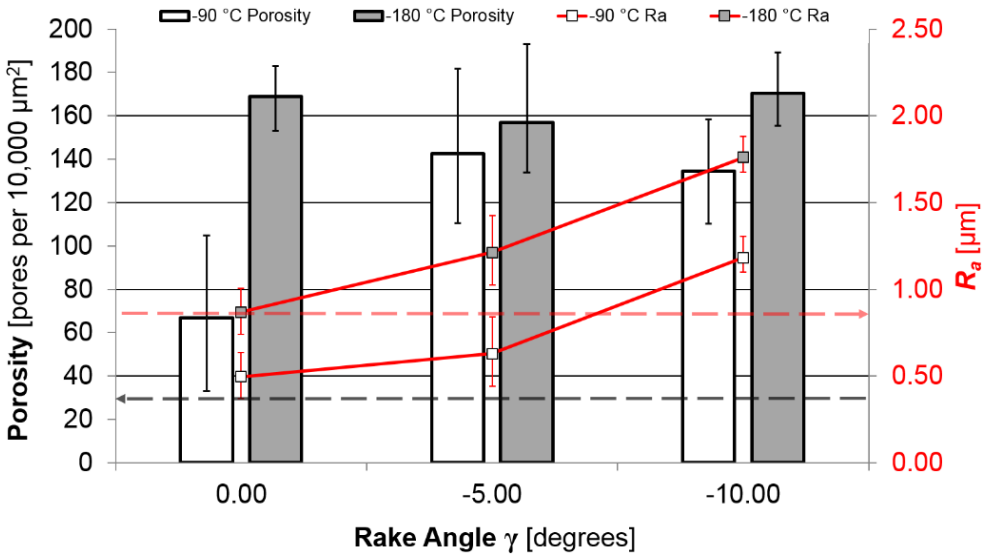

Figure 5-3. Surface morphology of cryogenically machined porous tungsten as a function of rake angle and as-pre-cooled cryogenic bulk workpiece temperature. Compax 1200 PCD cutting tools with an average cutting edge radius of $r_\beta \approx 6$ µm were used. Dashed arrow represent the acceptability limits for porosity (30, gray) and R_a (0.8, red). [v_c = 20 m/min, a_p = 0.1 mm, f = 0.025 mm/rev]

As can be seen in Figure 5-3, both rake angle and cryogenic pre-cooling temperature of the porous tungsten workpiece have significant effects on as-machined surface morphology. Surface roughness, which is represented by red lines in Figure 5-3, increases almost linearly as rake angle becomes more negative. It is hypothesized that there are three primary reasons for this effect. First, more negative rake angles have been documented by various researchers to increase cutting force/pressure, i.e., stress intensity in the primary deformation zone [87, 96, 101, 102, 104, 124]. As stress intensity is increased, porous tungsten becomes more prone to brittle intergranular fracture. Fracture

pits are formed on the machined surface because of the high cutting pressure exerted by the cutting edge.

The second reason for increased surface roughness is an increase in strain rate as rake angle decreases. This effect has been described in micromachining, where effective rake may become very negative due to small undeformed chip thickness values [93, 103, 105, 107]. Tungsten exhibits significant strain rate sensitivity, particularly at low temperatures when there is no thermal energy to allow for ductile deformation [211, 243, 244]. Therefore, more negative rake angles are expected to increase the severity of brittle fracture due to an increase in strain rate as well as stress intensity.

The third reason for increased surface roughness of cryogenically machined porous tungsten with more negative rake angles is difficulty of chip evacuation. The more negative rake angle is, the smaller the space for chips to accumulate ahead of the cutting edge becomes. Therefore, negative rake angles have a propensity towards BUE formation [79, 97, 98]. BUE has already been documented to have a detrimental effect on the surface roughness of porous tungsten in the previous chapter of cryogenic machining with cermet cutting tools as well as the author's published work [3, 4].

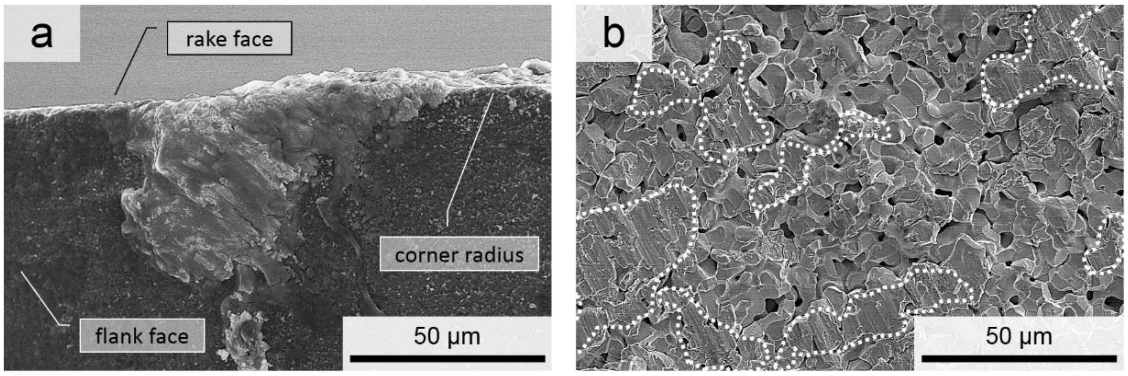

Figure 5-4. SEM micrographs of PCD cutting edge with significant BUE of tungsten on the flank face as well as the corresponding cryogenically machined surface. Smeared islands of re-deposited tungsten chip fragments are highlighted with white dashed lines. [v_c = 20 m/min, a_p = 0.1 mm, f = 0.025 mm/rev, $T_{pre\text{-}cooling}$ = -180 °C]

The primary mechanism of surface degradation when BUE is present during cryogenic machining of porous tungsten is hypothesized to be chip re-deposition, i.e., unstable BUE. By both effectively increasing cutting edge radius, i.e., effective rake angle, and also by creating randomly distributed smeared islands on the machined surface, BUE results in significant scatter in both surface roughness and porosity. Therefore, BUE needs to be eliminated in order to obtain a uniform, finely finished surface in porous tungsten. Evidence for BUE when cryogenically machining porous tungsten with a negative rake angle of $\gamma = -10^{o}$ can be seen in Figure 5-4.

Similar to the effect of rake angle, cryogenic pre-cooling temperature has a strong effect on both surface roughness and surface porosity. Surface roughness, which is shown in Figure 5-3, increased by a factor of 2 when cryogenic pre-cooling was increased from -90 ºC to -180 ºC. The primary reason for the increase in surface roughness with cryogenic pre-cooling was an increase in brittle fracture. Porous tungsten exhibits a brittle to ductile transition (BDT) as a result of its BCC crystal structure [230, 245-247]. Clearly, cryogenic pre-cooling to -180 ºC is sufficient to increase the amount of brittle fracture during machining by keeping the cutting temperature below the BDT temperature of porous tungsten. Microscopy evidence for this fact can be seen in Figure 5-4 as well as Figure 5-5.

Interestingly, limited pre-cooling to -90 ºC along with a neutral rake angle (i.e., $\gamma = 0^{o}$) resulted in significant smearing, which can be seen in Figure 5-5c. This observation suggests that when limited pre-cooling is used, the BDTT of tungsten is exceeded. When limited pre-cooling is employed with a negative rake angle of -5º, an excellent surface with low roughness yet high surface porosity may be obtained. The reason for the increase in surface porosity as rake angle becomes more negative is hypothesized the suppression of burr formation, i.e., smearing of pores. By increasing stress intensity ahead of the cutting edge, smearing is decreased because rather than filling in pores, a chip may be formed. In micromachining, as in finish machining, micro-burr formation is a common problem that may be reduced by selecting smaller cutting edge radius and more negative rake angle [248, 249]. It should be noted that larger cutting edge radii also result in more negative effective rake angles along the cutting edge, assuming that uncut chip thickness is smaller than cutting edge radius.

More negative effective rake angles from larger cutting edges do however not prevent smearing, as evidenced by the commonly observed reduction in porosity with increasing tool-wear, which leads to increased cutting edge radius. To better study the nature of rake angle of sharp ($r_\beta \approx 6$ μm) PCD cutting tools on as-machined surface morphology, the following Figures were prepared.

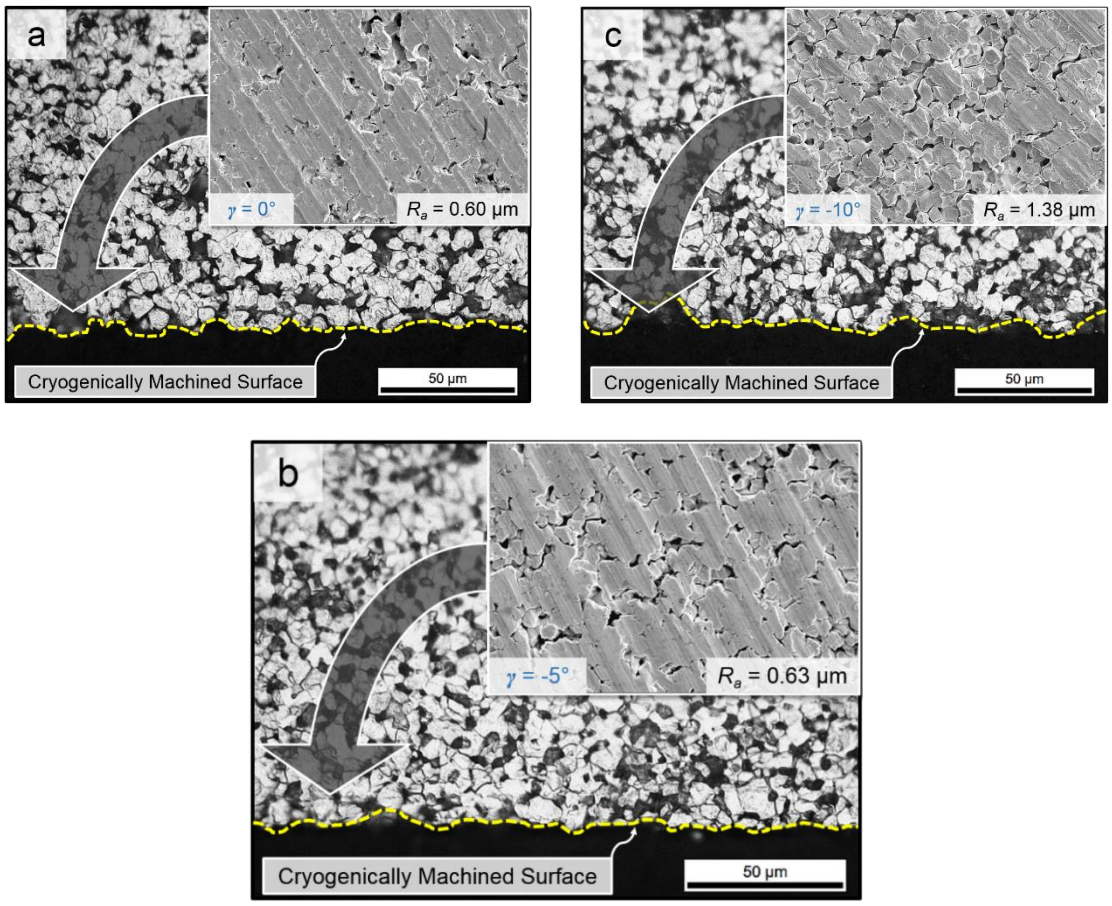

Figure 5-5. Combination of optical micrographs showing cross-sections of cryogenically machining tungsten as well as SEM micrographs of the machined surface. Surface roughness of the machined surface is included in the bottom left hand corner and each set of micrographs corresponds to a different rake angle, namely 0º (a), -5º (b), and -10º (c). The optimum surface morphology obtained can be seen in (b), which is a combination of low surface roughness and high surface porosity.

[v_c = 20 m/min, a_p = 0.1 mm, f = 0.025 mm/rev, $T_{pre\text{-}cooling}$ = -90 °C]

Figure 5-5 was included to illustrate the effect of rake angle on surface and sub-surface morphology of cryogenically machined porous tungsten. No 'white layer' or similar severely deformed layer can be observed in the optical cross-sectional micrographs. Because SEM images of the machined surface clearly show that some smearing, i.e., plastic flow, occurred, it can be concluded that the deformed layer is very thin (less than one micron). Therefore, even the highly smeared surface shown in Figure 5-5c did not result in closing of sub-surface pores. Considering the etching effect of the *Ba* impregnate that is introduced into the pores during the final stages of the manufacturing of dispenser cathodes, it is likely that the very thin smeared layer of all the surfaces shown in Figure 5-5 would be chemically removed. In fact, the amount of material removal by the *Ba-Ca* may be as high as several microns.

As a result, surface roughness may be prioritized over as-machined surface porosity. Highly porous surfaces, such as the ones shown in Figures 5-4 and 5-5c (i.e., $\gamma = -10^{o}$) suffer from deep fracture pits. When machining parameters are carefully chosen, both these fracture pits and smeared islands may be eliminated. Since no BUE was observed when limited pre-cooling was applied along with rake angles of 0^{o} and -5^{o}, it seems that limited pre-cooling and slightly negative rake angles allow for the elimination of BUE. Pre-cooling to -180 ^{o}C resulted in BUE under all conditions, further supporting the hypothesis that brittle fracture chips are primarily responsible for BUE in cryogenic machining of porous tungsten. Despite the low cutting speed and cryogenic pre-cooling to -90 ^{o}C used to machine porous tungsten with PCD cutting tools, sufficient heat is generated during the machining process to allow for enough ductile to prevent brittle fracture ahead of the cutting edge. Because achieving limited pre-cooling to -90 ^{o}C is difficult to reliably implement for automated production of a wide range of dispenser cathode geometries, a different solution from the one pursued during the controlled experimental conditions used in a laboratory needs to be developed. For this purpose, cryogenic high speed machining was investigated.

5.3.4 Cryogenic High Speed Machining of Porous Tungsten

In order to obtain the excellent surface quality shown in Figure 5-5c, a cutting speed of 20 m/min with a sharp (r_β = 6 µm), as-supplied fine grained PCD cutting tool was used. Moreover, a rake angle of -5º allowed for significantly increased surface porosity without sacrificing surface roughness. Unfortunately, limited cryogenic pre-cooling to a bulk workpiece temperature of -90 ºC was necessary for sufficient ductility in the workpiece material to prevent undesirable brittle fracture and BUE and thus reduce surface roughness. Because cutting speed has a direct impact on cutting temperature, it was hypothesized that by using higher cutting speed and long with easily implemented pre-cooling to -180 ºC (i.e., the temperature of liquid nitrogen) would allow for an optimum surface to be reliable obtained. At the same time, higher cutting speeds would also boost productivity, further justifying the increased cost per cutting edge of PCD cutting tools.

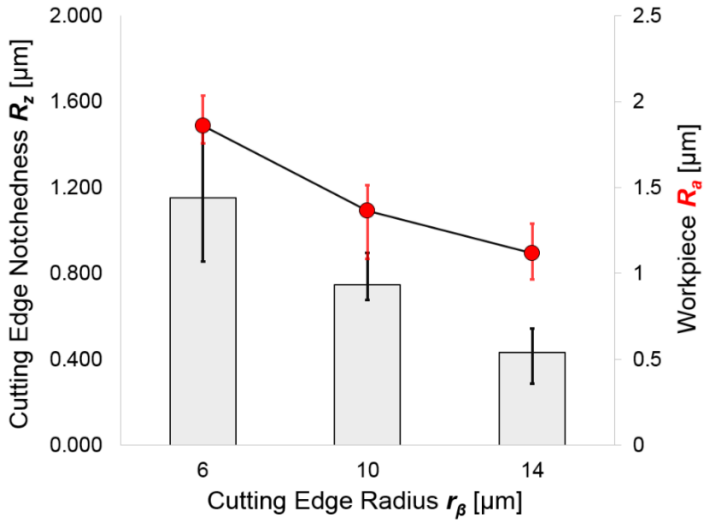

Figure 5-6. Correlation between cutting edge notchedness and as-machine workpiece roughness as a function of cutting edge radius for drag finished Compax 1200 PCD tools (from the author's published work [250], with permission of IEEE).
[v_c = 20 m/min, a_p = 0.1 mm, f = 0.025 mm/rev, $T_{pre\text{-}cooling}$ = -180 °C]

Figure 5-6 summarized the effect of drag finishing of PCD tools on cutting edge notchedness and workpiece surface roughness from cryogenic machining. Due to the

high brittleness and relatively low cutting edge strength of PCD cutting tools, cryogenic high speed machining with as-supplied upsharp ground tools resulted in unpredictable catastrophic tool failure beyond cutting speeds of approximately 100 m/min. In order to improve the resistance of PCD tools to edge chipping, drag finishing was used to reduce cutting edge notchedness and increase cutting edge radius.

As cutting edge radius is increased by longer drag finishing process time, which increases exponentially due to increased wear resistance of rounded tools, notchedness is likewise reduced. The processing time to achieve a radius of 14 μm was more than 5 times longer than that required to hone an upsharp edge from 6 μm to a light hone with 10 μm radius. Because of the substantial decrease in cutting edge notchedness with increasing drag finishing time (and thus r_β), tool-life was likewise expected to increase. The primary failure mechanism of upsharp PCD tools in porous tungsten was pullout of diamond grains and ultimately fracture of the cutting edge. By removing imperfections along the cutting edge, chip flow is improved while the likelihood of diamond grain pullout is dramatically reduced. As a result, abrasive wear may become the dominant wear mechanism, leading to predictable tool-life.

Using drag finished Compax 1200 PCD cutting tool with a uniformly rounded cutting edge (r_β = 10 μm), cryogenic high speed machining at cutting speeds up to 400 m/min was achieved. The as-machined surface roughness of the porous tungsten samples from this study can be seen in Figure 5-7. The motivation for modifying the cutting edge radius of PCD tools was to achieve both improved productivity (tool-life, cutting speed/feed) and more easily implemented cryogenic flood cooling by controlling cutting temperature, i.e., cutting mechanism.

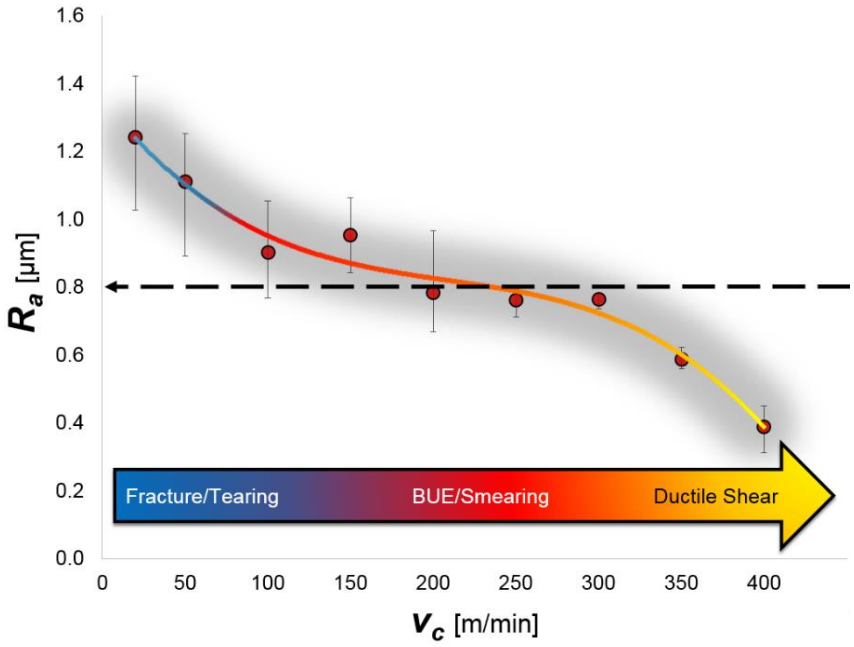

Figure 5-7. Surface roughness as a function of cutting speed with modified cutting edge radius PCD tool. By increasing cutting edge strength, cryogenic high speed machining was achieved. The cutting mechanism can be fine-tuned by altering cutting speed while cryogenic flood-cooling is applied.

[a_p = 0.1 mm, f = 0.025 mm/rev, $T_{pre\text{-}cooling}$ = -180 °C, r_β = 10 µm, γ = -5°]

The trend of surface roughness as a function of cutting speed shown in Figure 5-7 does indeed suggest that there is a shift between three distinct machining mechanisms as cutting speed (and thus temperature) increases. While there is large scatter in R_a at low cutting speeds (v_c < 100 m/min) due to brittle fracture and tearing of the workpiece surface, very low surface roughness was attained at high cutting speeds (v_c > 300 m/min). It is hypothesized that beyond a critical cutting speed, sufficient heat is generated in the primary deformation zone to exceed the BDTT of porous tungsten, leading to severe plastic deformation of the machined surface and thus low surface roughness. Under the experimental conditions used to obtain the data shown in Figure 5-7, this critical cutting speed likely occurred around $v_c \approx$ 250 m/min, since scatter in R_a is significantly reduced at this speed.

Between fracture and tearing and low cutting speeds and ductile shear at high cutting speeds, BUE and chip re-deposition occurs. As described in earlier chapters, BUE is hypothesized to be due to impingement of small fracture chips at low to intermediate cutting speeds. Therefore, BUE is of course present at low cutting speeds when fracture is the dominant machining mechanism. As cutting speed is increased, the BDTT of porous tungsten may be locally exceeded, allowing for localized plasticity. When adhered tungsten fragments begin to flow more easily as temperature increases, chip re-deposition likely occurs more frequently. Consequently, surface roughness is reduced since more even smearing fills in deep fracture pits that remain unsmeared at low cutting speeds. Once the BDTT is exceeded, BUE is hypothesized to disappear because both chips and the machined surface may flow without tearing. In other words, the necessary conditions for BUE, small fracture chips, is eliminated as ductile shear becomes dominant.

In addition to surface roughness, tool-wear also reflects the shift from fracture towards ductile shear as the dominant machining mechanisms. Even more pronounced than the transition from high surface roughness with significant scatter at low speeds to very low roughness with low scatter at high speeds, the data shown in Figure 5-8 exhibits a step like shift in nose wear at a critical cutting speed of $v_c \approx 250$ m/min. The sudden transition in nose wear at $v_c \approx 250$ m/min is hypothesized to coincide with the BDT of porous tungsten. At low cutting speeds up to 200 m/min, brittle fracture machining and the resultant phenomenon of BUE lead to both abrasive and attrition wear. The latter is a result of chip re-deposition, which involves sliding of tungsten fragments across the cutting edge. During this process, some material may be removed from the cutting edge. As cutting speed increases, more smearing occurs (i.e., BUE destabilizes). Consequently, tool-wear increases as cutting speed is increased, as would be expected in any machining operation. Once the BDTT of porous tungsten is exceeded, however, brittle fracture chips and thus BUE disappear. As a result, the dominant tool-wear mechanism changes from attrition wear towards abrasion.

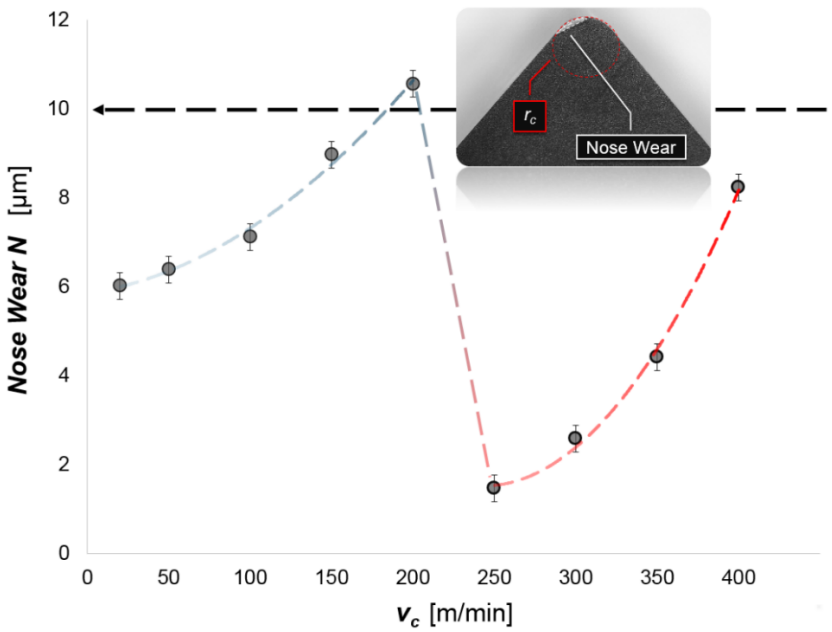

Figure 5-8. Nose wear as a function of cutting speed. At a critical cutting speed ($v_c \approx 250$ m/min), there is a shift in the dominant wear mechanism due to a change in the machining mechanism (i.e., material properties) of porous tungsten. An optical micrograph of a PCD cutting tool in plan view of the rake face is included to illustrate the meaning of nose wear.

[a_p = 0.1 mm, f = 0.025 mm/rev, $T_{pre\text{-}cooling}$ = -180 °C, r_β = 10 µm, γ = -5º]

Because the workpiece material and chip may slide freely during ductile shear machining, tool-wear is significantly reduced. However, the increase in cutting temperature necessary to achieve ductile deformation of porous tungsten also places significant thermal stress on the PCD cutting tool. As cutting speed is increased beyond the BDT cutting speed of $v_c \approx 250$ m/min, nose wear increases rapidly. Nevertheless, the acceptability condition of $N < 10$ µm is met even at $v_c = 400$ m/min. Because of the much lower tool-wear of PCD tools during cryogenically cooled ductile shear machining, significant improvements in productivity during rough and pre-finish machining of infiltrated porous tungsten may be realized.

While current industry practice is to machine plastic infiltrated porous tungsten pellets at cutting speeds of approximately 20 m/min, cryogenic high speed machining at

v_c = 250-350 m/min would result in a productivity increase of a factor of 10, without even considering potential increases in feed and depth of cut. Likewise, tool-wear of lightly honed (r_β = 10 μm) PCD tools during shear machining of porous tungsten is so low that a very large number of acceptable workpieces could be machined without changing the cutting tool. Because the amount of time necessary for an operator to change the cutting tool may be as much as 10 min due to the very small geometric tolerances of dispenser cathodes, the productivity increase due to tool-life alone may justify the cost of PCD over "less expensive" carbide and cermet tools; in other words, cost per cutting edge does not reflect the true cost of a given cutting tool material. Determining the most economical choice of cutting tool material is of course outside the scope of this present study. Nevertheless, the quantitative findings presented here (tool-life, attainable cutting speeds/feeds, etc.) will certainly be necessary in this endeavor.

Surface roughness and tool-wear data shown in Figures 5-7,8 have been interpreted as conclusive evidence of a transition in machining mechanism of porous tungsten with cutting speed. To further study the effect on cutting speed on the as-machined surface morphology of porous tungsten, Figure 5-9 was prepared.

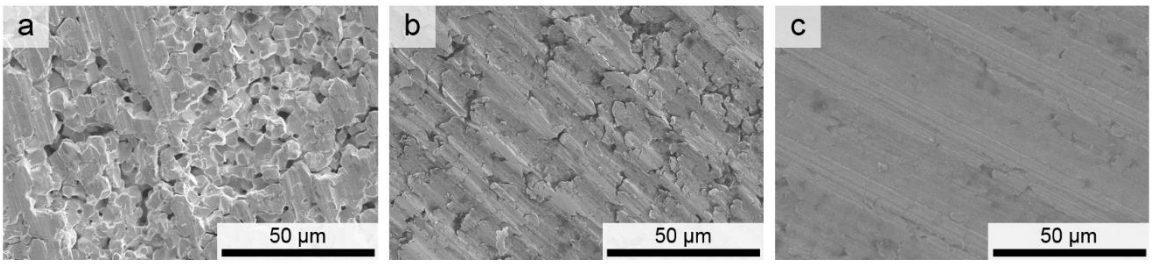

Figure 5-9. SEM micrographs of surface morphology of porous tungsten as a function of cutting speed. At low speeds (v_c = 100 m/min), fracture and tearing occurs (a). As cutting speed increases (v_c = 250 m/min), severe smearing due to localized plasticity reduces surface roughness (b) until ductile shear machining at very high cutting speeds (v_c = 350 m/min) yields very fine surface finish (c).
[a_p = 0.1 mm, f = 0.025 mm/rev, $T_{pre\text{-}cooling}$ = -180 °C, r_β = 10 μm, γ = -5°]

The morphology of cryogenically machined porous tungsten surfaces shown in Figure 5-9 further supports the hypothesized transition from brittle fracture towards ductile shear with increasing cutting speed. Deep fracture pits at a cutting speed of 100 m/min (Figure 5-9a) and smeared islands are consistent with the hypothesized machining mechanism of intergranular cracks moving ahead of the cutting edge, resulting in tearing and small fracture chips. Because not all dust-like fracture chips can be removed from the cutting area, some of these chips adhere to the cutting edge as shown in Figure 5-4. The increased cutting edge radius of r_β = 10 μm further decreases the effective rake angle, which further impedes chip flow/removal and thus increases the likelihood of BUE. Once the BDT of porous tungsten is exceeded at $v_c \approx 250$ m/min, fracture pits (and likely BUE) disappear, as can be seen in Figure 5-9b. At the very high cutting speed of v_c = 350 m/min, severe plastic deformation of the machined surface is clearly evident (see Figure 5-9c). In fact, the workpiece material flowed so freely that feed lines resulting from the rounded corner of the cutting tool are clearly visible.

Despite the excellent surface roughness of porous tungsten machined via ductile shear at high cutting speeds, little to no surface porosity was attained. The best combination of low surface roughness and high surface porosity is shown in see Figure 5-9b was achieved at a cutting speed of v_c = 250 m/min, i.e., at the BDT. Because reaching such high cutting speeds required the use of honed PCD cutting tools, most surface pores are smeared even under 'optimum' conditions. It can be concluded that a cutting edge radius of r_β = 10 μm is simply too large to avoid smearing of pores in 80% density porous tungsten.

By comparing the phenomenon of smearing to burr generation, it seems that the only way to prevent smearing is to select a (much) smaller ("sharp") cutting edge radius (r_β < 6 μm) along with a slight negative rake angle. Since it was already determined that a rake angle of $\gamma \approx -5^o$ yields optimum surface morphology (when r_β = 6 μm), it can be concluded that a sharp cutting edge is a necessary condition for open surface porosity in porous tungsten. Because low cutting speeds necessary to avoid catastrophic tool failure of sharp edged PCD tools, high speed finish machining of porous tungsten is problematic to implement. Improvements in PCD and PCBN materials research may lead to the development of very sharp yet tough (fracture resistant) cutting tools necessary to obtain

the best possible finish in porous tungsten. Chapter 6 will address finish machining of porous tungsten at relatively low cutting speeds (v_c < 100 m/min) with very sharp cutting tools (r_β = 2 μm), considering critical chip thickness effects. In this way, fracture can be avoided even when cryogenic flood cooling and low cutting speeds are used. Extending these findings to modern nano-grain PCD tool grades, which are beginning to be offered by several cutting manufacturers, will be the subject of future studies.

If surface pores were larger, as is the case in some powdered steels and porous titanium foams, a larger cutting edge radius would likely be sufficient to prevent smearing of pores (assuming open surface porosity is in fact a desirable characteristic). If a certain application requires complete smearing of surface pores, as is the case for the rear surface of dispenser cathodes, a larger cutting edge radius and very high cutting speed do allow for a quasi-dense surface to be obtained, as can be seen in Figure 5-9c. In short, the functional characteristics of each surface of a given component will dictate the most appropriate choice of cutting speed and edge radius for 'optimum' surface morphology.

5.4 CHAPTER CONCLUDING REMARKS

Cryogenic of porous tungsten with PCD cutting tools offered a variety of benefits compared to other cutting tool materials such as (tungsten-) carbide and cermet. Dry and pre-heated machining of porous tungsten with PCD tools was not feasible due to catastrophic edge chipping, which was hypothesized to occur as the result of high temperature chemical interactions between carbon, oxygen and tungsten. In cryogenic machining, the very high wear resistance of PCD led to low tool-wear, especially when a fine-grained PCD grade is selected. Using such tools (Diamond Innovations© grade Compax 1200, 1.7 μm average grain size), the effects of rake angle and cryogenic pre-cooling were explored. Limited cryogenic pre-cooling of the workpiece to -90 ºC and a negative rake angle of γ = -5º resulted in optimum surface morphology when as-received PCD tools were used (r_β = 6 μm).

Further improvements in terms of wear resistance and thus the maximum attainable cutting speed were made by modifying a set of PCD tools by using drag finishing (r_β = 10, 14 μm). A linear relationship between cutting edge notchedness and as-machined surface existed for drag finished (honed) PCD tools. As a result of increased edge stability, cryogenic high speed cutting up to v_c = 400 m/min was achieved. The relatively high cutting edge radius (r_β = 10 μm) of the modified PCD tools used for cryogenic high speed machining resulted in little to no surface porosity yet surface roughness as low as R_a = 0.4 μm (recall dispenser cathode acceptability criterion: R_a < 0.8 μm). Based on SEM micrographs of machined porous tungsten surfaces as well as tool-wear and surface roughness data, two key machining mechanisms were identified, namely fracture and ductile shear. The brittle to ductile transition (BDT) of porous tungsten was observed at a cutting speed of approximately $v_c \approx$ 250 m/min.

CHAPTER 6.

CHIP THICKNESS EFFECTS ON MODE OF MACHINING IN CRYOGENIC AND DRY MACHINING OF POROUS TUNGSTEN

6.1 INTRODUCTION

Cryogenic high speed machining of porous tungsten has been shown to be capable of producing excellent surface quality. However, in order to prevent catastrophic edge chipping of PCD tools at high cutting speeds, honing of the cutting edge to a radius of $r_\beta \geq 10$ µm is necessary. Since surface pores are smeared shut when cutting edge radius exceeds 6 µm, cryogenic high speed machining results in complete smearing of pores. Moreover, the machining mechanism of porous tungsten at high cutting speeds is ductile shear, which further increases smearing. Cryogenic high speed machining may therefore be used for efficient rough and semi-finish machining yet not for the final finishing pass of dispenser cathode emitting surfaces which require open surface porosity.

In order fulfill the dispenser cathode industry standard of at least 30 open pores per 10,000 µm^2, sharp-edged ($r_\beta \leq 6$ µm) cutting tools need to be used. To ensure process security (i.e., avoid unpredictable tool failure), low cutting speeds $v_c < 100$ m/min need to be used. Unfortunately, cryogenic machining of porous tungsten at low cutting speeds generally results in undesirable brittle fracture of the workpiece material. Fracture machining chips furthermore tend to adhere to the cutting edge and re-deposit onto the machined surface (unstable BUE). The resulting machined surface morphology is a combination of deep fracture pits and smeared islands, the latter being a result of re-deposition of small fracture chips. Using limited cryogenic pre-cooling along with a negative rake angle of -90 ºC has been shown to virtually eliminate fracture pits and thus BUE. Good surface roughness ($R_a \approx 0.6$ µm) and high surface porosity can be obtained when limited pre-cooling is used. However, pre-cooling to a specific workpiece temperature is nearly impossible to implement in an industrial setting and also leads to a number of undesirable problems such as thermal contraction and freezing of the machine tool spindle.

By considering critical chip thickness effects in porous tungsten, it is hypothesized that cryogenic flood cooling with upsharp cutting tools at low cutting speeds may be used to obtain fracture-free surfaces. Critical chip thickness is a concept developed in the context of machining of very brittle materials such as glass and ceramics [114, 117]. The most basic definition of *critical chip thickness* is the *undeformed chip thickness of a brittle material beyond which brittle fracture occurs*. Implied by this definition is the fact that below the critical chip thickness (h_c), ductile machining occurs [114, 116]. Much of the early work on ductile mode machining of brittle materials was carried out by Bifano, Blackley and Scattergood et al. [108, 109, 114] in the early 1990s. By using the theory of indentation of brittle materials, the critical feature size (i.e., critical infeed or critical chip thickness) can be calculated as a function of the hardness *H*, fracture toughness K_{1C} and Young's modulus *E* of the workpiece material, scaled by a constant α as $d_c = \alpha * \left(\frac{E}{H}\right)\left(\frac{K_{1c}}{H}\right)^2$ (i.e., equation 2.2) [111, 118, 251]. More recent work by Arif et al. [119, 124, 126] also considered the thermodynamic energy balance between brittle and ductile deformation in brittle materials as a function of feature size to analytically predict h_c.

Because porous tungsten is macroscopically brittle at room temperature, it is hypothesized that there is a critical chip thickness effect. However, the currently available theories regarding ductile mode machining of brittle materials assume dense and highly brittle materials. While porous tungsten is very brittle, it is not as brittle as most ceramic materials. When using equation 2.2 for dense polycrystalline tungsten, a critical uncut chip thickness of more than 40 μm is calculated, which is clearly larger than commonly encountered chip thickness values in finish turning. Consequently, any critical chip thickness effect in porous tungsten can be assumed to be a result of the pore and ligament morphology rather than the inherent brittleness of tungsten. Determining the hardness and fracture toughness of porous materials is problematic due to the effect of porosity on both measures [252-254]. Therefore, equation 2.2 cannot be used to meaningfully predict the h_c in porous tungsten. As an alternative, a qualitative empirical model for ductile mode machining of porous materials will be developed.

To empirically determine h_c for 80% density porous tungsten, dry and cryogenic machining experiments were carried out. Based on previous observations, it was assumed that $h_c < 20$ µm. Arif et al. [121, 122, 124, 125] described a method for productive ductile mode machining of tungsten carbide by controlling the point at which critical chip thickness occurs to prevent any cracks from reaching the final machined surface. Because cryogenic machining of porous tungsten often leaves deep fracture pits on the machined surface it was assumed that ductile mode machining would only occur when $h_{max} < h_c$. In other words, fracture is either avoided completely or cracks will reach and degrade the machined surface. To better illustrate the qualitative basis for the model of critical chip thickness effects in porous tungsten machining the following Figures were prepared.

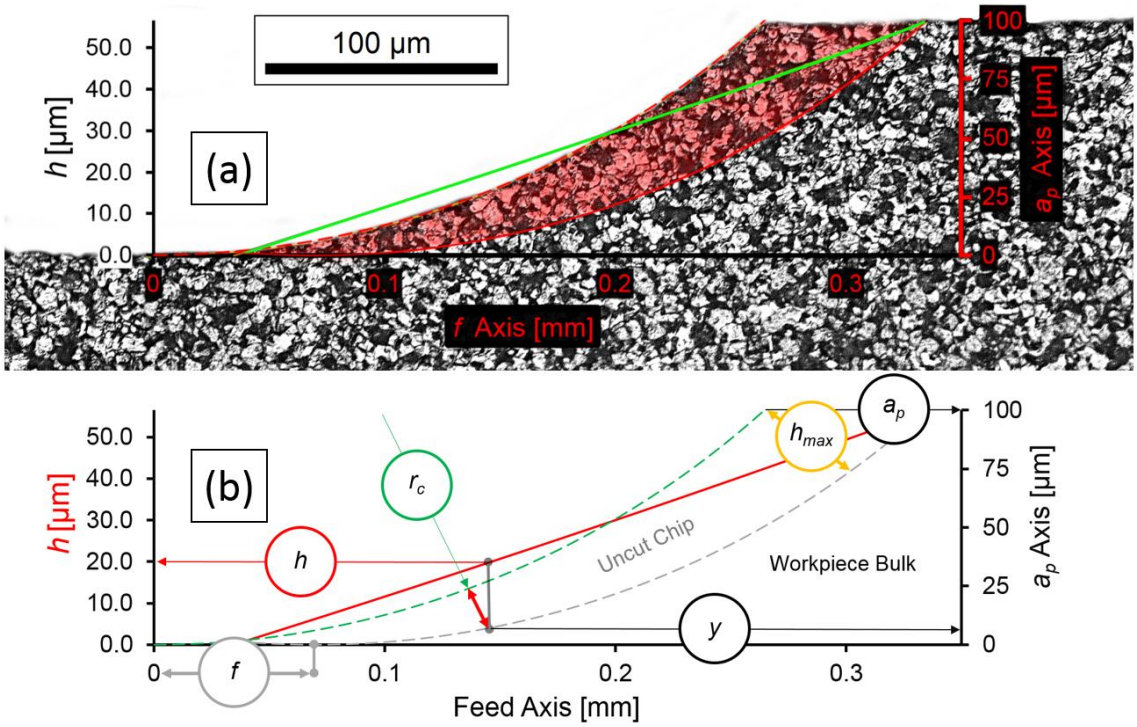

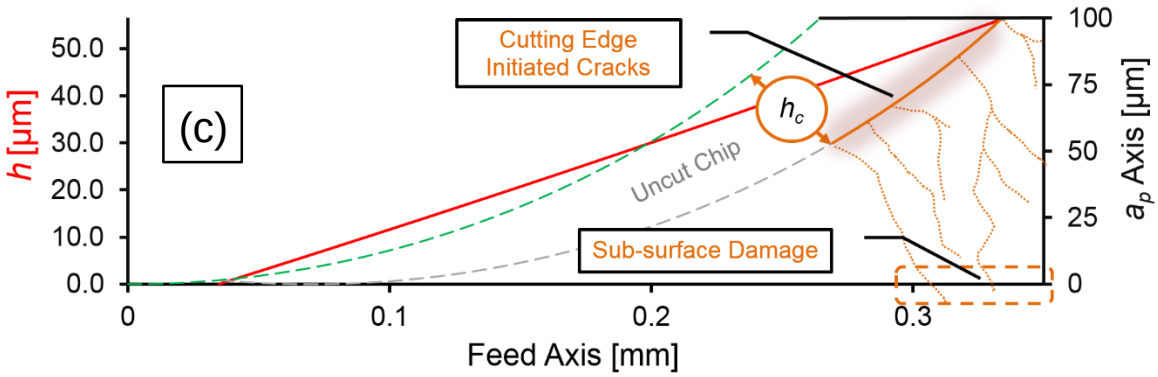

Figure 6-1. Optical micrograph of 80% density porous tungsten with overlay of uncut chip thickness geometry (f = 0.07 mm/rev, r_c = 0.8 mm) (a) and schematic of generic uncut chip geometry for machining with circular tool of radius r_c (b), as well as schematic of critical chip thickness model for porous tungsten machining (c).

Figure 6-1a shows the geometry of the uncut chip in 80% density porous tungsten with a depth of cut of a_p = 0.1 mm, feed of f = 0.03 mm/rev and tool corner radius r_c = 0.8 mm. When examining the left hand axis on the same Figure, it can be seen that the maximum chip thickness of this cut is approximately $h_{max} \approx 20$ µm. Figure 6-1b outlines the process of graphically determining the uncut chip thickness at a given point on the corner radius. As is common for finish machining, the uncut chip thickness near the final machined surface in Figure 6-1a becomes very small, in fact $h_{max} < 10$ µm at 25 µm above the machined surface and $h_{max} < 5$ µm at about 5 µm higher than the finished surface. Because of the finite sharpness of the cutting tool, some ploughing is therefore to be expected, especially when small feed and large corner radius are used. The minimum chip thickness h_{min}, below which ploughing occurs, is highlighted in green in Figure 6-1c. The critical chip thickness h_c, above which fracture occurs, is likewise emphasized with a red circle. The uncut chip thickness h at any point a distance y above the machined surface (in the direction of depth of cut a_p) can be calculated by Eq. (6-1):

$$h(f, r_c, y) = r_c - \sqrt{f^2 + r_c^2 - 2 f r_c \cos\left(\frac{\pi}{2} - cos^{-1}\left(\frac{r_c - y}{r_c}\right)\right)} \tag{6-1}$$

The maximum uncut chip thickness can be obtained from Eq. (6-1) by setting the distance *y* equal to the depth of cut a_p, i.e., $h_{(y = a_p)} = h_{max}$. The mathematical description of *y* as a function of the local chip thickness *h*, the feed *f* and the corner radius of the cutting tool r_c is given by Eq. (6-2):

$$y(h, f, r_c) = \frac{8f^2 r_c - \sqrt{64f^4 r_c^2 - 16f^2\left(f^4 - 2f^2h^2 + 4f^2 h r_c + h^4 - 4h^3 r_c + 4h^2 r_c^2\right)}}{8f^2} \tag{6-2}$$

Equation 6-2 can be used to determine the influence of feed and corner radius on the depth of cut necessary to achieve a certain desired uncut chip thickness. Practically, this allows for optimization of the feed, depth of cut and cutting tool nose radius when the minimum and/or critical chip thickness value are known. A simpler version of Eq. (6-2) can be obtained when the relationship between feed, corner radius and surface roughness (Eq. 6-3) is used to substitute *f* in Eq. (6-2).

$$R_a(kinematic) = \frac{f^2}{32 r_c} \rightarrow f = \sqrt{32 R_a r_c} \tag{6-3}$$

$$y(h, R_a, r_c) = \frac{256 r_c^2 R_a - \sqrt{\left(256 r_c^2 R_a\right)^2 - 512 r_c R_a\left(h^4 - 4h^3 r_c + 4h^2 r_c^2 - 64 r_c R_a + 128 h r_c^2 R_a + 1024 r_c R_a^2\right)}}{256 r_c R_a} \tag{6-4}$$

Since $r_c \gg R_a$, corner radius can be eliminated from Eq. 6-4, in other words:

$$\lim[y(h, r_c, R_a)]_{r_c \to 1} \approx y(h, R_a)$$

$$\text{Thus, } y(h, R_a) = \frac{256 R_a - \sqrt{(256 R_a)^2 - 512 R_a\left(h^4 - 4h^3 + 4h^2 - 64 R_a + 128 h R_a + 1024 R_a^2\right)}}{256 R_a} \tag{6-5}$$

Equation (6-5) is equivalent to Eq. (6-2), yet it enables the calculation of the depth of cut necessary to achieve a certain uncut chip thickness (in this context h_c) as a function of kinematic roughness only. The manner in which a given value of kinematic roughness is achieved, i.e., which combination of feed and corner radius is used, evidently does not affect the depth of cut at which a certain chip thickness occurs. Therefore, Eq. (6-5)

places a firm limit on the maximum depth of cut that may be taken when $h \leq h_{max}$ as function of kinematic roughness. This geometric phenomenon can be exploited to achieve significant productivity increases since it allows for the use of very large corner radii as long as feed is adjusted accordingly to keep kinematic roughness fixed (or within an acceptable range), as can be seen in the following plot.

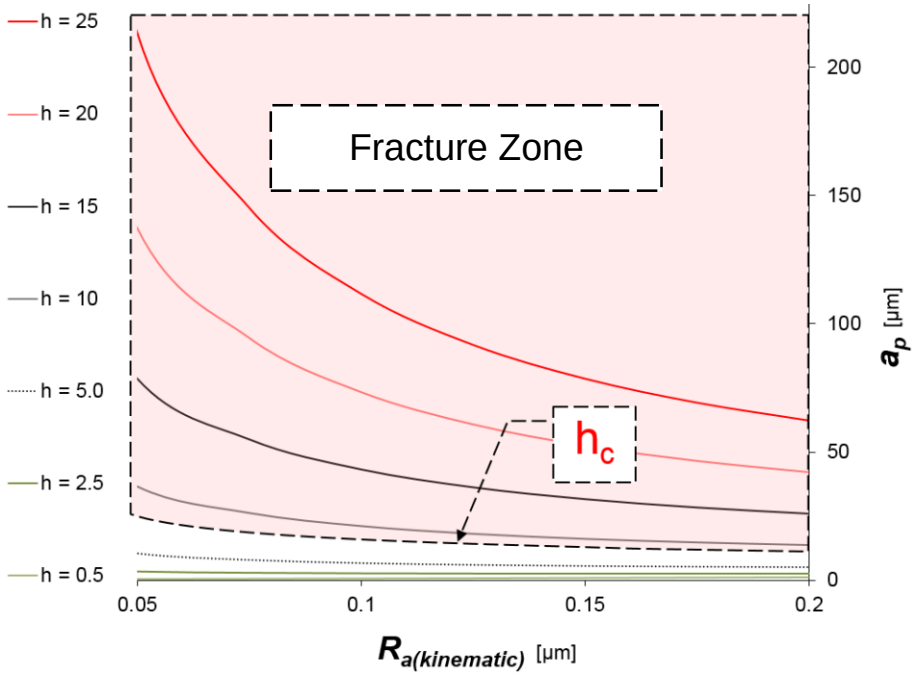

Figure 6-2. Plot of the maximum possible depth of cut (given by Eq. (6-5)) to achieve uncut chip thickness values between h = 0.5 – 25 µm as a function of kinematic roughness (within a range applicable to this current study). The dashed outline representing the critical chip thickness ($h_c \approx 9$ µm) is based on experimental results for 80% density porous tungsten.

In certain cases it is convenient to express maximum uncut chip thickness in terms of kinematic surface roughness and depth of cut. Analogously to the manner in which Eq. (6-2) was transformed into Eq. (6-5) by substituting feed for Eq. (6-3), the maximum chip thickness (Eq. (6-2)) can be expressed as:

$$h_{max} = r_c - \sqrt{32R_a r_c + r_c^2 - 2r_c\sqrt{32R_a r_c}\cos\left(\frac{\pi}{2} - cos^{-1}\left(\frac{r_c - y}{r_c}\right)\right)} \qquad (6\text{-}6)$$

where y practically represents the depth of cut a_p and given by Eq. (6-5). When the latter is substituted into Eq. (6-6), a lengthy yet powerful formula is obtained. It should be noted that corner radius r_c can seemingly be eliminated in the fully expanded expression of Eq. (6-6); however, the effects of r_c and f are still contained in $R_{a(kinematic)}$. This is of particular importance when considering the implications of choosing a particular value of kinematic roughness for practical machining applications. A graphical representation of Eq. (6-6) is shown in Figure 6-2 on the following page.

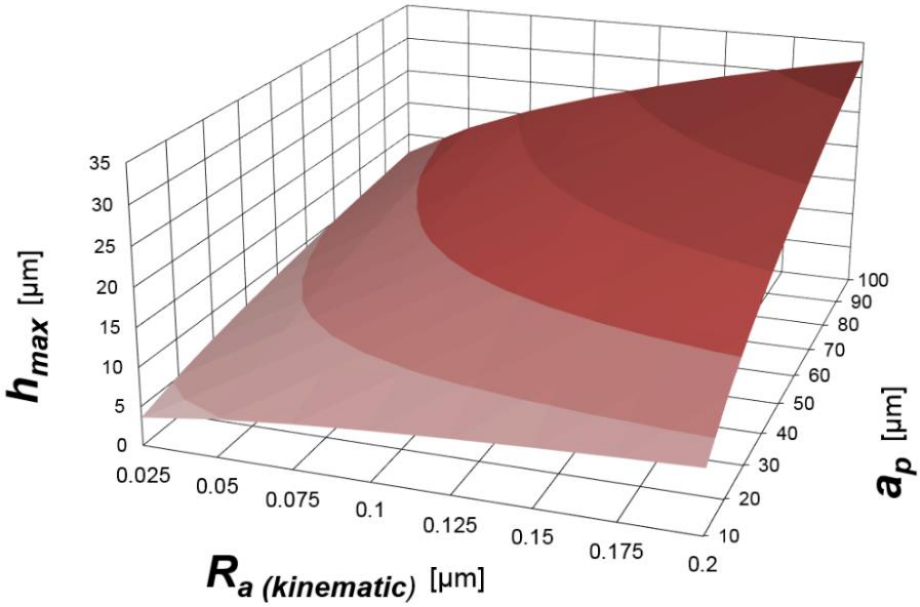

Figure 6-3. Contour plot of maximum uncut chip thickness h_{max} as a function of kinematic surface roughness R_a and depth of cut a_p.

The most important observation from this contour plot is the fact that the maximum chip thickness increases with both kinematic roughness and depth of cut. Therefore, when a small value of h_{max} needs to be achieved, as is the case when $h_{max} \leq h_c$, very low depth of cut and kinematic roughness need to be selected. The precise manner in which h_{max} is achieved i.e., whether small kinematic roughness and large depth of cut or large kinematic roughness is chosen depends on a variety of factors. On the one hand, low

depth of cut results in a large force component perpendicular to the machined surface and thus the likelihood of chatter is increased. When small kinematic roughness is selected, minimum chip thickness effects become dominant, i.e., ploughing occurs. Much like small depth of cut, ploughing at any depth of cut leads to an increase in cutting force and potentially chatter. In porous tungsten machining ploughing furthermore causes the smearing of pores. Additionally, cutting distance is increased with low kinematic roughness since the most common (practical) way to reduce kinematic roughness is to reduce feed. In face turning, cutting distance Γ may be calculated by Eq. (6-7).

$$\Gamma = \frac{\pi r^2}{f} = \frac{\pi r^2}{\sqrt{32 R_a r_c}} \tag{6-7}$$

According to Eq. (6-7), even a small reduction in feed (or kinematic roughness) leads to a significant increase in cutting distance (as $1/f$). Since tool-wear is increased approximately proportionally with cutting distance, selecting small kinematic roughness (i.e., feed) results in large tool-wear. This effect may be offset to a degree by choosing a larger corner radius, yet this in turn leads to chatter due to the low depth of cut necessary to maintain a given maximum chip thickness (see Eq. (6-6)). Precisely balancing the problems of tool-wear, ploughing and chatter requires comprehensive empirical optimization as well as selection of a suitable machine tool (high stiffness, high spindle speed, high accuracy) which lies outside of the scope of this current study. Nevertheless, an appropriate set of machining parameters was selected to first determine the critical chip thickness, which needs to be known in order to begin the optimization process. To give a visual representation for the influences of kinematic roughness and corner radius on (relative) cutting distance (i.e., tool-wear) can be seen in Figure 6-4 on the following page.

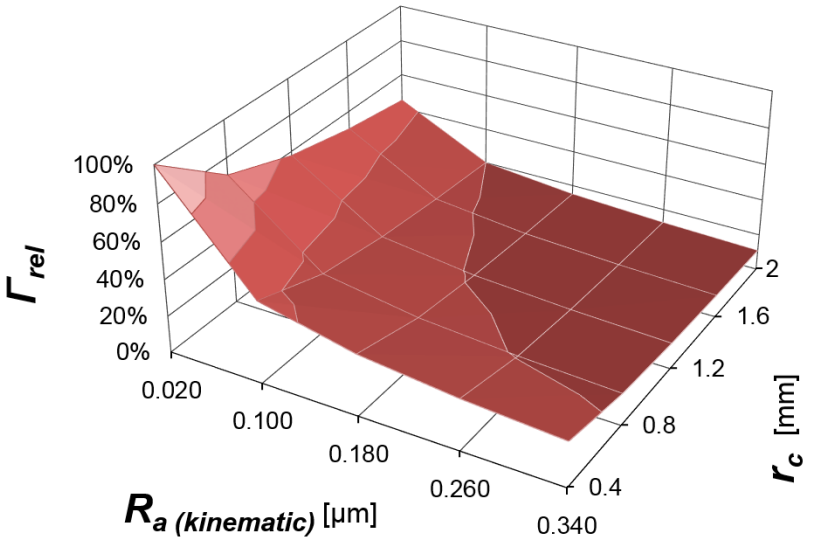

Figure 6-4. Contour plot of relative cutting distance as a function of kinematic roughness (equivalent to feed according Eq. (6-3)) and the corner radius of the cutting tool. When low kinematic roughness is selected, cutting distance, which directly affects tool-wear, necessarily increases.

6.2 EXPERIMENTAL DETAILS

In order to determine the critical chip thickness h_c of 80% density porous tungsten, side milling of 2.5 mm thick sheet was carried out. Since porous tungsten is fabricated by pressing and sintering of 3-5 µm diameter tungsten powder, only round bar stock is conventionally prepared. Porous tungsten plates were cut from a 60 mm diameter round bar using wire EDM. Prior to EDM cutting, rectangular recesses were 4 axis CNC milled into the round bar, leaving two 10 mm long protrusions on each of the four sides of each plate. Therefore, each plate featured a total of 8 sample surfaces. Using a custom made fixture, up-cut side milling was carried out on 54 surfaces (requiring 7 plates). For more information regarding sample preparation chapter 3.2 may be consulted. The machine tool was a HAAS VF-2 CNC milling machine and the cutting tools were GARR TOOL 222M straight flute end mills with a diameter of 6.35 mm (0.25 in) and average cutting edge radius of $r_\beta \approx 2$ µm (upsharp ground). The experimental matrix is shown in Table 6-1 on the following page.

Table 6-1. Experimental matrix for side milling experiments of 80% density porous tungsten for critical chip thickness determination.

Cooling condition	$R_{a\ (kinematic)}$ [μm]	v_c [m/min]	h_{max} [μm]	a_p [μm]
Dry, cryogenic	0.05, 0.1, 0.15	20, 60, 100	5.4, 7.2, 8.3, 10.1, 13.8, 16.4, 12.8, 17.6, 21.2	12, 37, 58

It should be noted that while the most relevant parameter for this particular investigation was h_{max}, there is no 'direct' way to achieve a particular value of maximum chip thickness. According to Eq. (6-6), corner radius (end mill diameter), depth of cut and kinematic roughness (r_c and f) all influence h_{max}. Since cutting tool diameter was kept constant, only R_a (i.e., feed) and a_p controlled h_{max}. To achieve an optimum spread of the various values of h_{max} thus determined by feed and depth of cut, an iterative procedure was used, yielding the values shown in Table 6-1. The reason $R_{a\ (kinematic)}$, rather than feed per tooth, was reported is the fact that feed/tooth (feed/rev in turning) is strongly influenced by the radius of the cutting tool. To allow for generalized application of the results from this study, kinematic roughness can easily be converted into feed when a tool with a specific corner radius is selected.

Cryogenic "flood" cooling was applied simultaneously to the rake face of the cutting tool and workpiece surface at a flow rate of 0.5 l/min. Cutting forces were acquired using a KISTLER type 9257B three-channel dynamometer. Ten representative values of maximum cutting force of each channel were recorded and used to calculate the (maximum) specific cutting force k_c. For more information regarding cutting force acquisition please review chapter 3.3. Cutting temperature measurements for dry machining were taken with a FLIR SC7000 infrared thermal camera, as described in chapter 3.2. Surface roughness and cutting edge radius measurements were taken on a ZYGO NewView 7300 scanning white light (non-contact) profilometer.

6.3 RESULTS AND DISCUSSION

6.3.1 Determining the Critical Chip Thickness of Porous Tungsten

Surface roughness of dry and cryogenically machined porous tungsten was measured in order to determine h_c. Based on the hypothesis that surface roughness will increase when $h_{max} > h_c$, finding the value of maximum uncut chip thickness beyond which R_a increases should allow for extrapolation of h_c. Arif et al. [120, 123, 124] had performed similar experiments to measure critical chip thickness in machining of brittle materials such as glass and ceramics. In porous tungsten, brittle fracture during machining has been hypothesized by the author to lead to the formation of BUE and chip re-deposition on the machined surface (see chapter 5). Previous attempts to eliminate brittle fracture have been partially successful yet certain practical issues have prevented these approaches from being implemented for cryogenic finish machining of un-infiltrated porous tungsten.

High speed cryogenic machining and limited pre-cooling have been shown to prevent brittle fracture and thus eliminate BUE. However, both of these approaches have limitations. Limited pre-cooling is difficult and time-consuming to implement reliably in an industrial environment when batch sizes are small, as is the case for dispenser cathodes. High speed machining of porous tungsten has so far only been achieved with lightly honed PCD cutting tools, which lead to excessive smearing. Low-speed machining of porous tungsten with very sharp cutting tools generally leads to brittle fracture when easily implemented "flood" cryogenic cooling is used. In this chapter, fracture-free cryogenic finish machining of porous tungsten with sharp edged tools will be developed. Again, the central hypothesis motivating this investigation is that fracture can be avoided as long as $h_{max} < h_c$.

The surface roughness data shown in Figure 6-5 showed similar trends for both dry and cryogenic machining. The critical chip thickness, as determined by extrapolation of surface roughness before and after the minimum value of R_a, did not change significantly cutting speed. Cryogenic cooling increased h_c by approximately 1 μm (about 10% increase). The absolute value of surface roughness at h_c (designated $R_{a\,(c)}$) remained practically unchanged under all conditions tested, as can be seen in Figure 6-6.

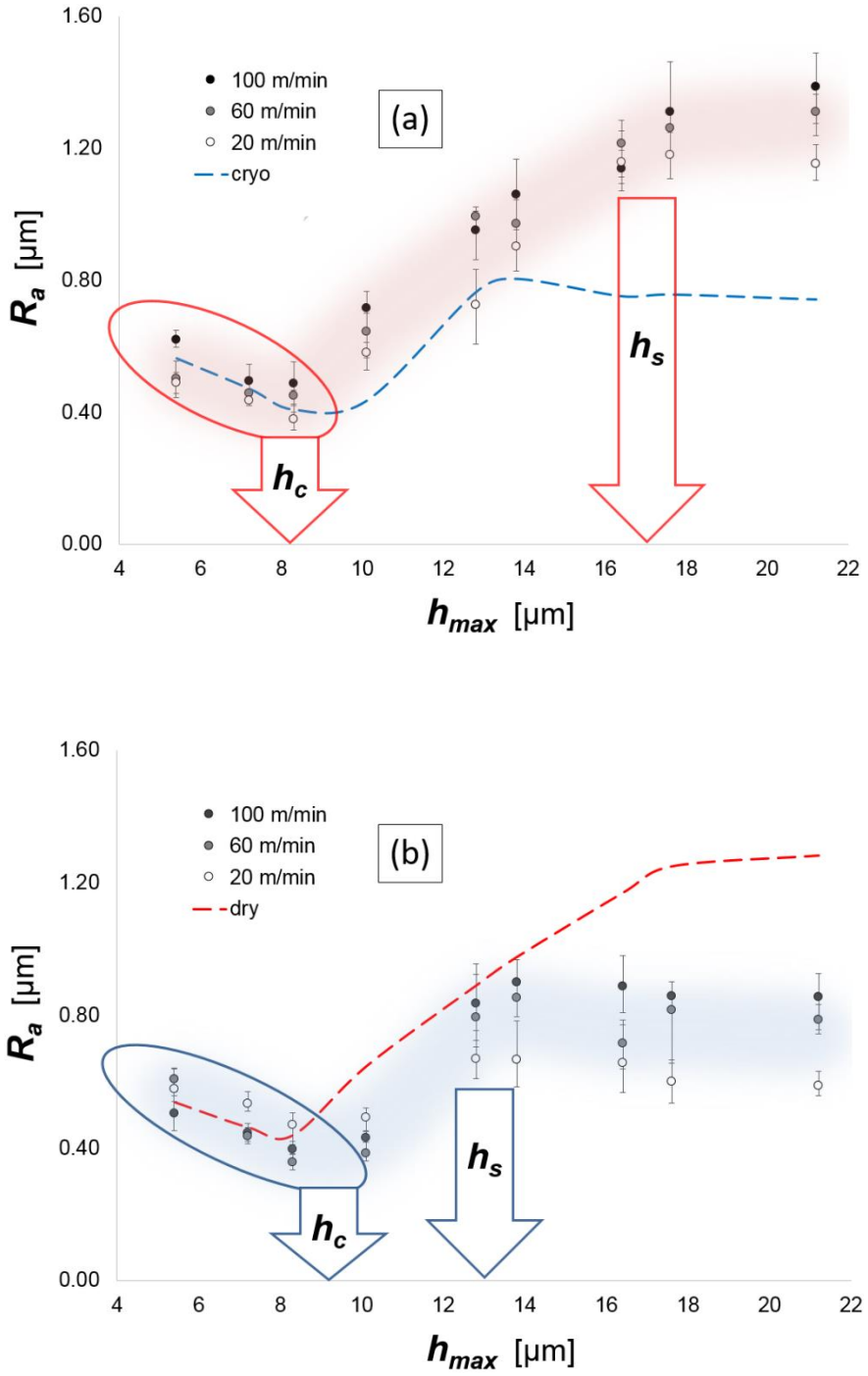

Figure 6-5. As-machined surface roughness of dry (a, red) and cryogenically (b, blue) machined porous tungsten for three cutting speeds. Both the critical chip thickness h_c and a new measure, termed the 'steady-state chip thickness' h_s were determined from R_a data.

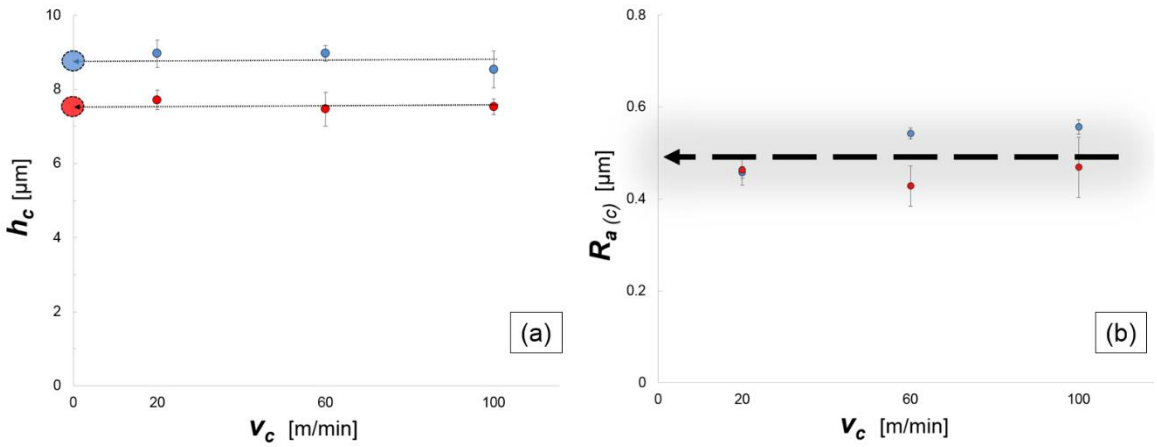

Figure 6-6. Critical chip thickness (a) and surface roughness at the critical chip thickness (b) for dry (red) and cryogenic (blue) machining as a function of cutting speed.

Interestingly, the value of h_c for both dry and cryogenic machining (8 µm, ± 1 µm) was approximately equal to the average ligament size of the workpiece material. Moreover, the fact that $R_{a\ (c)}$ seemed to be unchanged by either cutting speed or the cooling condition suggests that the deformation mechanism when $h_{max} = h_c$ was the same for all conditions. Based on the hypothesis that (only) ductile mode machining occurs when $h_{max} \leq h_c$, ductile machining of porous tungsten seems to be possible under both dry and cryogenic conditions. When $h_{max} < h_c$, surface roughness increased linearly with decreasing h_{max}. This behavior is a result of ploughing and tearing at very small undeformed chip thickness values and was first explained by Brammertz [90] for a variety of (dense) materials. According to deformation cutting theory, ductile mode machining of porous materials results in the cutting edge encountering only compacted material due to the collapse of pores ahead of the cutting/ploughing region [46]. As more severely strain hardened material is piled up ahead of the cutting edge, cutting forces and thus tool-wear are expected to increase. Evidence of such an increase in cutting force due to the size effect will be presented in section 6.3.3 of this chapter.

Once h_c is exceeded, fracture may take place and surface roughness will increase. Figure 6-5 clearly shows this behavior, supporting the hypothesis that a ductile to brittle transition with uncut chip thickness does in fact occur in porous tungsten. Rather than continuing to increase linearly with h_{max}, R_a reached a steady-state. This 'steady state

surface roughness', termed $R_{a\,(s)}$, was quite different for dry and cryogenic machining. Interestingly, $R_{a\,(s)}$ was largest for dry machining with the highest cutting speed and lowest when cryogenic cooling and the lowest cutting speed were used. Because surface roughness is mainly due to brittle fracture when $h_{max} > h_c$, the steady state surface roughness is hypothesized to be equivalent to the largest piece of porous tungsten that can be broken out of the workpiece surface. Since the yield strength of tungsten increases significantly at low temperatures, it seems reasonable that cryogenic cooling increased the strength of the workpiece material [244, 255, 256]. Likewise, dry machining and increasing cutting speeds both weaken the workpiece material by thermal softening, allowing for larger fracture pits to be formed.

Regardless of the mechanism responsible for the 50% decrease in $R_{a\,(s)}$ with cryogenic cooling, limiting the depth of fracture pits during rough and pre-finish machining of porous is highly desirable. Finish machining should clearly occur at $h_{max} = h_c$ so that surface roughness is as low as possible. Since maximum uncut chip thickness depends mainly on depth of cut and kinematic roughness (feed) when a given corner radius is used, h_{max} directly affects metal removal rate and thus productivity. It is therefore desirable during rough machining to use the largest possible value of h_{max} that permits rapid material removal while avoiding damage to the workpiece. Fracture and chipping are the most important kinds of damage in porous tungsten machining. Therefore, cryogenic machining allows for increased productivity by reducing fracture at large values of h_{max}. The way in which cryogenic cooling achieves this strengthening effect will be addressed in the following discussion.

6.3.2 Cutting Temperature Effects

Because cryogenic cooling reduces both the steady state surface roughness $R_{a\,(s)}$ and the steady state uncut chip thickness h_s, cutting temperature is hypothesized to be the primary factor affecting the extent of brittle fracture in machining of porous tungsten. Fracture of porous tungsten is different than that of dense materials because of the strong influence of the porous microstructure. Francois et al. [198] reported the shear and tensile strengths of 80% dense porous tungsten to be only half that of dense

polycrystalline tungsten. In other words, 80% dense porous tungsten is about 30% weaker than would be expected by a simple rule of mixtures approximation. The apparent lack of (macroscopic) mechanical strength of porous tungsten is likely due to the weakening effect of pores and relatively low strength of grain boundaries. In fact, during the course of this study, intergranular fracture was the most commonly observed failure mode observed in fracture pits generated during both cryogenic and dry machining of porous tungsten. It is therefore hypothesized that cryogenic machining reduces $R_{a\,(s)}$ by strengthening tungsten grains and thus increases the overall yield strength, which in turn reduces the depth of fracture pits by limiting the number of ligaments being pulled out. Further evidence for the effect of temperature, as well as cutting edge radius, can be seen in the Figure 6-7.

Figure 6-7 was prepared in the same format as Figure 6-5, showing effect of maximum uncut chip thickness on surface roughness. To further illustrate the importance of cutting temperature, experimental results from a cryogenic machining with modified cutting edge radius PCD tools were included as well. Within the ductile/ploughing region of $h_{max} < h_c$, all experimental conditions resulted in a linear increase in as-machined surface roughness with decreasing h_{max}. The three larger cutting edge radii of r_β = 6, 10, 14 μm did all exhibited this same trend, with the largest cutting edge radius (r_β = 14 μm) resulting in the largest surface roughness at very low h_{max}. This observation is consistent with the hypothesis of ploughing and tearing at low chip thickness values, where larger cutting edge radii are expected to lead to more severe ploughing induced surface degradation.

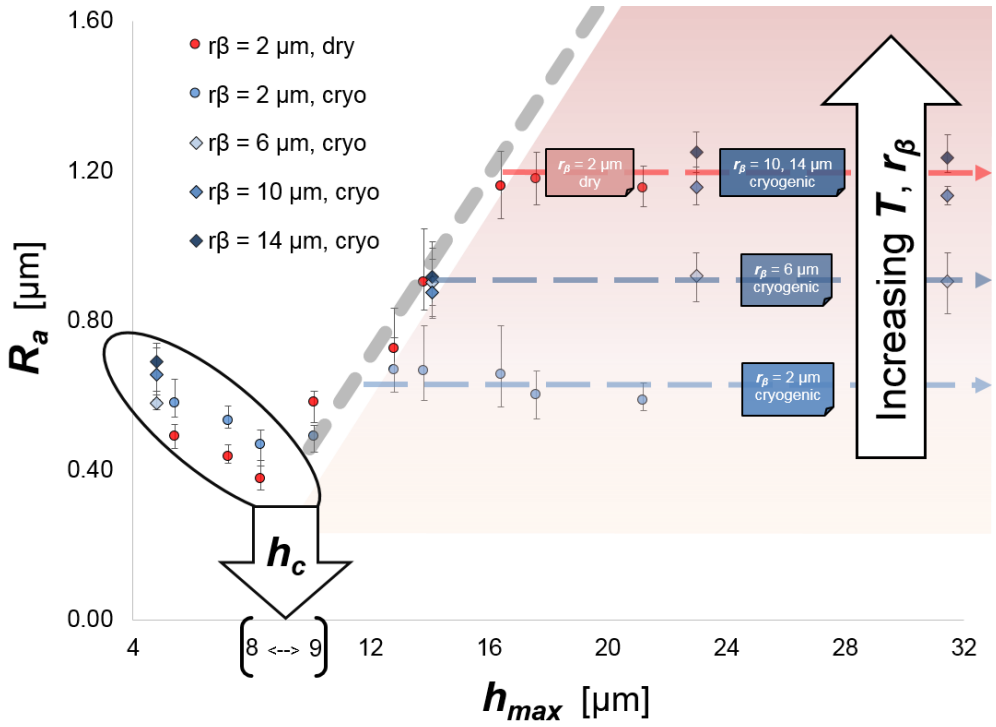

Figure 6-7. Surface roughness as a function of maximum chip thickness for dry and cryogenically machined porous tungsten for v_c = 20 m/min. In addition to upsharp tools (r_β = 2 µm), results for three additional cutting edge radii from a previous study are included.

The most striking observation from Figure 6-7 is the fact that all machining conditions resulted in approximately the same trend in surface roughness in between h_c and h_s. In other words, regardless of cryogenic cooling or changes in cutting edge radius, surface roughness increases linearly and with the same slope until the steady state roughness $R_{a\,(s)}$ is reached. The magnitude of $R_{a\,(s)}$ has already been observed to be dependent upon the cooling condition and cutting speed, and Figure 6-7 seems to suggest that cutting edge radius also has a strong effect. In fact, $R_{a\,(s)}$ for cryogenic machining with cutting edge radii of 10 and 14 µm was approximately the same as $R_{a\,(s)}$ of dry machined porous tungsten when a sharper cutting tool with r_β = 2 µm was used. The steady state roughness for a 'sharp' PCD tool with a cutting edge radius of 6 µm was about 30% larger compared to the results obtained for cryogenic machining with a 2 µm

edge radius tool. It is hypothesized that cutting edge radius has a direct impact on cutting temperature and thus the deformation and failure mode of porous tungsten since the size of the plastic zone (i.e., the primary deformation zone) is largely a function of cutting edge radius (smaller $r_\beta \rightarrow$ smaller plastic zone). The lower that cutting edge radius becomes, the lower cutting temperature will be. Cryogenic cooling has the ability to significantly reduce cutting temperature, allowing for the use of larger cutting edge radii with similar results as those from dry machining using sharp-edged tools.

To better understand the impact of different cutting speeds or modified edge radii on the mode of deformation in porous tungsten, it is necessary to quantify cutting temperature for both dry and cryogenic machining. Unfortunately, measuring cutting temperature during cryogenic machining is extremely difficult. A jacket of liquid nitrogen surrounding the cutting area makes indirect measurement by infrared radiation nearly impossible. Frozen water vapor further decreases the visibility between an external camera and the primary deformation zone, where heat is generated. Internal measurement methods such as thermocouples and pyrometers embedded in and on the cutting tool are also highly limited in their ability to measure cutting temperature during cryogenic machining. Previous attempts during this study to measure cutting temperature during cryogenic high speed machining with modified cutting edge radius PCD tools resulted in no discernable temperature rise from a pyrometer inside of the tool. The minimum accurately measureable temperature from black body radiation with a pyrometer is approximately 500 °C, which is likely more than cutting temperatures during cryogenic finish machining of porous tungsten. For the purposes of this present study, an indirect method of determining cutting temperature during cryogenic machining was developed based on surface roughness data.

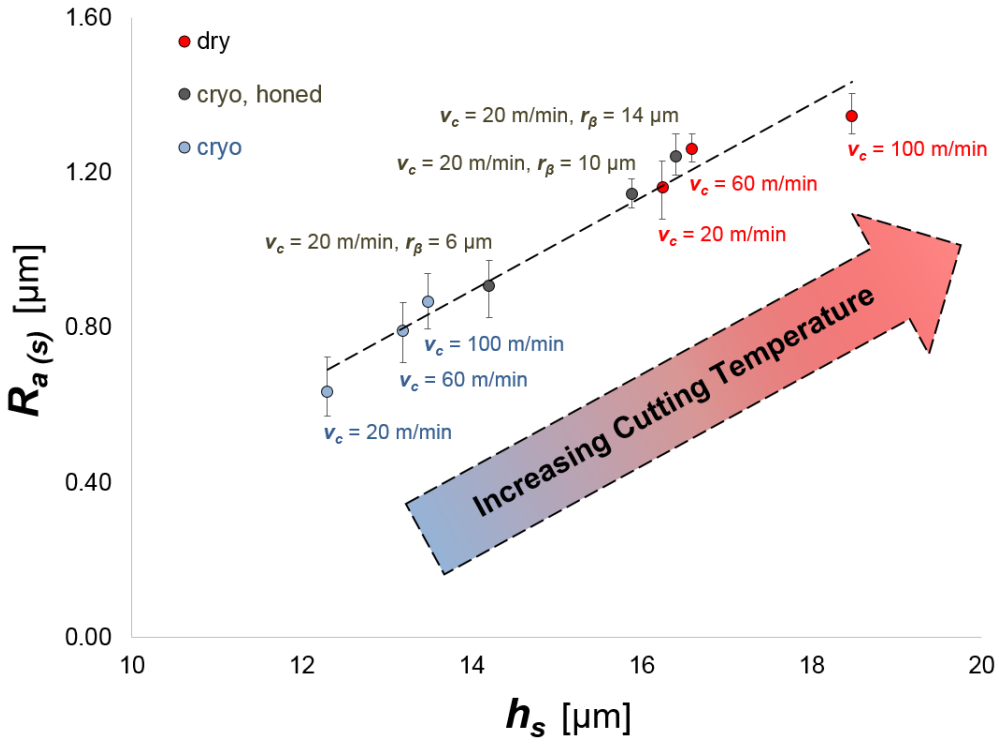

Figure 6-8. Steady state surface roughness data for a variety of cutting speeds and cutting edge radii. The values of $R_{a\,(s)}$ and h_s were determined by both linear and parabolic curve fitting, yielding 50% of the scatter shown. The remainder of scatter is a result of measurement uncertainties. Considering the approximately linear increase in $R_{a\,(s)}$ with respect to h_s as cutting speed, cooling temperature (i.e., dry vs. cryo) and edge radius are increased, temperature is hypothesized to influence $R_{a\,(s)}$.

By averaging the values of surface roughness within the steady state region $h_{max} \geq h_s$ and extrapolating the linear region between h_c and h_s, Figure 6-8 was prepared. As may be expected from Figures 6-5 and 6-7, $R_{a\,(s)}$ increases linearly with h_s, both of which depend on cutting speed, edge radius and cryogenic cooling. Because lower cutting speed and cryogenic cooling result in lower values of $R_{a\,(s)}$, cutting speed is hypothesized to be increasing in the same manner as $R_{a\,(s)}$. By measuring cutting temperature for dry machining at the exact (calculated/interpolated) value of h_s, temperature for all of the conditions shown in Figure 6-8 may be estimated as shown in Figure 6-9.

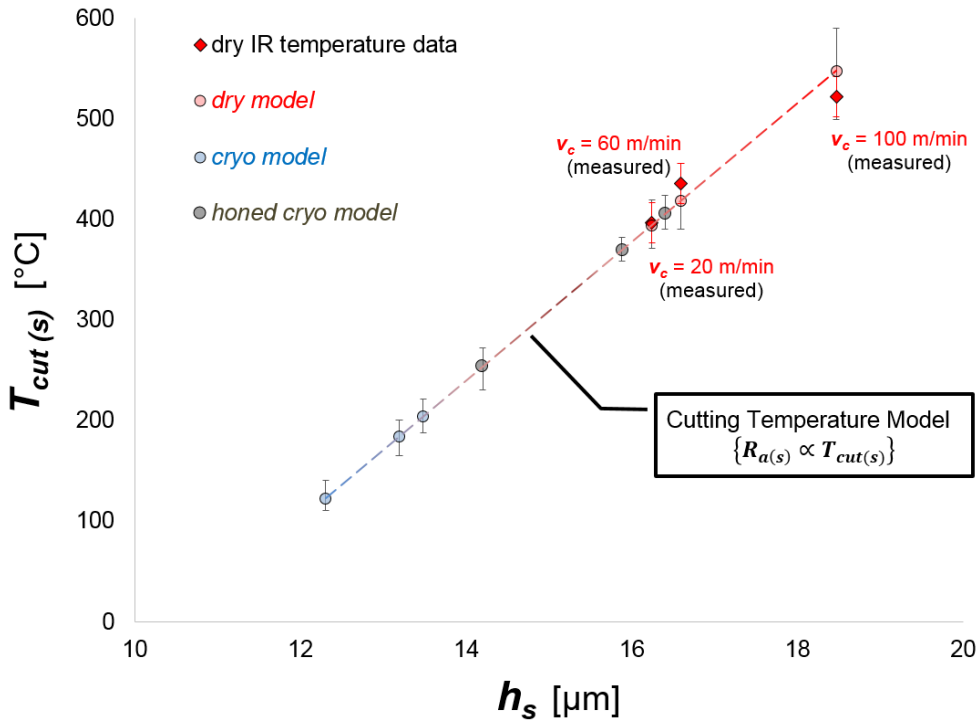

Figure 6-9. Calibrated cutting temperature model based on surface roughness data shown in Figure 6-8. Red diamonds represent infrared temperature measurement of dry machining at h_s for three different cutting speeds.

Based on the assumption that cutting temperature at the steady state chip thickness h_s is proportional to trend in steady state roughness, Figure 6-9 was created. To obtain absolute values of temperature, infrared temperature measurements were carried out under the conditions predicted in Figure 6-8 (i.e., at $h_{max} = h_s$). Since the measured temperature value appear to follow a nearly linear trend, it seems reasonable to assume that a cutting temperature model based on surface roughness may give a relevant approximation of temperatures during cryogenic machining. This is particularly interesting when considering the difficulties in accurately measuring cutting temperatures during cryogenic machining experiments. Both the frozen water vapor and the liquid nitrogen coolant itself obscure the line of sight between an infrared camera and the primary deformation zone. Approximating the temperature during cryogenic machining

from dry machining data is therefore a convenient means to studying the effect of liquid nitrogen on cutting temperature and the mode of deformation of porous tungsten.

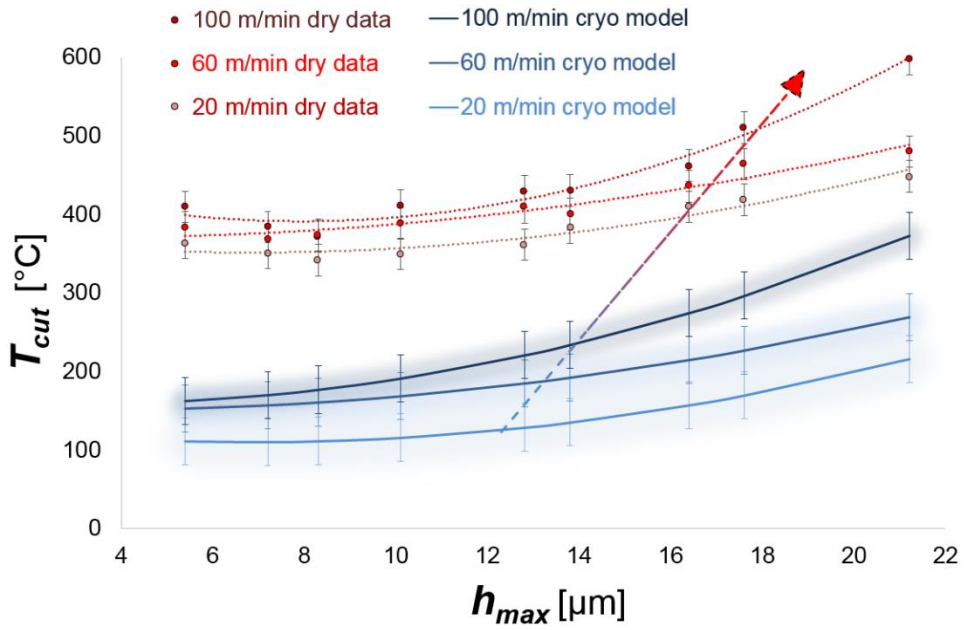

Figure 6-10. Infrared cutting temperature data for dry machining and modeled cryogenic cutting temperatures. The dashed line colored as a blue to red gradient was used to estimate cryogenic cutting temperature and is the same as the curve shown in Figure 6-9.

Using the cutting temperature model from Figure 6-9, cryogenic cutting temperature was estimated based on dry machining data in Figure 6-10. While cutting speed had some effect on temperature during dry machining of porous tungsten, maximum chip thickness affected the temperature more strongly. Surprisingly, there was no significant increase in temperature at very low value of h_{max}. Ploughing, and ductile mode machining in general, generate a lot of heat due to external (tool/chip) and internal (workpiece/chip) friction [78, 95, 101]. Therefore, one would expect a rise in cutting temperature as $h_{max} \leq h_c$.

The most likely reason for the relatively 'low' cutting temperatures at low h_{max} is hypothesized to be increased thermal conductivity of the highly compacted chip. Francois et al. had measured the thermal conductivity of 80% porous tungsten as only

50% that of dense tungsten (see Figure 2-15) [198]. Consequently, heat generated during machining of porous tungsten will tend to stay within the primary deformation zone. During ploughing, the material in the chip becomes compacted and thus thermal conductivity is expected to increase to approximate that of dense tungsten. Therefore, cutting temperature will be slightly lower because the material in the primary deformation zone, part of which will become the chip, may transport heat more efficiently. The fact that cutting temperature remained approximately constant below h_c suggests that the amount of compaction due to ploughing was approximately resulted in an increase in thermal conductivity approximately equal to the increase in heat primarily due to internal friction.

The increase in cutting temperature with h_{max} in Figure 6-10 is consistent with the trend in as-machined surface roughness shown in Figures 6-5,7. As chip thickness increases, so does the volume of the chip. Moreover, less compaction (or loss of porosity) is expected with increasing h_{max} because the dominant machining mechanism is brittle fracture. Rather than internal friction, external (tool/chip) friction is hypothesized to be responsible for the majority of the heat generated during brittle fracture machining. Previous results had already established the existence of BUE and chip re-deposition during brittle fracture machining. The latter process leads to rapid tool-wear by attrition, which in turn generates significant heat. Sliding of brittle fracture chips across the cutting edge and subsequent smearing of these chips onto the machined surface could generate sufficient heat to locally allow for severe plastic deformation.

Cutting temperatures from dry machining were approximately 220 °C higher than temperatures during cryogenic machining, yet the temperature of liquid nitrogen was 'only' -180 °C. Dry machining therefore appears to generate more net heat than cryogenic machining. It is hypothesized that liquid nitrogen provides a slight lubricating effect and also aids in chip evacuation, both of which reduce the amount of heat generated from friction at the tool/chip interface. Also, while the cutting length of the experiments discussed here was intentionally kept short to eliminate the effect of tool-wear, dry machining likely leads to an increase in cutting edge radius due to tool-wear. As shown in Figures 6-8,9, larger cutting edge radii are expected to increase cutting temperature. Some of the temperature increase with dry machining is therefore likely due

to (limited) tool-wear. Optical microscopy of cutting edges after machining did however not allow for precise determination of tool-wear because of the very small size of the worn area (VB_C < 10 μm).

6.3.3 Cutting Force and Deformation Mechanisms

Based on surface roughness and cutting temperature data, ductile and brittle mode machining of porous tungsten have been shown to strongly influenced by the maximum uncut chip thickness. Both dry and cryogenic machining exhibit similar patterns, although cryogenic machining resulted in significantly lower surface roughness beyond $h_{max} > h_c$, i.e., in the brittle fracture regime. Below h_c, brittle fracture is avoided and ductile mode machining takes place. To better study the deformation mechanism of porous tungsten during both brittle and ductile mode machining, cutting force was measured. The specific cutting force (or specific cutting pressure) k_c, which has units of N/mm^2 (i.e., MPa), was then computed by dividing the maximum cutting force by the maximum cross sectional area of the chip.

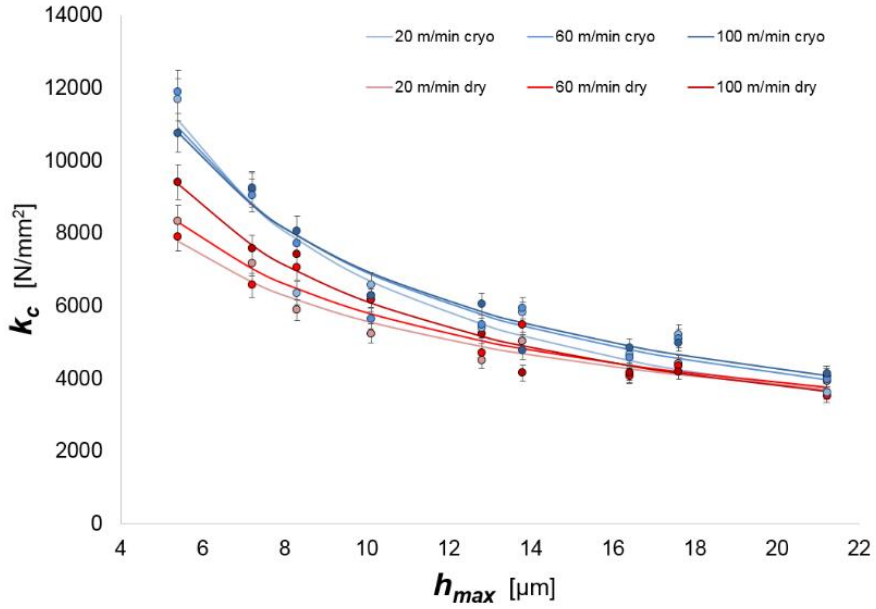

Figure 6-11. Specific cutting force data from dry and cryogenic machining of 80% dense porous tungsten for three different cutting speeds, as a function of maximum undeformed chip thickness. Solid lines represent best fit curves by a power law.

Cutting force data shown in Figure 6-10 illustrates the significant effect of maximum uncut chip thickness on machining of porous tungsten. Both cryogenic and dry machining exhibited a power law increase in k_c with decreasing h_{max}. Cutting speed had comparatively little to no effect on the specific cutting force during cryogenic machining. In dry machining, increasing the cutting speed from 20 m/min to 100 m/min resulted in a 17% increase in k_c in the range $h_{max} < h_s$. Since cutting speed is approximately proportional to strain rate, the increase in cutting force with cutting speed during dry machining is hypothesized to be due to strain rate hardening of the porous tungsten workpiece. In cryogenic machining the competing effects of thermal softening and strain hardening seem to offset each other, so that cutting force did not change as speed was increased.

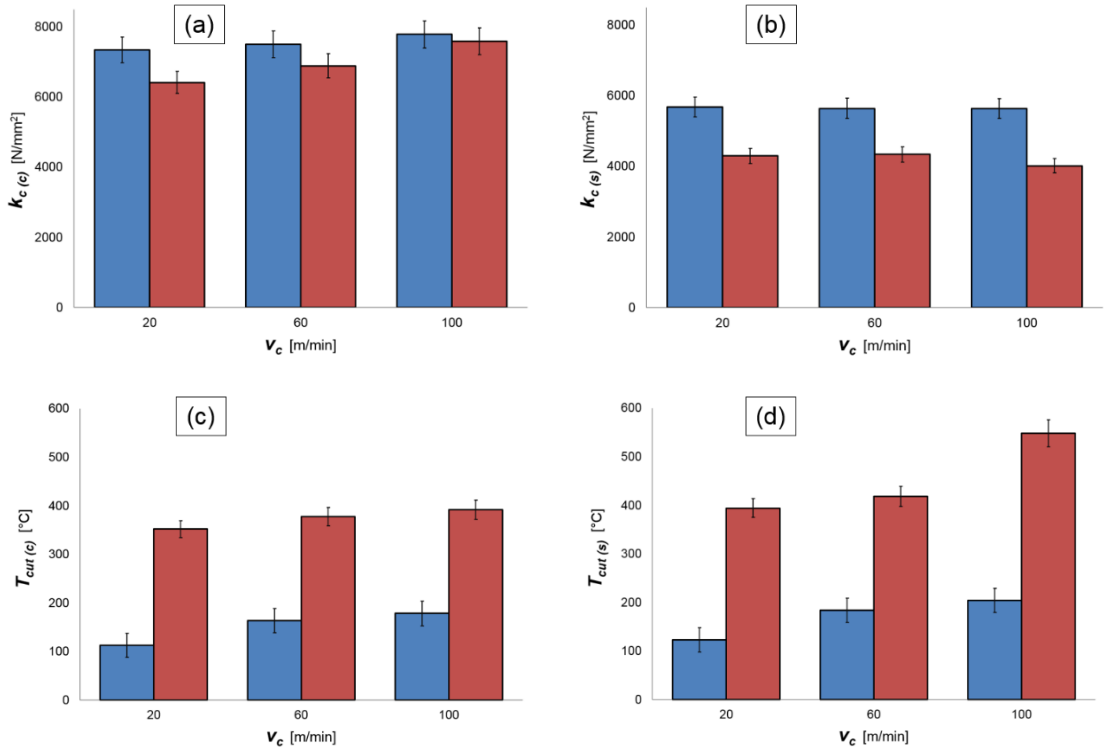

Figure 6-12. Specific cutting force at the critical (a) and steady state (b) uncut chip thicknesses as a function of cutting speed, interpolated from measured force data in Figure 6-11. Also included are plots of cutting temperature at h_c (c) and h_s (d) for dry (red, measured) and cryogenic (blue, modeled) machining.

Figure 6-12 summarizes the key parameters from Figures 6-10 (temperature) and 6-11 (force). The specific cutting force when $h_{max} = h_c$, designated $k_{c\,(c)}$, i.e., the unit pressure at the ductile/brittle transition of surface generation in porous tungsten machining, varied relatively little with either cutting speed or cooling condition. As can be seen in Figure 6-12a, $k_{c\,(c)}$ was approximately equal to 7 ± 0.5 GPa. While cutting speed had almost no effect on $k_{c\,(c)}$ during cryogenic machining, dry machining exhibited some strain rate hardening induced increase in $k_{c\,(c)}$. Interestingly, Dandekar et al. reported that during shock compression of 80% dense porous tungsten at strain rates of $\dot{\epsilon} \approx 10^6\ s^{-1}$, stiffness increased significantly beyond a critical stress of 6.4 GPa due to the formation of a stable two wave structure [209]. It is therefore hypothesized that the critical chip thickness in porous tungsten coincides with this strengthening mechanism.

Dandekar et al. [209] also observed that beyond a stress of 4.9 GPa, full compaction of porous tungsten took place. The specific cutting force at the steady state chip thickness, $k_{c\,(s)}$, shown in Figure 6-12b, was approximately 4.1 GPa during dry machining and 5.8 GPa during cryogenic machining. Cutting speed had essentially no effect on $k_{c\,(s)}$, which suggests that the machining mechanism responsible for the transition towards steady state (constant fragment size) fracture in porous tungsten is not strain rate sensitive. However, it is proposed that the transition from fracture towards ductile mode machining coincides with full compaction of material comprising the chip. As pores and voids collapse, the number of crack initiation sites is dramatically reduced. Therefore, fracture becomes much less likely when $h_{max} \leq h_s$, i.e., when the compaction pressure $k_{c\,(s)}$ is exceeded. Surface roughness reaches a minimum at $k_{c\,(c)}$ (h_c), because fracture is essentially eliminated as the compacted and highly deformed material in the primary deformation zone is further strengthened according to the mechanism proposed by Dandekar et al. (steady two wave structure beyond 6.4 GPa).

While the specific cutting force decreased significantly between the critical and steady state chip thickness, cutting temperature remained almost constant. Only dry machining at a cutting speed of v_c = 100 m/min resulted in a temperature increase of more than 10% from $T_{c\,(c)}$ to $T_{c\,(s)}$. As mentioned earlier, strain rate hardening is hypothesized to exceed thermal softening in ductile mode dry machining. This theory is

consistent with the fact that $T_{c\,(c)}$ remained unchanged with cutting speed for dry machining while cutting force increased. Based on the simultaneous increase in $T_{c\,(s)}$ and $R_{a\,(s)}$ with cutting speed, thermal softening is hypothesized to be dominant during brittle fracture machining for both dry and cryogenic machining. The lower thermal conductivity of porous tungsten compared with compacted/dense tungsten is the most likely reason for this behavior.

The phenomenon of significantly increased specific cutting force with a decrease in uncut chip thickness is often referred to as the 'size effect' in machining. As can be seen in Figure 6-11, porous tungsten clearly exhibits a size effect. However, the nature of this effect is more complex than would be the case for a similar dense material. Under conventional machining conditions, porous tungsten is machined via brittle fracture (assuming the cutting tool remains sufficiently sharp to prevent smearing). Only at low values of uncut chip thickness ($h_{max} \leq h_s$), complete compaction of porous tungsten pores initiates a transition from brittle fracture machining towards ductile chip formation and thus fracture free surfaces. The extremely high pressures encountered when machining porous tungsten in this manner are the result of severe strain and strain rate hardening of the workpiece material. As uncut chip thickness is decreased, the strain rate increases in the same manner as cutting force (i.e., by a power law). Denkena et al. [88] had reported this very effect from finite element modeling (FEM) of *AISI 1045* steel, a *BCC* metal (α-*Fe* + *C*).

There now is a consensus that the size effect in machining arises primarily due to the finite sharpness of the cutting tool [93, 103-105, 222, 257]. At low uncut chip thickness, the ratio between cutting edge radius r_β and h becomes very large near the machined surface. In other words, the cutting tool appears to become duller at small values of h_{max}. Because chip formation becomes very difficult due to highly negative local rake angles (tangent to the cutting edge radius), ploughing occurs. As the material within and ahead of the primary deformation zone is ploughed, it becomes highly strain hardened. Both cutting force and cutting temperature consequently increase. In porous tungsten, compaction of the ploughed material changes the material properties in such a way that thermal conductivity and yield strength are significantly increased [198].

Therefore, strain hardening dominates during ploughing of porous tungsten at very small h_{max} and cutting force increases even more dramatically than would be expected. While already difficult to machine under conventional machining conditions (i.e., relatively large h_{max}), ploughing makes porous tungsten harder to machine than even hardened steels ($k_{c1} \approx$ 3-5 GPa). Ploughing consequently leads to severe tool-wear that in turn degrades the quality of the machined surface. Moreover, severe ploughing is hypothesized to lead to localized cracking of the machined surface due to strain hardening induced fatigue, also referred to as spalling. It should be noted that ploughing induced spalling is quite different from fracture that occurs when $h_{max} > h_c$, the latter of which involve crack initiation at the cutting edge. Burnishing, which is essentially a type of chip-less metal forming by ploughing of the workpiece surface, has been reported to induce spalling by sub-surface crack initiation due to excessive burnishing pressure [258, 259]. Whether spalling occurs during ploughing of porous tungsten when $h_{max} < h_c$ requires microscopic study of the machined surface.

6.3.4 Correlating Chip Thickness Effects and As-Machined Surface Morphology of Porous Tungsten

In order to verify the various hypotheses with regard to the influence of undeformed chip thickness on the mode of machining of porous tungsten, SEM imaging was performed for a selected number of samples. Since the effects of h_{max} and cryogenic cooling on surface roughness, cutting temperature and cutting force were more significant than that of cutting speed, only v_c = 60 m/min was selected for SEM investigation. Surface morphology of cryogenically and dry machined porous tungsten samples can be seen in Figure 6-13. From the micrographs shown in Figure 6-13, it is possible to deduce the mode of deformation under which the machined surface was created. In this way, further evidence for the correlation between maximum uncut chip thickness and machining mechanisms of porous tungsten is obtained, as will become clear in the ensuring discussion.

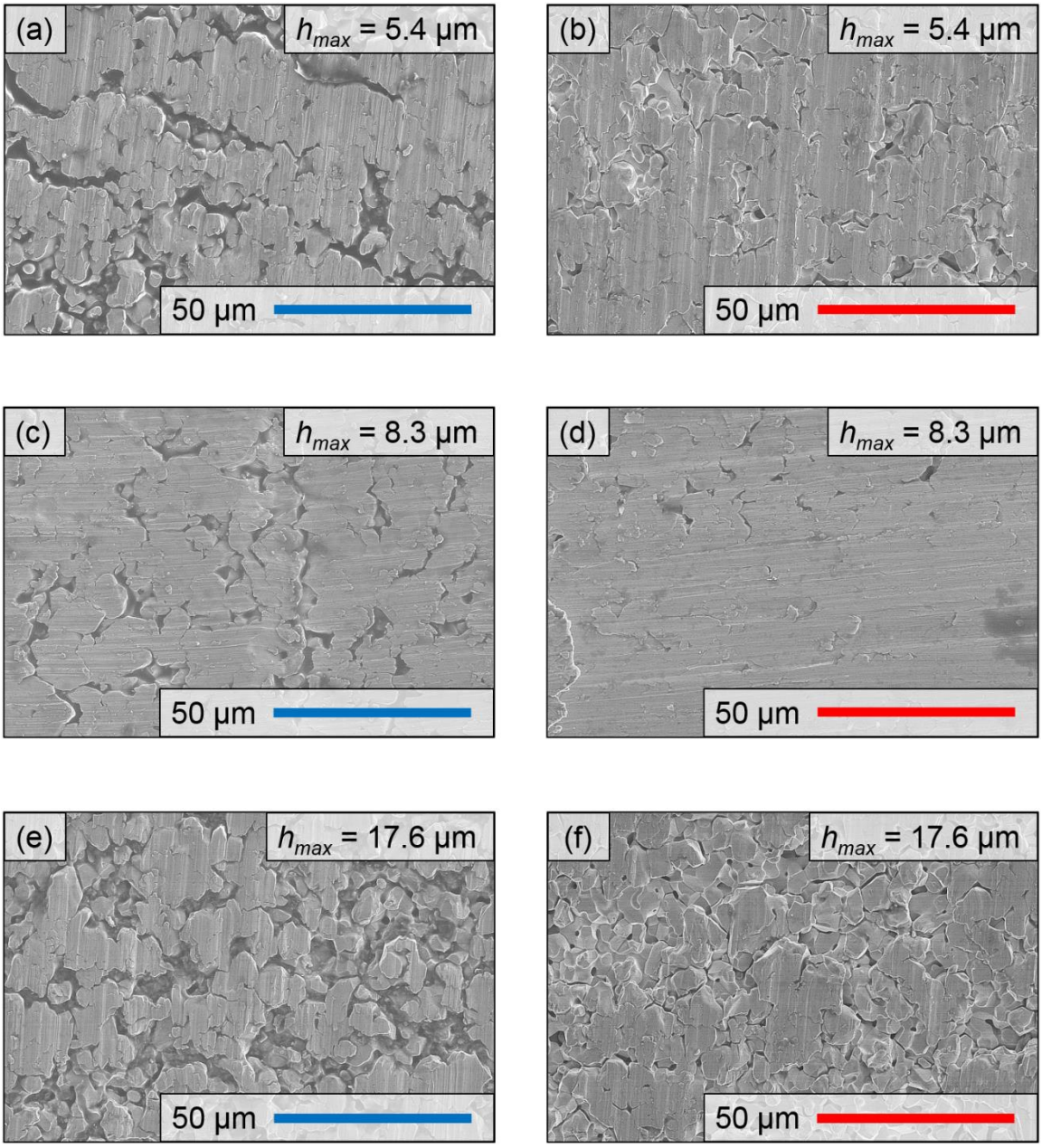

Figure 6-13. SEM micrographs of cryogenically (a, c, e) and dry (b, d, f) machined porous tungsten surfaces. A transition from ploughing (a, b) to ductile shear (c, d) and finally brittle fracture (e, f) with an increase in h_{max} can be clearly observed.

The scanning electron micrographs shown in Figure 6-13 are consistent with the hypothesized machining mechanisms involving ploughing, shear and fracture. At h_{max} = 17.6 µm (Figures 6-13e,f), both fracture pits and smeared islands are visible.

Cryogenic machining resulted in slightly more shallow pits than dry machining. Steady state surface roughness had already been shown to be lower with cryogenic cooling. The reason for this phenomenon was hypothesized to be increased strength of porous tungsten at lower temperatures. Near the critical chip thickness at h_{max} = 8.3 μm in Figures 6-13c,d the strengthening effect of cryogenic cooling can also be observed. Cryogenic machining resulted in much larger and more evenly distributed surface porosity. The majority of both dry and cryogenically machined surfaces have been severely plastically deformed, supporting the hypothesis of ductile mode machining. Moreover, no cracks or fracture pits were observed on either surface. In fact, Figure 6-13c shows evidence of some side flow that occurred during cryogenic machining at a peak of the kinematic roughness profile. Dry machining left only a small number of surface pores unsmeared, which is likely due to increased plasticity of porous tungsten at elevated temperatures encountered during dry machining. By sufficiently limiting plasticity to avoid micro-burr formation, cryogenic cooling increases surface porosity while maintaining low surface roughness.

At very small uncut chip thickness (h_{max} = 5.4 μm), ploughing and severe strain hardening led to spalling. Especially with cryogenic cooling, large (≈ 30 μm) lateral cracks were uniformly distributed across the machined surface. Similar to burnishing with excessive force, the extreme pressure from ploughing resulted in micro cracks within the sub-surface of the workpiece. The rest of the machined surface was severely smeared with little to no residual porosity. Dry machining did not result in spalling to the degree that cryogenic cooling did. However, as can be seen in Figure 6-13b, flake-like spalling left randomly distributed shallow pits on the machined surface.

It should be noted that the surface morphology of dry machining with h_{max} = 5.4 μm resembles that from cryogenic and dry machining with excessively large cutting edge radii at larger values of h_{max}. It therefore stands to reason that the ratio between cutting edge radius and uncut chip thickness is a key factor in determining whether ploughing occurs in porous tungsten machining. Because the critical chip thickness appears to be closely tied to the microstructure of the porous tungsten workpiece material (i.e., the average ligament size), there likely is no generalizable ratio of cutting edge radius and critical chip thickness. In other words, ductile mode machining of porous tungsten

without excessive ploughing requires sharp cutting tools. Because of the relatively low tool-life of sharp cutting tools, and the fact that cryogenic cooling significantly decreases tool-wear (at least 50% lower than dry machining), cryogenic cooling is a necessity for sustained machining of infiltrant-free porous tungsten. Especially when considering the limitations placed on appropriate coolants for machining of vacuum devices, specifically the requirement to leave absolutely no residue, there is no obviously superior alternative to liquid nitrogen cooling. When fine-grained PCD tools with very sharp cutting edges are used in conjunction with cryogenic cooling and proper machining parameters ($h_{max} \approx h_c$), equal or better surface quality than infiltrant-assisted machining can be achieved through cryogenic machining of porous tungsten while also ensuring long tool-life.

6.4 CHAPTER CONCLUDING REMARKS

It has been demonstrated that in both dry and cryogenic machining of porous tungsten there is a value of critical chip thickness, approximately equal to the average ligament size (h_c = 8 - 9 μm). Below h_c, ductile mode machining and ploughing occur, the latter leading to poor surface quality at low values of h_{max}. Sub-surface cracking and spalling were observed as a result of very high cutting pressures resulting from ploughing. Above h_c, brittle fracture originates from the cutting edge, resulting in deep fracture pits. The small brittle fracture fragments lead to the formation of built-up edge (BUE) which is re-deposited to form randomly distributed smeared islands, as described in previous studies.

It should be noted that brittle fracture occurred for both dry and cryogenic machining, indicating that maximum uncut chip thickness has a stronger effect on the brittle to ductile transition of porous tungsten than even cutting temperature. Increasing uncut chip thickness led to larger cutting temperature, while ploughing at low uncut chip thickness surprisingly did not result in significantly increased cutting temperatures. It was hypothesized that increased thermal conductivity of fully compacted tungsten in the chip and primary deformation zone was responsible for this effect.

When $h_{max} \approx h_c$, ductile mode machining with little to no detrimental ploughing or brittle fracture is achieved. Very low surface roughness ($R_a \approx 0.4$ μm) and surface

porosity well in excess of the acceptability limit of 30 pores per 10,000 μm^2 can be achieved when liquid nitrogen cooling is applied. While dry machining does allow for ductile mode machining, as-machined surface porosity is very low due to excessive plasticity resulting in smearing of pores. The mechanism of eliminating fracture (originating from the cutting edge) at $h_{max} \leq h_c$ was hypothesized to involve a combination of compaction of the workpiece material in the primary deformation zone and the establishment of a stable two wave shock structure, based on work performed by Dandekar et al. [209].

Cutting temperature for cryogenic machining was estimated by means of a surface roughness based model. Based on the observation that the surface roughness reaches a steady state point, and that point increases linearly as a function of cutting speed, edge radius and cooling condition, it was hypothesized that $R_{a\,(s)}$ is proportional to cutting temperature. Infrared temperature measurements of dry machining at the steady state chip thickness h_s did confirm the expected pattern of an approximately linear increase in cutting temperature with cutting speed (within the range v_c = 20 - 100 m/min). Cutting temperatures for dry machining were in the range of 320 – 520 °C while cryogenic machining resulted in (estimated) cutting temperatures between 100 – 300 °C. The fact that the temperature differential between dry and cryogenic machining was larger than the difference between room temperature (dry) and liquid nitrogen (cryo, -180 °C) was hypothesized to be due to lubrication and chip clearing provided by pressurized LN2.

Based on the results from this current study on the effect of maximum uncut chip thickness on surface morphology in porous tungsten it can be concluded that cryogenic cooling is necessary to achieve optimum surface quality. Liquid nitrogen cooling, along with the very low cutting edge radii of the tools used in this study ($r_\beta \approx 2$ μm), allowed for excellent surface porosity to be obtained at $h_{max} \approx h_c$ due to the suppression of burr formation between ligaments (i.e., smearing). Dry machining left insufficient surface porosity because of higher cutting temperatures that led to increased smearing. While tool-wear was insignificant during the short cutting length of the experiments performed during this study, previous work on machining of porous tungsten has shown that dry machining results in significant large tool-wear, particularly at small values of uncut chip thickness (low feed) [4, 22].

Larger cutting edge radii are an effective means of reducing tool-wear, but they in turn cause ploughing and smearing due to very large effective negative rake angles in the vicinity of the machined surface. Therefore, cryogenic cooling along with sharp cutting edges such as the ones used during this study are necessary requirements for achieving optimum surface morphology in porous tungsten. By selecting $h_{max} \approx h_c$, fracture originating from the cutting edge can be avoided along with BUE, and tool-life will likely be increased substantially. Quantifying tool-wear during cryogenic ductile mode turning of porous tungsten with recently developed sub-micron (nano) grain, sharp edged superabrasive (PCD, PCBN) cutting tools ought to be the focus of subsequent studies.

CHAPTER 7.

CONCLUSIONS AND FUTURE WORK

7.1 CONCLUSIONS

Cryogenic machining of porous tungsten has been demonstrated to be capable of producing excellent surface quality. The manner in which cryogenic cooling improves the machining characteristics of porous tungsten is complex and cannot be reduced to a single mechanism. Moreover, cryogenic machining offers the ability to fine-tune surface morphology by altering the mode of machining. Which kind of machining mode is the 'best' depends on the functional requirements of the particular surface. For example, dispenser cathodes consist of an emitting surface which requires high surface porosity yet low surface roughness. To achieve both of these requirements, ductile mode machining without smearing is necessary. The rear and side surfaces of dispenser cathodes need to be completely smeared to retain the Ba impregnate, which should only be dispensed by the emitting surface. Ploughing and severe smeared are therefore actually desirable for the non-emitting surfaces of dispenser cathodes. The third possible mode of machining porous tungsten, brittle fracture, may also be appropriate in certain cases. Applications requiring very high surface porosity such as rocket nozzles, filters and other gas and liquid flow devices made from porous tungsten are best machined by brittle fracture. While the attainable surface roughness may not be very low, it is still more than sufficient for the majority of applications and tolerances on the order of ± 20 μm can be easily obtained.

Since tool-wear directly affects the achievable geometric tolerance of a machined component, limiting tool-wear is very important to maintain product quality and functional performance. In porous tungsten machining with cermet cutting tools, cryogenic cooling lowers tool-wear by more than 50% compared to dry machining. Cermet tools are capable of producing acceptable surface quality, yet tool-wear increases near exponentially with cutting speed. Even at low cutting speeds, only a small number of finish machining cuts can be performed before tool-wear exceeds an acceptable limit. Despite their inability to be used for automated machining of porous tungsten, cermet

tools were successfully used to evaluate the effects of various machining and cooling parameters.

It was found that cryogenic cooling results in twice the compressive residual surface stress as dry machining under the same machining conditions. Practically, increased compressive stress of the machined surface reduces the likelihood of undesirable chipping and fracture. In this way, more delicate features such as the knife edge at the corner of the concave emitting surface of dispenser cathodes may be produced more reliably. Cutting edge radius affects both tool-wear and residual stress of the machined surface. Increasing cutting edge radius results in more tensile residual stress due to ploughing. Very sharp ($r_\beta < 2$ μm) cutting edges do however also produce less compressive stress than lightly honed ($r_\beta = 5$ μm) tools. Tool-wear is also lowest when lightly honed tools and larger nose radii are used.

By controlling depth of cut and cryogenic pre-cooling time, ductile mode and brittle fracture machining of porous tungsten can be achieved. Increasing the amount of cryogenic pre-cooling allows for a deeper cut to be taken while maintaining very good surface porosity as a result of fracture machining. It was shown that brittle fracture machining leads to unstable BUE formation and large tool-wear from sliding/extruding of chips along the cutting edge and onto the machined surface. Only a small range of depths of cut and limited pre-cooling led to acceptable surface roughness because brittle fracture was limited.

To achieve more sustained machining performance, PCD cutting tools were investigated. It was found that a fine grained PCD grade is necessary to avoid catastrophic edge chipping. Edge stability may be further improved by using negative rake angles, which also limit burr formation (i.e., smearing). A slight negative rake angle of $\gamma \approx -5°$ limits the problem of poor chip evacuation common to negative rake angles while providing significantly better surface porosity than neutral rake angle. It should be noted that there is no visible ‘white layer’ in cryogenically machined porous tungsten, even when surface porosity is relatively low.

When limited cryogenic pre-cooling of the workpiece bulk to -90 °C is applied, superior surface quality compared to cryogenic ‘flood’ cooling to -180 °C is obtained.

To avoid difficult to implement pre-cooling to -90 °C, cutting temperature may be increased with cutting speed while using cryogenic flood cooling. Because PCD is prone to fracture at increasing cutting speeds in porous tungsten as a result of vibrations induced by the porous workpiece microstructure, drag finishing was used to allow for higher cutting speeds to be attained.

Cryogenic high speed machining at cutting speeds up to v_c = 400 m/min is feasible with modified cutting edge radius (r_β = 10 μm) PCD tools, allowing for efficient rough and pre-finish machining. Beyond a critical cutting speed ($v_c \approx$ 250 m/min), ductile mode machining of porous tungsten leads to dramatically reduced tool-wear and excellent surface finish due to the elimination of BUE, which is a result of brittle fracture machining. Because of the relatively large cutting edge radius used for cryogenic high speed cutting, surface porosity during ductile mode machining was very low. While this means that high speed cutting of porous tungsten may not be ideal for finish machining of dispenser cathode emitting surfaces, it may be an efficient means to machine the rest of the cathode body where smearing is in fact desired. Moreover, eliminating fracture is very important for both finish and pre-finish machining of porous tungsten because fracture pits and smeared islands also degrade the surfaces from subsequent cuts by unpredictably affecting the uncut chip thickness.

To achieve ductile mode machining of porous tungsten with sharp cutting tools, the effect of uncut chip thickness of the mode of machining at relatively low cutting speeds (20 – 100 m/min) was explored. It was found that there is a critical value of maximum uncut chip thickness h_c, beyond which brittle fracture originates from the cutting tool. The theoretical basis for this effect has been established in the field of ultraprecision machining of brittle materials such as ceramics and glass. Ductile mode machining of dense brittle materials depends a critical ratio between uncut chip thickness and cutting edge radius. In 80% density porous tungsten, h_c is approximately the same as the average ligament size (i.e., h_c = 8-9 μm).

By selecting $h_{max} = h_c$, brittle fracture can be eliminated and cryogenic flood cooling may be used to limit tool-wear and improve surface porosity. Cutting forces in ductile mode machining of porous tungsten are very high and indicate the deformation

mechanism during machining. By comparing cutting force data from this present study to shock loading results of porous tungsten of identical microstructure it was found that the unit cutting pressure (specific cutting force) at the critical chip thickness is approximately the same as the stress at which a steady two wave structure is established. In other words, the critical chip thickness of porous tungsten occurs when the material is loaded/cut in such a way that stable shock waves may propagate within the chip. At very low uncut chip thickness, severe ploughing leads to sub-surface cracking and spalling as a result of very high specific cutting force.

Compaction and collapse of pores in the primary deformation zone change the mechanical properties of porous tungsten during machining, and are necessary for ductile mode machining. Based on the same external results from shock loading of 80% density porous tungsten it was hypothesized that the complete collapse of pores occurs at a certain chip thickness. Cutting force data indicates that the specific cutting force at the steady state chip thickness h_s, beyond which brittle fracture machining does not lead to a further increase in surface roughness, coincides with the stress of complete compaction. As the material in the chip becomes compacted, thermal conductivity and mechanical properties change.

Cutting temperature in finish machining of porous tungsten is a function of maximum uncut chip thickness. The fact that ploughing and low values of h_{max} does not result in very large temperature is likely a result of improved thermal conductivity of the highly compacted chip and machined surface. There is relatively little difference in measured cutting temperature between the critical and steady state chip thickness, suggesting cutting temperature does not play a major role in controlling the brittle to ductile transition at low cutting speeds. Both dry and cryogenic machining resulted in brittle fracture when $h_{max} > h_c$. In this regime, as-machined surface roughness is a result of brittle fracture pits, the size of which is proportional to cutting temperature.

By estimating cryogenic cutting temperature as being proportional to the steady state surface roughness, it was estimated the cryogenic cooling resulted in an average temperature reduction of approximately 220 °C. Since this value is larger than the temperature differential between liquid nitrogen and room temperature ($T_{LN2} \approx$ -180 °C),

it was hypothesized the cryogenic cooling further lowers cutting temperature by clearing abrasive chips and providing some lubrication.

As a whole, cryogenic machining of porous tungsten is a sustainable, highly effective technology that can eliminate the currently used plastic infiltration process. Infiltrant free cryogenic machining is not only a means to streamline the dispenser cathode manufacturing process, but it also leads to significantly improved product quality. Brittle fracture, ploughing and ductile mode material removal can be realized by simply altering the maximum uncut chip thickness. Cryo-cooling is able to provide a level of surface quality unattainable by conventional machining by offering the means to precisely engineer the surface properties of porous tungsten according to specific requirements. The results presented in the present study should provide the basis for reliable implementation of cryogenic machining of porous tungsten for application in dispenser cathodes.

7.2 FUTURE WORK

7.2.1 Further Optimization of Cryogenic Machining Performance

The most immediate work necessary to further improve cryogenic machining of porous tungsten would be to investigate the performance of modern nano-grain PCD and PCBN grades, especially with upsharp edge preparation. While the fine grained PCD tools used for the present study were certainly adequate, fracture toughness of newly developed superabrasive cutting tool materials has been reported to be significantly higher. Moreover, smaller grain size of the cutting tool directly translates into better surface finish of machined components. Currently, only relatively large cutting edge radii of PCD tools allow for high cutting speeds to be attained, limiting this highly productive method to rough and semi-finish machining. With a hypothetical tough yet extremely abrasion resistant tool with very small cutting edge radius, cryogenic high speed finish machining of porous tungsten may be possible.

In addition to high speed finish machining, it would also be highly informative to conduct detailed a tool-wear study as function of cutting speed at $h_{max} = h_c$. Previous work presented in this dissertation showed that even when uncut chip thickness is chosen such that brittle fracture occurs at low cutting speeds, high speed machining provides sufficient heat to exceed the brittle to ductile transition temperature. With improved understanding of critical chip thickness effects in porous tungsten, it would be interesting to conduct high speed machining at or below the critical chip thickness. In this way, tool-wear may potentially be reduced sufficiently to permit the use of sharper cutting tools. Understanding the wear mechanism during ductile mode machining both at low and high cutting speeds will be very helpful for more efficient implementation of cryogenic machining of porous tungsten.

7.2.2 Expansion of Critical Chip Thickness Theory to Other Porous Metals

An important step in expanding the scope of the present study would be to evaluate critical chip thickness effects for a variety of porosities and grain sizes of porous tungsten. It has become clear that the critical chip thickness of 80% density porous tungsten produced from 3-5 μm powder with an average as-sintered ligament size of 8-9 μm is approximately equal to the latter. Based on the current understanding of the nature of the critical chip thickness effect in 80% porous tungsten, it would be expected that h_c will also be equal to average ligament size at other porosity and grain size levels. In simple terms, it is hypothesized that fracture-free ductile mode machining of porous tungsten is only possible when no more than a single ligament is contained within the uncut chip. Due to the intense stress applied by the cutting tool, the chip is completely compacted, leaving little to no imperfections (stress risers) to serve as crack initiation sites. Testing this hypothesis for a range of porous tungsten microstructures would provide the information necessary for developing a more generally applicable model.

Lastly, the most important next step would be to evaluate the applicability of findings from the present study to machining of other porous metals. There exists a range of porous metals in which either high surface porosity (titanium foams) or low surface roughness (PM steel) is a major concern. Cryogenic machining may be an efficient

means to achieve higher surface porosity in titanium foams for bone implants. A possible mechanism for improving surface porosity is controlled fracture machining, which may be possible a suitable combination of cutting edge radius, rake angle and uncut chip thickness is selected. Titanium has a hexagonal close packed crystal structure, which does suggest that cryo-cooling would induce brittleness.

PM steel likewise would benefit from cryogenic machining, though ductile mode or even ploughing would yield more desirable surface quality. If Cryogenic high speed machining of PM steel could lead to similar results as it has in porous tungsten, i.e., lower tool-wear and very low surface roughness with no residual porosity, it could potentially eliminate a whole host of secondary finishing steps (polishing, burnishing, impregnation, etc.). Based on the similarities between PM steel and porous tungsten (hardness, fracture toughness, grain morphology), it is certainly possible that cryogenic machining will provide beneficial effects in both materials. Gaining a better understanding of critical chip thickness effects in porous metals would likewise help to improve product quality by preventing both excessive ploughing (burr formation) and fracture.

7.2.3 Micro-Specimen Four Point Bend Testing to Assess Surface Integrity

While the relationship between machining induced surface integrity and functional performance such as fatigue life and wear resistance has been widely studied and documented, relatively little work has been done to assess the precise mechanical properties of machined surfaces. Commonly used characterization techniques such as XRD residual stress measurement and mico/nano-hardness provide some insight into the difference between the machined surface and sub-surface compared to the bulk material. However, neither technique is capable of isolating the mechanical properties of the machined surface from those of the near sub-surface. In other words, both XRD and micro/nano-hardness measurements assess the state of a certain volume of material rather than the properties of a single layer. Moreover, edge effects prevent even ultra-low force nano-hardness techniques to take measurements closer than approximately 5 μm away from the machined surface.

Because of the setup geometry of bend testing, only the very top layer of a sample is subject to the maximum tensile stress. A three point loading geometry results in the maximum bending moment and stress to occur underneath the central load pin. Therefore, mechanical property result obtained from three point loading are highly susceptible to localized flaws. While this is usually not a problem in highly uniform dense materials, porous and highly brittle materials are generally subjected to four point bending rather than three point. Four point loading results in a constant stress and bending moment between the two central load pins, allowing for a more consistent 'average' flexural strength of the top layer to be obtained. For this reason, four point bend testing will be chosen to assess the mechanical properties of the machined surfaces of porous tungsten from the present study.

REFERENCES

[1] J.O. Tarter, M. Effgen, F. Pusavec, I.S. Jawahir, Cryogenic Machining of Porous Tungsten for Dispenser Cathode Applications, in: IEEE 9th IVEC Monterey, CA, USA 2008.

[2] F. Pusavec, Porous tungsten machining under cryogenic conditions, Int. J. Refract. Met. Hard Mater., 35 (2012) 84-89.

[3] J. Schoop, M. Effgen, T.J. Balk, I.S. Jawahir, Improved Product Quality and Resource Efficiency in Porous Tungsten Machining for Dispenser Cathode Application by Elimination of the Infiltration Process, in: 20th CIRP LCE Singapore, 2013.

[4] J. Schoop, M. Effgen, T.J. Balk, I.S. Jawahir, The Effects of Depth of Cut and Precooling on Surface Porosity from Cryogenic Machining of Porous Tungsten, in: 14th CIRP CMMO, Torino, Italy, 2013.

[5] J. Schoop, I.S. Jawahir, T.J. Balk, D. Busbaher, High performance infiltrant-free cryogenic machining of 82% density porous tungsten under computer numerical control, in: Vacuum Electronics Conference, IEEE International, 2014, pp. 167-168.

[6] S. Chen , D. Head, M. Effgen, I.S. Jawahir, An Investigation of Sustained Machining Performance for Controlled Surface Quality Requirements in Porous Tungsten, IEEE Transactions on Electron Devices, 52 (2005) 903-908.

[7] E. Brinksmeier, A. Walter, G. Reucher, J. Solter, Influence of characteristic material properties on machinability under high speed cutting, International Journal of Machining and Machinability of Materials, 4 (2008) 419-428.

[8] I.J. Stewart, P.R. Arzt, Machining characteristics of the refractory metal systems of Columbium, molybdenum, tantalum, and tungsten, in: National Aero-Nautical Meeting, April 8, 1963 - April 11, 1963, SAE International, Washington, DC, United states, 1963.

[9] A. Chilton, A. Wronski, The effects of strain rate and pressurization on the ductile-brittle transition temperature of polycrystalline sintered tungsten, Journal of the Less Common Metals, 17 (1969) 447-450.

[10] R. Levi, New method for machining sintered tungsten, Precision Metal Molding, 13 (1955) 58-60.

[11] F. Pusavec, A. Deshpande, J. Tarter, M. Effgen, O.W. Dillon Jr., J. Kopac, I.S. Jawahir, Optimization of Machining Performance in Finish Turning of Porous Tungsten under Cryogenic Conditions, in: 2nd Intl. Conference “Innovative Cutting Processes & Smart Machining” Cluny. , 2008

[12] A. Sil, N.K. Samria, A. Chatterjee, D.S. Venkateswarlu, Estimation of dispenser cathode surface temperature of a practical potted heater cathode assembly, IEEE Transactions on Electron Devices, 40 (1993) 1855-1862.

[13] O. Richardson, On the positive ionization produced by hot platinum in air at low pressures, Proceedings of the Physical Society of London, 18 (1903) 524.

[14] O.W. Richardson, Thermionic phenomena and the laws which govern them, Nobel Lecture, December, 12 (1929) 1929.

[15] E.L. Murphy, R. Good Jr, Thermionic emission, field emission, and the transition region, Physical review, 102 (1956) 1464.

[16] J. Wang, L. Li, L. Zhao, Y. Wang, W. Liu, X. Zhang, 17.6: Evaporation behavior of scandia doped dispenser cathode, in: 2010 IEEE International Vacuum Electronics Conference, IVEC 2010, May 18, 2010 - May 20, 2010, IEEE Computer Society, Monterey, CA, United states, 2010, pp. 427-428.

[17] A. Hull, The Dispenser Cathode. A New Type of Thermionic Cathode for Gaseous Discharge Tubes, Physical review, 56 (1939) 86.

[18] G. Gaertner, S. Ording, T. Bisschops, Comparison of Ba evaporation from different Ba dispenser cathode types, ITG-Fachbericht, 150 (1998) 489-494.

[19] H. Glascock Jr Homer, Dispenser cathode and method of manufacture, in, Google Patents, 1966.

[20] H. Wang, Z. Yu, J. Li, W. Shao, A. Yang, L. Xia, J. Shi, P3-32: Fabrication of the big-size thermionic dispenser cathode, in: 2010 IEEE International Vacuum Electronics Conference, IVEC 2010, May 18, 2010 - May 20, 2010, IEEE Computer Society, Monterey, CA, United states, 2010, pp. 393-394.

[21] Anon, Machining pure tungsten, Tooling and Production, 27 (1962) 50-51.

[22] J. Schoop, F. Ambrosy, F. Zanger, V. Schulze, I.S. Jawahir, T.J. Balk, Increased Surface Integrity in Porous Tungsten from Cryogenic Machining with Cermet Cutting Tool, Mater. Manuf. Processes, (2015) 150610065751007.

[23] D. Levina, L. Chernyshev, N. Mikhailovskaya, Contemporary powder metallurgy: Achievements and problems, Powder Metall. Met. Ceram., 46 (2007) 202-205.

[24] J. Banhart, Manufacture, characterisation and application of cellular metals and metal foams, Prog. Mater Sci., 46 (2001) 559-632.

[25] D.G. White, Powder metallurgy. A dynamic industry, in: Proceedings of the 1990 Powder Metallurgy Conference and Exhibition, May 20, 1990 - May 23, 1990, Publ by Metal Powder Industries Federation, Pittsburgh, PA, USA, 1990, pp. 1-13.

[26] S.O. Shah, J.R. McMillen, P.K. Samal, E. Klar, Development of powder metal stainless steel materials for exhaust system applications, in, SAE Technical Paper, 1998.

[27] G. Hoffman, K. Lipp, K. Michaelis, C.M. Sonsino, J.A. Rice, Testing P/M materials for high loading gear applications, International Journal of Powder Metallurgy (Princeton, New Jersey), 35 (1999) 35-44.

[28] E. Alizadeh, Factors influencing the machinability of sintered steels, Powder Metall. Met. Ceram., 47 (2008) 304-315.

[29] N. Narutaki, H. Usuki, Machinability of Sintered Steels, in: Horizons of Powder Metallurgy. Proceedings of the 1986 International Powder Metallurgy Conference and Exhibition: The Future of Powder Metallurgy, P/M '86., Verlag Schmid GmbH, Duesseldorf, W Ger, 1986, pp. 393-396.

[30] J. Denafas, H.N. Hansen, G. Bissacco, J.H. Hales, T. Lund-Olesen, Quantified evaluation of machined surfaces on sintered porous stainless steel samples, in: 12th International Conference of the European Society for Precision Engineering and Nanotechnology, EUSPEN 2012, June 4, 2012 - June 7, 2012, euspen, Stockholm, Sweden, 2012, pp. 53-56.

[31] S. Uenosono, S. Unami, K. Ogura, New improvement in the machinability of P/M steel due to retained graphite particles, in: Proceedings of the 1995 International Conference & Exhibition on Powder Metallurgy & Partuculate Materials. Part 1 (of 3), May 14, 1995 - May 17, 1995, Metal Powder Industries Federation, Seattle, WA, USA, 1995, pp. 8/171-178/176.

[32] E. Robert-Perron, C. Blais, S. Pelletier, Y. Thomas, Drilling of high quality features in green powder metallurgy components, Materials Science and Engineering: A, 458 (2007) 195-201.

[33] A. alak, M. Selecka, K. Vasilko, H. Danninger, Face turning of PM steels: Effect of porosity and carbon level, International Journal of Powder Metallurgy (Princeton, New Jersey), 44 (2008) 49-61.

[34] Z. Zurecki, R. Ghosh, J.H. Frey, Finish-turning of hardened powder metallurgy steel using cryogenic cooling, International Journal of Powder Metallurgy (Princeton, New Jersey), 40 (2004) 19-31.

[35] J. Desbiens, E. Robert-Perron, C. Blais, F. Chagnon, Effect of green machining on the tensile properties and fatigue strength of powder metallurgy sinter-hardenable steel components, Mater. Sci. Eng., A, 546 (2012) 218-222.

[36] M. Hamiuddin, Q. Murtaza, Machinability of phosphorous containing sintered steels, Mater. Chem. Phys., 67 (2001) 78-84.

[37] N. Crisan, A.-M. Trunfio-Sfarghiu, D. Gordin, H. Gheorghiu, G. Stoica, Y. Berthier, A new titanium alloy for biomedical applications, in: 2011 E-Health and Bioengineering Conference, EHB 2011, November 24, 2011 - November 26, 2011, IEEE Computer Society, Iasi, Romania, 2011.

[38] M. Balazic, J. Kopac, Machining of titanium alloy TI-6AL-4V for biomedical applications, Strojniski Vestnik/Journal of Mechanical Engineering, 56 (2010).

[39] Y.J. Chen, B. Feng, Y.P. Zhu, J. Weng, J.X. Wang, X. Lu, Fabrication of porous titanium implants with biomechanical compatibility, Mater. Lett., 63 (2009) 2659-2661.

[40] M. Atapour, A.L. Pilchak, G.S. Frankel, J.C. Williams, Corrosion behavior of titanium alloys for biomedical applications, Mater. Sci. Eng., C, 31 (2011) 885-891.

[41] A.T. Sidambe, Biocompatibility of advanced manufactured titanium implants-A review, Materials, 7 (2014) 8168-8188.

[42] W. Serbinski, T. Seramak, S. Sobieszczyk, A. Zielinski, Fabrication and microstructure characteristics of sintered porous biomaterial based on titanium alloy for orthopedic applications, in: 12th World Conference on Titanium, Ti 2011, June 19, 2011 - June 24, 2011, Science Press, Beijing, China, 2012, pp. 614-619.

[43] M. Gauthier, R. Menini, M.N. Bureau, S.K.V. So, M.J. Dion, L.P. Lefebvre, Properties of novel titanium foams intended for biomedical applications, in: Medical Device Materials - Proceedings of the Materials and Processes for Medical Devices Conference 2003, September 8, 2003 - September 10, 2003, ASM International, Anaheim, CA., United states, 2003, pp. 382-387.

[44] M. Bram, C. Kempmann, A. Laptev, D. Stover, K. Weinert, Investigations on the machining of sintered titanium foams utilizing face milling and peripheral grinding, Adv. Eng. Mater., 5 (2003) 441-447.

[45] R. Singh, P.D. Lee, R.J. Dashwood, T.C. Lindley, Titanium foams for biomedical applications: A review, Materials Technology, 25 (2010) 127-136.

[46] O. Tutunea-Fatan, M. Fakhri, E. Bordatchev, Porosity and cutting forces: from macroscale to microscale machining correlations, Proceedings of the Institution of Mechanical Engineers, Part B: Journal of Engineering Manufacture, 225 (2011) 619-630.

[47] M. Bram, A. Laptev, H.P. Buchkremer, D. Stover, Near-net-shape manufacturing of highly porous titanium parts for biomedical applications

Herstellung von hochporosen, endkonturnahen titan-formkorpern fur biomedizinische anwendungen, Materialwiss. Werkstofftech., 35 (2004) 213-218.

[48] S. Amin Yavari, S.M. Ahmadi, J. van der Stok, R. Wauthle, A.C. Riemslag, M. Janssen, J. Schrooten, H. Weinans, A.A. Zadpoor, Effects of bio-functionalizing surface treatments on the mechanical behavior of open porous titanium biomaterials, Journal of the Mechanical Behavior of Biomedical Materials, 36 (2014) 109-119.

[49] S. Pervaiz, A. Rashid, I. Deiab, M. Nicolescu, Influence of tool materials on machinability of titanium- and nickel-based alloys: A review, Mater. Manuf. Processes, 29 (2014) 219-252.

[50] M.A. Fakhri, E.V. Bordatchev, O.R. Tutunea-Fatan, Framework for evaluation of the relative contribution of the process on porosity-cutting force dependence in micromilling of titanium foams, in, SAGE Publications Ltd, 55 City Road, London, EC1Y 1SP, United Kingdom, 2013, pp. 1635-1650.

[51] M. Abolghasemi Fakhri, E.V. Bordatchev, O.R. Tutunea-Fatan, An image-based methodology to establish correlations between porosity and cutting force in micromilling of porous titanium foams, International Journal of Advanced Manufacturing Technology, 60 (2012) 841-851.

[52] D.A. Axinte, N. Gindy, K. Fox, I. Unanue, Process monitoring to assist the workpiece surface quality in machining, International Journal of Machine Tools and Manufacture, 44 (2004) 1091-1108.

[53] M. Thomas, S. Turner, M. Jackson, Microstructural damage during high-speed milling of titanium alloys, Scripta Mater., 62 (2010) 250-253.

[54] E. Brinksmeier, State-of-the-art of non-destructive measurement of sub-surface material properties and damages, Precision Engineering, 11 (1989) 211-224.

[55] R. M'Saoubi, J.C. Outeiro, H. Chandrasekaran, O.W. Dillon Jr, I.S. Jawahir, A review of surface integrity in machining and its impact on functional performance and life of machined products, International Journal of Sustainable Manufacturing, 1 (2008) 203-236.

[56] A. Yamamoto, T. Yamada, S. Nakahigashi, L. Liu, M. Terasawa, H. Tsubakino, Effects of surface grinding on hardness distribution and residual stress in low carbon austenitic stainless steel SUS316L, ISIJ Int., 44 (2004) 1780-1782.

[57] P.J. Withers, Residual stress and its role in failure, Rep. Prog. Phys., 70 (2007) 2211-2264.

[58] A. Ramesh, S.N. Melkote, L.F. Allard, L. Riester, T.R. Watkins, Analysis of white layers formed in hard turning of AISI 52100 steel, Mater. Sci. Eng., A, 390 (2005) 88-97.

[59] D.K. Aspinwall, S.L. Soo, A.E. Berrisford, G. Walder, Workpiece surface roughness and integrity after WEDM of Ti-6Al-4V and Inconel 718 using minimum damage generator technology, CIRP Annals - Manufacturing Technology, 57 (2008) 187-190.

[60] I.S. Jawahir, E. Brinksmeier, R. M'Saoubi, D.K. Aspinwall, J.C. Outeiro, D. Meyer, D. Umbrello, A.D. Jayal, Surface integrity in material removal processes: Recent advances, CIRP Annals - Manufacturing Technology, 60 (2011) 603-626.

[61] H.K. Tönshoff, W. v. Schmieden, I. Inasaki, W. König, G. Spur, Abrasive Machining of Silicon, CIRP Annals - Manufacturing Technology, 39 (1990) 621-635.

[62] J. Yan, T. Asami, H. Harada, T. Kuriyagawa, Fundamental investigation of subsurface damage in single crystalline silicon caused by diamond machining, Precision Engineering, 33 (2009) 378-386.

[63] R. Teti, K. Jemielniak, G. O'Donnell, D. Dornfeld, Advanced monitoring of machining operations, CIRP Annals - Manufacturing Technology, 59 (2010) 717-739.

[64] T. Semba, K. Sakuma, Y. Tani, H. Sato, Thickness Measurement of a Metallurgically Damaged Layer on a Ground Surface Using an Acoustic Microscope, CIRP Annals - Manufacturing Technology, 38 (1989) 549-552.

[65] P.J. Withers, M. Turski, L. Edwards, P.J. Bouchard, D.J. Buttle, Recent advances in residual stress measurement, International Journal of Pressure Vessels and Piping, 85 (2008) 118-127.

[66] J.C. Outeiro, A.M. Dias, I.S. Jawahir, On the effects of residual stresses induced by coated and uncoated cutting tools with finite edge radii in turning operations, CIRP Annals - Manufacturing Technology, 55 (2006) 111-116.

[67] D.W. Schwach, Y.B. Guo, A fundamental study on the impact of surface integrity by hard turning on rolling contact fatigue, Int. J. Fatigue, 28 (2006) 1838-1844.

[68] H.K. Tonshoff, C. Arendt, R. Ben Amor, Cutting of hardened steel, CIRP Annals - Manufacturing Technology, 49 (2000) 547-566.

[69] J. Barry, G. Byrne, TEM study on the surface white layer in two turned hardened steels, Mater. Sci. Eng., A, 325 (2002) 356-364.

[70] D.A. Axinte, R.C. Dewes, Surface integrity of hot work tool steel after high speed milling-experimental data and empirical models, J. Mater. Process. Technol., 127 (2002) 325-335.

[71] N.F.M. Aris, K. Cheng, Characterization of the surface functionality on precision machined engineering surfaces, International Journal of Advanced Manufacturing Technology, 38 (2008) 402-409.

[72] X.P. Xu, Y.Q. Yu, H.J. Xu, Effect of grinding temperatures on the surface integrity of a nickel-based superalloy, J. Mater. Process. Technol., 129 (2002) 359-363.

[73] M.F. DeVries, M. Field, J.F. Kahles, Relationship of Surface Roughness and Surface Integrity to Functional Properties, Ann CIRP, 25 (1976) 569-573.

[74] X. Jiang, Robust solution for the evaluation of stratified functional surfaces, CIRP Annals - Manufacturing Technology, 59 (2010) 573-576.

[75] M.E. Merchant, Basic mechanics of the metal cutting process, Journal of Applied Mechanics, 11 (1944) 168-175.

[76] M.E. Merchant, Mechanics of the metal cutting process. II. Plasticity conditions in orthogonal cutting, J. Appl. Phys., 16 (1945) 318-324.

[77] M.E. Merchant, Mechanics of the metal cutting process. I. Orthogonal cutting and a type 2 chip, J. Appl. Phys., 16 (1945) 267-275.

[78] P. Albrecht, New Developments in the Theory of the Metal-Cutting Process: Part I. The Ploughing Process in Metal Cutting, Journal of Manufacturing Science and Engineering, 82 (1960) 348-357.

[79] K. Nakayama, M. Shaw, R. Brewer, Relationship between cutting forces, temperatures, built-up edge and surface finish, CIRP ANN, 14 (1966) 211-223.

[80] J.D. Thiele, S. N. Melkote, Effect of cutting edge geometry and workpiece hardness on surface generation in the finish hard turning of AISI 52100 steel, J. Mater. Process. Technol., 94 (1999) 216-226.

[81] B. Denkena, D. Biermann, Cutting edge geometries, CIRP Annals - Manufacturing Technology, 63 (2014) 631-653.

[82] B. Denkena, J. Kohler, B. Bergmann, Development of cutting edge geometries for hard milling operations, CIRP Journal of Manufacturing Science and Technology, 8 (2015) 43-52.

[83] P.C. Priarone, S. Rizzuti, L. Settineri, G. Vergnano, Effects of cutting angle, edge preparation, and nano-structured coating on milling performance of a gamma titanium aluminide, J. Mater. Process. Technol., 212 (2012) 2619-2628.

[84] D. Biermann, A. Baschin, Influence of cutting edge geometry and cutting edge radius on the stability of micromilling processes, Prod. Eng. Res. Devel., 3 (2009) 375-380.

[85] D. Biermann, I. Terwey, Cutting edge preparation to improve drilling tools for HPC processes, CIRP Journal of Manufacturing Science and Technology, 1 (2008) 76-80.

[86] D. Biermann, M. Wolf, R. Aßmuth, Cutting edge preparation to enhance the performance of single lip deep hole drills, in: Procedia CIRP, 2012, pp. 172-177.

[87] T. Ozel, T.-K. Hsu, E. Zeren, Effects of cutting edge geometry, workpiece hardness, feed rate and cutting speed on surface roughness and forces in finish turning of hardened AISI H13 steel, International Journal of Advanced Manufacturing Technology, 25 (2005) 262-269.

[88] B. Denkena, L. de Leon, J. Köhler, Influence of scaled undeformed sections of cut on strain rate, cutting force and temperature, Prod. Eng. Res. Devel., 4 (2010) 457-464.

[89] F. Schultheiss, S. Hägglund, V. Bushlya, J. Zhou, J.-E. Ståhl, Influence of the Minimum Chip Thickness on the Obtained Surface Roughness During Turning Operations, Procedia CIRP, 13 (2014) 67-71.

[90] P. Brammertz, Die Entstehung der Oberflachenrauheit beim Feindrehen, Industrieanzeiger, 2 (1961) 25-32.

[91] K. Liu, S.N. Melkote, Effect of plastic side flow on surface roughness in micro-turning process, International Journal of Machine Tools and Manufacture, 46 (2006) 1778-1785.

[92] H. Weule, V. Hüntrup, H. Tritschler, Micro-cutting of steel to meet new requirements in miniaturization, CIRP Annals-Manufacturing Technology, 50 (2001) 61-64.

[93] X. Liu, R.E. DeVor, S.G. Kapoor, An analytical model for the prediction of minimum chip thickness in micromachining, Journal of Manufacturing Science and Engineering, Transactions of the ASME, 128 (2006) 474-481.

[94] J.E. Ståhl, F. Schultheiss, S. Hägglund, Analytical and Experimental Determination of the Ra Surface Roughness during Turning, Procedia Engineering, 19 (2011) 349-356.

[95] H.A. Kishawy, A.J. Haglund, I.M. Deiab, An analysis of machining with honed tools using ale finite element model: Ploughing force and minimum chip thickness, in: 34th North American Manufacturing Research Conference, May 23, 2006 - May 26, 2006, Society of Manufacturing Engineers, Milwaukee, WI, United states, 2006, pp. 277-284.

[96] T.H.C. Childs, D. Dornfeld, D.E. Lee, S. Min, K. Sekiya, R. Tezuka, Y. Yamane, The influence of cutting edge sharpness on surface finish in facing with round nosed cutting tools, CIRP Journal of Manufacturing Science and Technology, 1 (2008) 70-75.

[97] K. Oishi, Finish cutting of hardened steel (1st report) - Influence of workpiece hardness for the forming of built-up edge, Seimitsu Kogaku Kaishi/Journal of the Japan Society for Precision Engineering, 59 (1993) 509-516.

[98] J. Kummel, D. Braun, J. Gibmeier, J. Schneider, C. Greiner, V. Schulze, A. Wanner, Study on micro texturing of uncoated cemented carbide cutting tools for wear improvement and built-up edge stabilisation, J. Mater. Process. Technol., 215 (2015) 62-70.

[99] R. Yousefi, Y. Ichida, Study on ultra-high-speed cutting of aluminum alloy: Formation of welded metal on the secondary cutting edge of the tool and its effects on the quality of finished surface, Precision Engineering, 24 (2000) 371-376.

[100] M.E.A. Moneim, Tool Edge Roundness in Finish Machining at High Cutting Speeds, Wear, 58 (1980) 173-192.

[101] D.J. Waldorf, R.E. DeVor, S.G. Kapoor, An evaluation of ploughing models for orthogonal machining, Journal of Manufacturing Science and Engineering, Transactions of the ASME, 121 (1999) 550-558.

[102] T.H.C. Childs, Surface energy, cutting edge radius and material flow stress size effects in continuous chip formation of metals, CIRP Journal of Manufacturing Science and Technology, 3 (2010) 27-39.

[103] F.B. de Oliveira, A.R. Rodrigues, R.T. Coelho, A.F. de Souza, Size effect and minimum chip thickness in micromilling, International Journal of Machine Tools and Manufacture, 89 (2015) 39-54.

[104] N. Ikawa, S. Shimada, H. Tanaka, Minimum thickness of cut in micromachining, Nanotechnology, 3 (1992) 6.

[105] Z.G. Wang, X. Cheng, K. Nakamoto, S. Kobayashi, K. Yamazaki, Modeling of minimum chip thickness in micromachining of hard tool steels with the modified slip line model, in: 24th Annual Meeting of the American Society for Precision Engineering, ASPE 2009, October 4, 2009 - October 9, 2009, American Society for Precision Engineering, ASPE, Monterey, CA, United states, 2009, pp. Elsevier Science, Inc.; 3M Company; Corning Tropel Corporation; ADCOLE Corporation; Equilibria.

[106] X. Lai, H. Li, C. Li, Z. Lin, J. Ni, Modelling and analysis of micro scale milling considering size effect, micro cutter edge radius and minimum chip thickness, International Journal of Machine Tools and Manufacture, 48 (2008) 1-14.

[107] Z.Y. Shi, Z.Q. Liu, Y.B. Guo, An assessment, definition, and determination of the minimum uncut chip thickness of microcutting and impact on machining new powder metallurgy nickel-based superalloys, in: ASME 2011 International Mechanical Engineering Congress and Exposition, IMECE 2011, November 11, 2011 - November 17, 2011, American Society of Mechanical Engineers, Denver, CO, United states, 2011, pp. 691-700.

[108] T.G. Bifano, T. Dow, R. Scattergood, Ductile-regime grinding: a new technology for machining brittle materials, Journal of Manufacturing Science and Engineering, 113 (1991) 184-189.

[109] T.G. Bifano, T.A. Dow, R.O. Scattergood, Ductile-regime grinding of brittle materials: experimental results and the development of a model, in: 32nd Annual Technical Symposium, International Society for Optics and Photonics, 1989, pp. 108-115.

[110] Z. Zhong, Ductile or partial ductile mode machining of brittle materials, The International Journal of Advanced Manufacturing Technology, 21 (2003) 579-585.

[111] D.B. Marshall, B.R. Lawn, Indentation of brittle materials, Microindentation Techniques in Materials Science and Engineering, ASTM STP, 889 (1986) 26-46.

[112] D. Gamzina, Machining Methods for Nano-Composite Scandate Tungsten Cathodes, in, University of California, Davis, Ann Arbor, 2012, pp. 75.

[113] B.V. Bell, K. Okazaki, Mechanical and microstructural properties of porous tungsten, in: Proceedings of the 1994 International Conference & Exhibition on Powder Metallurgy & Particulate Materials. Part 5 (of 7), May 8 - 11 Metal Powder Industries Federation, Toronto, Canada, 1994, pp. 237-237.

[114] W.S. Blackley, R.O. Scattergood, Ductile-regime machining model for diamond turning of brittle materials, Precision Engineering, 13 (1991) 95-103.

[115] J.B. Bryan, Design and construction of an ultraprecision 84 inch diamond turning machine, Precision Engineering, 1 (1979) 13-17.

[116] T. Nakasuji, S. Kodera, S. Hara, H. Matsunaga, N. Ikawa, S. Shimada, Diamond turning of brittle materials for optical components, CIRP Annals-Manufacturing Technology, 39 (1990) 89-92.

[117] J. Yan, K. Syoji, T. Kuriyagawa, H. Suzuki, Ductile regime turning at large tool feed, J. Mater. Process. Technol., 121 (2002) 363-372.

[118] K. Liu, X. Li, S. Liang, The mechanism of ductile chip formation in cutting of brittle materials, The International Journal of Advanced Manufacturing Technology, 33 (2007) 875-884.

[119] X. Zhang, M. Arif, K. Liu, A.S. Kumar, M. Rahman, A model to predict the critical undeformed chip thickness in vibration-assisted machining of brittle materials, International Journal of Machine Tools and Manufacture, 69 (2013) 57-66.

[120] M. Arif, M. Rahman, W. San, N. Doshi, An experimental approach to study the capability of end-milling for microcutting of glass, The International Journal of Advanced Manufacturing Technology, 53 (2011) 1063-1073.

[121] M. Arif, M. Rahman, W.Y. San, Analytical modeling of ductile-regime machining of tungsten carbide by endmilling, The International Journal of Advanced Manufacturing Technology, 55 (2011) 53-64.

[122] M. Arif, M. Rahman, W.Y. San, Analytical model to determine the critical conditions for the modes of material removal in the milling process of brittle material, J. Mater. Process. Technol., 212 (2012) 1925-1933.

[123] M. Arif, M. Rahman, W.Y. San, An experimental study on the machining characteristics in ductile-mode milling of BK-7 glass, in, Springer London, The

Guildway, Old Portsmouth Road, Artington, Guildford, GU3 1LP, United Kingdom, 2012, pp. 487-495.

[124] M. Arif, M. Rahman, W.Y. San, A study on the effect of tool-edge radius on critical machining characteristics in ultra-precision milling of tungsten carbide, International Journal of Advanced Manufacturing Technology, 67 (2013) 1257-1265.

[125] M. Arif, M. Rahman, W. Yoke San, Analytical model to determine the critical feed per edge for ductile–brittle transition in milling process of brittle materials, International Journal of Machine Tools and Manufacture, 51 (2011) 170-181.

[126] M. Arif, Z. Xinquan, M. Rahman, S. Kumar, A predictive model of the critical undeformed chip thickness for ductile-brittle transition in nano-machining of brittle materials, International Journal of Machine Tools and Manufacture, 64 (2013) 114-122.

[127] N. Fang, I.S. Jawahir, An analytical predictive model and experimental validation for machining with grooved tools incorporating the effects of strains, strain-rates, and temperatures, CIRP Annals - Manufacturing Technology, 51 (2002) 83-86.

[128] G. Poulachon, A. Moisan, I.S. Jawahir, On modelling the influence of thermo-mechanical behavior in chip formation during hard turning of 100Cr6 bearing steel, CIRP Annals - Manufacturing Technology, 50 (2001) 31-36.

[129] O. Dillon Jr, Thermal stresses in machining, Journal of thermal stresses, 15 (1992) 241-251.

[130] O. Dillon, R. De Angelis, W. Lu, J. Gunasekera, J. Deno, The effects of temperature on the machining of metals, Journal of Materials Shaping Technology, 8 (1990) 23-29.

[131] S.Y. Hong, Z. Zhao, Thermal aspects, material considerations and cooling strategies in cryogenic machining, Clean Products and Processes, 1 (1999) 107-116.

[132] D. Umbrello, S. Caruso, S. Yang, F. Crea, O.W. Dillon Jr, I.S. Jawahir, The effect of cryogenic cooling on white layer formation in hard machining, in: ASME 2011 International Mechanical Engineering Congress and Exposition, IMECE 2011, November 11, 2011 - November 17, 2011, American Society of Mechanical Engineers, Denver, CO, United states, 2011, pp. 341-348.

[133] K. Uehara, S. Kumagai, Chip formation, surface roughness and cutting force in cryogenic machining, Ann. CIRP, 17 (1968) 409-416.

[134] A. Bhattacharya, T. Roy, A. Chattopadhyay, Application of cryogenic in metal machining, J. of Institution of Engs, India, 52 (1972) 73-81.

[135] K. UEHARA, S. KUMAGAI, Characteristics of tool-wear in cryogenic machining, Defense Technical Information Center, 1970.

[136] J. Li, Z. Yuan, M. Zhou, Cryogenic ultra-precision machining of ferrous metals with natural diamond tools, Jixie goneheng Xuebao, 25 (1989) 69-72.

[137] R.L. Lundin, D.D. Stewart, C.J. Evans, Diamond tool machining of materials which react with diamond, in, Google Patents, 1992.

[138] C. Evans, J. Bryan, Cryogenic diamond turning of stainless steel, CIRP Annals-Manufacturing Technology, 40 (1991) 571-575.

[139] S.Y. Hong, Advancement of economical cryogenic machining technology, in: Proceedings of 3rd International Conference on Manufacturing, 1995.

[140] D. Bhattacharyya, M. Allen, S. Mander, Cryogenic machining of Kevlar composites, Mater. Manuf. Processes, 8 (1993) 631-651.

[141] Z. Zhao, S.Y. Hong, Cooling strategies for cryogenic machining from a materials viewpoint, J. Mater. Eng. Perform., 1 (1992) 669-678.

[142] S.Y. Hong, Economical and ecological cryogenic machining, Journal of Manufacturing Science and Engineering, 123 (2001) 331-338.

[143] S.Y. Hong, Investigation of liquid nitrogen lubrication effect in cryogenic machining, in: 2005 World Tribology Congress III, September 12, 2005 - September 16, 2005, American Society of Mechanical Engineers, Washington, D.C., United states, 2005, pp. 801-802.

[144] S.Y. Hong, M. Broomer, Economical and ecological cryogenic machining of AISI 304 austenitic stainless steel, Clean Products and Processes, 2 (2000) 157-166.

[145] S.Y. Hong, Y. Ding, Cooling approaches and cutting temperatures in cryogenic machining of Ti-6Al-4V, International Journal of Machine Tools and Manufacture, 41 (2001) 1417-1437.

[146] S.Y. Hong, Y. Ding, Micro-temperature manipulation in cryogenic machining of low carbon steel, J. Mater. Process. Technol., 116 (2001) 22-30.

[147] S.Y. Hong, Y. Ding, J. Jeong, Experimental evaluation of friction coefficient and liquid nitrogen lubrication effect in cryogenic machining, Machining Science and Technology, 6 (2002) 235-250.

[148] S.Y. Hong, Y. Ding, W.-c. Jeong, Friction and cutting forces in cryogenic machining of Ti–6Al–4V, International Journal of Machine Tools and Manufacture, 41 (2001) 2271-2285.

[149] S.Y. Hong, I. Markus, W.-c. Jeong, New cooling approach and tool-life improvement in cryogenic machining of titanium alloy Ti-6Al-4V, International Journal of Machine Tools and Manufacture, 41 (2001) 2245-2260.

[150] C. Courbon, F. Pusavec, F. Dumont, J. Rech, J. Kopac, Tribological behaviour of Ti6Al4V and Inconel718 under dry and cryogenic conditions—Application to the context of machining with carbide tools, Tribology International, 66 (2013) 72-82.

[151] J. Caudill, B. Huang, C. Arvin, J. Schoop, K. Meyer, I. Jawahir, Enhancing the Surface Integrity of Ti-6Al-4V Alloy through Cryogenic Burnishing, Procedia CIRP, 13 (2014) 243-248.

[152] R. Bassani, E. Ciulli, B. Piccigallo, M. Pirozzi, U. Staffilano, Hydrostatic lubrication with cryogenic fluids, Tribology International, 39 (2006) 827-832.

[153] R. Ghosh, B. Lindsley, Role of machining additives and cryogenic cooling in machining of sinterhardened materials, in: 2008 World Congress on Powder Metallurgy and Particulate Materials, PowderMet 2008, June 8, 2008 - June 12, 2008, Metal Powder Industries Federation, Washington, DC, United states, 2008, pp. 613-621.

[154] R. Ghosh, J.A. Knopf, D.J. Gibson, T. Mebrahtu, G. Currie, Cryogenic machining of polymeric biomaterials: An intraocular lens case study, in: Medical Device Materials IV: Materials and Processes for Medical Devices Conference 2007, September 23, 2007 - September 25, 2007, ASM International, Palm Desert, CA, United states, 2008, pp. 54-64.

[155] Z. Zurecki, R. Ghosh, J.H. Frey, Investigation of White Layers Formed in Conventional and Cryogenic Hard Turning of Steels, in: 2003 ASME International Mechanical Engineering Congress, November 15, 2003 - November 21, 2003, American Society of Mechanical Engineers (ASME), Washington, DC., United states, 2003, pp. 211-220.

[156] R. Ghosh, Z. Zurecki, J.H. Frey, Cryogenic Machining with Brittle Tools and Effects on Tool-life, in: 2003 ASME International Mechanical Engineering Congress, November 15, 2003 - November 21, 2003, American Society of Mechanical Engineers (ASME), Washington, DC., United states, 2003, pp. 201-209.

[157] Y. Kakinuma, N. Yasuda, T. Aoyama, Micro machining of soft polymer material applying cryogenic cooling, in: 4th International Conference on Leading Edge Manufacturing in 21st Century, LEM 2007, November 7, 2007 - November 9, 2007, Japan Society of Mechanical Engineers, Fukuoka, Japan, 2007, pp. Japan Society of Mechanical Engineers (JSME),; Manufacturing and Machine Tool Division; Japan Society of Mechanical Engineers (JSME),; Manufacturing System Division.

[158] V.G. Dhokia, S.T. Newman, P. Crabtree, M.P. Ansell, A methodology for the determination of foamed polymer contraction rates as a result of cryogenic CNC machining, in, Elsevier Ltd, Langford Lane, Kidlington, Oxford, OX5 1GB, United Kingdom, 2010, pp. 665-670.

[159] A. Huang, Y. Kaynak, D. Umbrello, I.S. Jawahir, Cryogenic machining of hard-to-machine material, AISI 52100: A study of chip morphology and comparison with dry machining, in: 10th Asia-Pacific Conference on Materials Processing, APCMP 2012, June 14, 2012 - June 17, 2012, Trans Tech Publications, Jinan, China, 2012, pp. 140-145.

[160] D. Umbrello, S. Yang, O.W. Dillon Jr, I.S. Jawahir, Effects of cryogenic cooling on surface layer alterations in machining of AISI 52100 steels, Materials Science and Technology (United Kingdom), 28 (2012) 1320-1331.

[161] D. Umbrello, F. Micari, I.S. Jawahir, The effects of cryogenic cooling on surface integrity in hard machining: A comparison with dry machining, CIRP Annals - Manufacturing Technology, 61 (2012) 103-106.

[162] D. Umbrello, Z. Pu, S. Caruso, J.C. Outeiro, A.D. Jayal, O.W. Dillon Jr, I.S. Jawahir, The effects of cryogenic cooling on surface integrity in hard machining, in: 1st CIRP Conference on Surface Integrity, CSI 2012, January 30, 2012 - February 1, 2012, Elsevier Ltd, Bremen, Germany, 2011, pp. 371-376.

[163] Z. Pu, D. Umbrello, O.W. Dillon, T. Lu, D.A. Puleo, I.S. Jawahir, Finite element modeling of microstructural changes in dry and cryogenic machining of AZ31B magnesium alloy, Journal of Manufacturing Processes, 16 (2014) 335-343.

[164] Z. Pu, J.C. Outeiro, A.C. Batista, O.W. Dillon Jr, D.A. Puleo, I.S. Jawahir, Enhanced surface integrity of AZ31B Mg alloy by cryogenic machining towards improved functional performance of machined components, International Journal of Machine Tools and Manufacture, 56 (2012) 17-27.

[165] Z.W. Pu, S. Caruso, D. Umbrello, O.W. Dillon Jr, D.A. Puleo, I.S. Jawahir, Analysis of surface integrity in dry and cryogenic machining of AZ31B Mg alloys, in: 17th CIRP Conference on Modelling of Machining Operations, May 12, 2011 - May 13, 2011, Trans Tech Publications, Sintra, Portugal, 2011, pp. 439-448.

[166] Z. Pu, D.A. Puleo, O.W. Dillon Jr, I.S. Jawahir, Controlling the biodegradation rate of magnesium-based implants through surface nanocrystallization induced by cryogenic machining, in: Magnesium Technology 2011 - TMS 2011 Annual Meeting and Exhibition, February 27, 2011 - March 3, 2011, Minerals, Metals and Materials Society, San Diego, CA, United states, 2011, pp. 637-642.

[167] Z. Pu, J.C. Outeiro, A.C. Batista, O.W. Dillon Jr, D.A. Puleo, I.S. Jawahir, Surface integrity in dry and cryogenic machining of AZ31B Mg alloy with varying cutting edge radius tools, in: 1st CIRP Conference on Surface Integrity, CSI 2012, January 30, 2012 - February 1, 2012, Elsevier Ltd, Bremen, Germany, 2011, pp. 282-287.

[168] Z. Pu, O.W. Dillon Jr, I.S. Jawahir, D.A. Puleo, Microstructural changes of AZ31 magnesium alloys induced by cryogenic machining and its influence on corrosion resistance in simulated body fluid for biomedical applications, in: ASME 2010 International Manufacturing Science and Engineering Conference, MSEC 2010, October 12, 2010 - October 15, 2010, American Society of Mechanical Engineers, Erie, PA, United states, 2010, pp. 271-277.

[169] M. Meyers, O. Vöhringer, V. Lubarda, The onset of twinning in metals: a constitutive description, Acta Mater., 49 (2001) 4025-4039.

[170] A. Staroselsky, L. Anand, A constitutive model for hcp materials deforming by slip and twinning: application to magnesium alloy AZ31B, Int. J. Plast., 19 (2003) 1843-1864.

[171] Y. Kaynak, T. Lu, I.S. Jawahir, Cryogenic machining-induced surface integrity: A review and comparison with dry, mql, and flood-cooled machining, Machining Science and Technology, 18 (2014) 149-198.

[172] F. Ambrosy, F. Zanger, V. Schulze, I.S. Jawahir, An experimental study of cryogenic machining on nanocrystalline surface layer generation, in: 2nd CIRP Conference on Surface Integrity, CSI 2014, May 28, 2014 - May 30, 2014, Elsevier, Nottingham, United kingdom, 2014, pp. 169-174.

[173] A. Shokrani, V. Dhokia, P. Munoz-Escalona, S.T. Newman, State-of-the-art cryogenic machining and processing, International Journal of Computer Integrated Manufacturing, 26 (2013) 616-648.

[174] F. Klocke, D. Lung, A. Kramer, T. Cayli, H. Sangermann, Potential of modern lubricoolant strategies on cutting performance, in: 16th ESAFORM Conference on Material Forming, ESAFORM 2013, April 22, 2013 - April 24, 2013, Trans Tech Publications Ltd, Aveiro, Portugal, 2013, pp. 2062-2071.

[175] G. Rotella, D. Umbrello, Numerical simulation of surface modification in dry and cryogenic machining of AA7075 alloy, in: 2nd CIRP Conference on Surface Integrity, CSI 2014, May 28, 2014 - May 30, 2014, Elsevier, Nottingham, United kingdom, 2014, pp. 327-332.

[176] S. Cordes, F. Hubner, T. Schaarschmidt, Next generation high performance cutting by use of carbon dioxide as cryogenics, in, Elsevier, 2014, pp. 401-405.

[177] S. Sun, M. Brandt, S. Palanisamy, M.S. Dargusch, Effect of cryogenic compressed air on the evolution of cutting force and tool-wear during machining of Ti–6Al–4V alloy, J. Mater. Process. Technol., 221 (2015) 243-254.

[178] Y. Kaynak, H.E. Karaca, R.D. Noebe, I.S. Jawahir, Analysis of tool-wear and cutting force components in dry, preheated, and cryogenic machining of NiTi shape memory alloys, in: 14th CIRP Conference on Modeling of Machining Operations, CIRP CMMO 2013, June 13, 2013 - June 14, 2013, Elsevier, Turin, Italy, 2013, pp. 498-503.

[179] M.J. Bermingham, J. Kirsch, S. Sun, S. Palanisamy, M.S. Dargusch, New observations on tool-life, cutting forces and chip morphology in cryogenic machining Ti-6Al-4V, International Journal of Machine Tools and Manufacture, 51 (2011) 500-511.

[180] K. Venugopal, S. Paul, A. Chattopadhyay, On Effect of Cryogenic Cooling on Tool-wear in Turning Ti-6AI-4V Alloy, in: Proceedings of the 34th International MATADOR Conference, Springer, 2004, pp. 127-132.

[181] Y. Kaynak, H.E. Karaca, I.S. Jawahir, Cutting Speed Dependent Microstructure and Transformation Behavior of NiTi Alloy in Dry and Cryogenic Machining, J. Mater. Eng. Perform., 24 (2014) 452-460.

[182] F. Pusavec, A. Deshpande, S. Yang, R. M'Saoubi, J. Kopac, O.W. Dillon Jr, I.S. Jawahir, Sustainable machining of high temperature Nickel alloy - Inconel 718: Part 1 - Predictive performance models, Journal of Cleaner Production, 81 (2014) 255-269.

[183] E. Ezugwu, Key improvements in the machining of difficult-to-cut aerospace superalloys, International Journal of Machine Tools and Manufacture, 45 (2005) 1353-1367.

[184] M. Rahman, Y.S. Wong, A.R. Zareena, Machinability of Titanium Alloys, JSME International Journal Series C, 46 (2003) 107-115.

[185] E. Ezugwu, J. Bonney, Y. Yamane, An overview of the machinability of aeroengine alloys, J. Mater. Process. Technol., 134 (2003) 233-253.

[186] D. Dudzinski, A. Devillez, A. Moufki, D. Larrouquere, V. Zerrouki, J. Vigneau, A review of developments towards dry and high speed machining of Inconel 718 alloy, International Journal of Machine Tools and Manufacture, 44 (2004) 439-456.

[187] E. Ezugwu, J. Bonney, Effect of high-pressure coolant supply when machining nickel-base, Inconel 718, alloy with coated carbide tools, J. Mater. Process. Technol., 153 (2004) 1045-1050.

[188] Y. Chen, Y. Liao, Study on wear mechanisms in drilling of Inconel 718 superalloy, J. Mater. Process. Technol., 140 (2003) 269-273.

[189] G. Rotella, O.W. Dillon Jr, D. Umbrello, L. Settineri, I.S. Jawahir, The effects of cooling conditions on surface integrity in machining of Ti6Al4V alloy, International Journal of Advanced Manufacturing Technology, 71 (2014) 47-55.

[190] Y. Kaynak, H.E. Karaca, I.S. Jawahir, Surface integrity characteristics of NiTi shape memory alloys resulting from dry and cryogenic machining, in: 2nd CIRP Conference on Surface Integrity, CSI 2014, May 28, 2014 - May 30, 2014, Elsevier, Nottingham, United kingdom, 2014, pp. 393-398.

[191] K. Venugopal, R. Tawade, P. Prashanth, S. Paul, A. Chattopadhyay, Turning of titanium alloy with TiB2-coated carbides under cryogenic cooling, Proceedings of the Institution of Mechanical Engineers, Part B: Journal of Engineering Manufacture, 217 (2003) 1697-1707.

[192] S. Sharafat, M. Demetriou, N. Ghoniem, B. Williams, R. Nygren, Enhanced surface heat removal using a porous tungsten heat exchanger, in: 14th Topical Meeting on the Technology of Fusion Energy, October 15, 2000 - October 19, 2000, American Nuclear Society, Park City, UT, United states, 2001, pp. 863-867.

[193] Y.A. Trishin, S.A. Kinelovskij, Effect of porosity on the cumulative flow, Fizika Goreniya i Vzryva, 36 (2000) 122-132.

[194] C. Selcuk, R. Bentham, N. Morley, J.V. Wood, Microhardness as a measure of homogeneity of porous tungsten, Mater. Lett., 58 (2004) 1873-1876.

[195] Y. Weihong, P. Hongwan, T. Xiurong, Some properties of porous tungsten at high temperature, High Temperatures - High Pressures, 26 (1994) 109-113.

[196] K.T. Kim, J. Suh, Elastic-plastic strain hardening response of porous metals, International Journal of Engineering Science, 27 (1989) 767-778.

[197] K.T. Kim, Elastic-plastic response of porous metals under triaxial loading, International Journal of Solids and Structures, 24 (1988) 937-945.

[198] D. Francois, C. Terraz, R. Meyer, H. Pastor, Electric and Thermal Conductivities, Elastic Properties and Resistance to Bending of Porous Tungsten as a Function of the Whole Range of Porosity, Planseeberichte fuer Pulvermetallurgie, 20 (1972) 185-202.

[199] R.R. Boade, Dynamic Compression of Porous Tungsten, J. Appl. Phys., 40 (1969) 3781-3785.

[200] M.E. Kirkpatrick, R.A. Mendelson, Investigation of porous tungsten formed from spherical tungsten powders, Int. J. Powder Metall., 2 (1966) 35-44.

[201] V.I. Vnukov, B.A. Gnesin, M.I. Karpov, M.M. Myshlyaeva, N.Y. Tkachenko, A.N. Shapoval, A.P. Shevchenko, On the state of subsurface coarse porosity zone in sintered refractory metals, Izvestiya Akademii Nauk SSSR. Metally, (1996) 56-61.

[202] O. Blaschko, M. Prem, G. Leichtfried, Porosity evolution during sintering in tungsten powders of different grain size, Scripta Mater., 34 (1996) 1045-1049.

[203] G.A. Goryaev, Z.I. Dzneladze, Variation of the Open and Closed Porosity of Porous Tungsten During Sintering, Soviet Powder Metallurgy and Metal Ceramics (English translation of Poroshkovaya Metallurgiya), 16 (1977) 149-150.

[204] T. Xiuren, Z. Hanliang, Study of Some Factors Effecting the Porosity of Porous Tungsten, Xiyou Jinshu Cailiao Yu Gongcheng/Rare Metal Materials and Engineering, 27 (1998) 380-380.

[205] C. Selcuk, N. Morley, J.V. Wood, Densification of porous tungsten by low temperature sintering, Powder Metall., 48 (2005) 245-248.

[206] C. Selcuk, N. Morley, J.V. Wood, Porous tungsten with controlled porosity by low temperature sintering, Powder Metall., 48 (2005) 17-22.

[207] C. Selcuk, R. Bentham, N. Morley, J.V. Wood, Effect of basic powder particle properties on densification of porous tungsten, Powder Metall., 46 (2003) 117-120.

[208] V.V. Skorokhod, O.I. Get'man, A.E. Zuev, S.P. Rakitin, Correlation between the particle size, pore size, and porous structure of sintered tungsten, Soviet powder metallurgy and metal ceramics, 27 (1989) 941-947.

[209] D.P. Dandekar, R.M. Lamothe, Behavior of Porous Tungsten Under Shock Compression at Room Temperature J. Appl. Phys., 48 (1977) 2871-2879.

[210] A.V. Logunov, O.B. Chevela, A.F. Silaev, High Temperature Investigation of the Thermophysical Properties of Porous Tungsten, Soviet Powder Metallurgy and Metal Ceramics (English translation of Poroshkovaya Metallurgiya), 13 (1974) 304-308.

[211] D.P. Dandekar, R.M. Lamothe, Behavior of porous tungsten under shock compression at room temperature, J. Appl. Phys., 48 (1977) 2871-2879.

[212] G. Paez, Emissivity and detected incidance from a thermal source, in: Infrared Spaceborne Remote Sensing IX, August 1, 2001 - August 3, 2001, SPIE, San Diego, CA, United states, 2002, pp. 181-192.

[213] E. Brodu, M. Balat-Pichelin, J.L. Sans, J.C. Kasper, Influence of roughness and composition on the total emissivity of tungsten, rhenium and tungsten-25% rhenium alloy at high temperature, J. Alloys Compd., 585 (2014) 510-517.

[214] D.P. Verret, K.G. Ramanathan, Total Hemispherical Emissivity of Tungsten, 68 (1978) 1167-1172.

[215] L.A. Wojcik, A.J. Sievers, G.W. Graham, T.N. Rhodin, Total Hemispherical Emissivity of W(100), Journal of the Optical Society of America, 70 (1980) 443-450.

[216] A. Electronic Components, & Materials Association, Engineering specification for dispenser cathodes, in: EIA-941, Nov. 2002.

[217] C. Eberl, D.S. Gianola, K.J. Hemker, Mechanical Characterization of Coatings Using Microbeam Bending and Digital Image Correlation Techniques, Exp Mech, 50 (2010) 85-97.

[218] S. Furuya, N. Ozoe, K. Sekiya, Y. Yamane, The improvement of machinability of gray cast iron using nonmetallic inclusions in high speed cutting (2nd report) - the effects of reducing wear of cermet tools in high speed face milling, Seimitsu Kogaku Kaishi/Journal of the Japan Society for Precision Engineering, 76 (2010) 775-780.

[219] G. Ostberg, H.-O. Andren, Microstructural changes during wear by plastic deformation of cemented carbide and cermet cutting inserts, Metall. Mater. Trans. A, 37 (2006) 1495-1506.

[220] K. Hirose, K. Tsuda, Y. Fukuyasu, A. Sakamoto, H. Yonekura, K. Nishi, K. Yamagata, H. Moriguchi, Development of cermet "T1500A" for steel turning, SEI Technical Review, (2011) 107-111.

[221] X.D. Fang, I.S. Jawahir, The effects of progressive tool-wear and tool restricted contact on chip breakability in machining, Wear, 160 (1993) 243-252.

[222] B. Denkena, A. Lucas, E. Bassett, Effects of the cutting edge microgeometry on tool-wear and its thermo-mechanical load, CIRP Annals - Manufacturing Technology, 60 (2011) 73-76.

[223] I.S. Jawahir, P.X. Li, R. Gosh, E.L. Exner, A New Parametric Approach for the Assessment of Comprehensive Tool-wear in Coated Grooved Tools, CIRP Annals - Manufacturing Technology, 44 (1995) 49-54.

[224] A.M.A. Electronic Components, EIA-941: Engineering specification for dispenser cathodes, in, Nov. 2002.

[225] A.F. A. Wronszki, The Ductile-Brittle Transition in Polycrystalline Tungsten, Journal of the Less-Common Metals, 6 (1964) 413-429.

[226] D.H. A. P. Valentine, Effect of Temperature on the Brittle Fracture of Polycrystalline Tungsten, Journal of the Less-Common Metals, 17 (1969) 353-361.

[227] E. Pink, K. Sedlatschek, Ductile Brittle Transition of BCC Metals, With Emphasis on Tungsten and Molybdenum, 23 (1969) 1249-1257.

[228] S. Caruso, J. OUTEIRO, D. Umbrello, A.C. Batista, Residual Stresses in Machining of AISI 52100 Steel under Dry and Cryogenic Conditions: A Brief Summary, (2014).

[229] A. Chilton, A. Wronzki, The Effect of Strain Rate and Pressurization on the Ductile-Brittle Transition Temperature of Polycrystalline Sintered Tungsten, Journal of the Less-Common Metals, 17 (1969) 447-450.

[230] A. Giannattasio, Z. Yao, E. Tarleton, S. Roberts, Brittle–ductile transitions in polycrystalline tungsten, Philosophical Magazine, 90 (2010) 3947-3959.

[231] P.M. Amaral, A. Coelho, C.A. Anjinho, J.C. Fernandes, L.G. Rosa, Evaluation of the relationship between diamond tool-wear performance and the mechanical properties of the individual metallic binders, in: 5th International Materials Symposium MATERIAiS 2009 - 14th meeting of SPM - Sociedade Portuguesa de Materiais, April 5, 2009 - April 8, 2009, Trans Tech Publications Ltd, Lisbon, Portugal, 2010, pp. 1467-1474.

[232] A.V. Belyakov, S.I. Tserman, Cutting features of almost unworkable refractories with a diamond tool based on a metal binder, Refract. Ind. Ceram, 54 (2013) 51-53.

[233] H.C.P. De Oliveira, A. Coelho, P.M. Amaral, J.C. Fernandes, L.G. Rosa, Comparison between cobalt and niobium as a matrix component for diamond impregnated tools used for stone cutting, in: 4th Global Stone Congress 2012, July 16, 2012 - July 20, 2012, Trans Tech Publications Ltd, Alentejo, Borba, Portugal, 2013, pp. 98-105.

[234] H.C.P. Oliveira, S.C. Cabral, R.S. Guimaraes, M. Filgueira, Is Ni a good substitute for Co in PM diamond cutting tools?, in: 7th International Latin-American Conference on Powder Technology, November 10, 2009 - November 10, 2009, Trans Tech Publications Ltd, Atibaia - SP, Brazil, 2010, pp. 363-369.

[235] L. Tian, Y. Fu, L. Yang, J. Xu, H. Li, W. Ding, Investigations of the "speed effect" on critical thickness of chip formation and grinding force in high speed and ultra-high speed grinding of superalloy, Jixie Gongcheng Xuebao/Journal of Mechanical Engineering, 49 (2013) 169-177.

[236] T. Ozel, I. Llanos, J. Soriano, P.J. Arrazola, 3d finite element modelling of chip formation process for machining inconel 718: Comparison of FE software predictions, Machining Science and Technology, 15 (2011) 21-46.

[237] C.Z. Duan, M.J. Wang, Y.J. Cai, T. Dou, Microcosmic mechanism of material softening and fracture in primary shear zone during high speed machining of hardened steel, Mater. Sci. Technol., 27 (2011) 625-630.

[238] T. Ozel, M. Sima, A.K. Srivastava, Finite element simulation of high speed machining Ti-6Ai-4V alloy using modified material models, in: 38th Annual North American Manufacturing Research Conference, NAMRC 38, May 25, 2010 - May 28, 2010, Society of Manufacturing Engineers, Kingston, ON, Canada, 2010, pp. 49-56.

[239] S. Tavakoli, H. Attia, R. Vargas, V. Thomson, Laser assisted finish turning of inconel 718- process optimization, in: ASME International Manufacturing Science and Engineering Conference 2009, MSEC2009, October 4, 2009 - October 7, 2009, American Society of Mechanical Engineers, West Lafayette, IN, United states, 2009, pp. 833-840.

[240] A. Li, J. Zhao, D. Wang, J. Zhao, Y. Dong, Failure mechanisms of a PCD tool in high-speed face milling of Ti–6Al–4V alloy, The International Journal of Advanced Manufacturing Technology, 67 (2012) 1959-1966.

[241] H. Tanaka, S. Shimada, M. Higuchi, T. Yamaguchi, T. Kaneeda, K. Obata, Mechanism of Cutting Edge Chipping and its Suppression in Diamond Turning of Copper, CIRP Annals - Manufacturing Technology, 54 (2005) 51-54.

[242] X. Xiao, L.C. Lev, M.J. Lukitsch, Material transfer during machining of aluminum alloys with polycrystalline diamond cutting tools, J. Mater. Process. Technol., 209 (2009) 5760-5765.

[243] D. Lassila, G. Gray III, Ductile-brittle transition behavior of tungsten under shock loading, Le Journal de Physique IV, 4 (1994) C8-349-C348-354.

[244] P.L. Raffo, Yielding and fracture in tungsten and tungsten-rhenium alloys, Journal of the Less-Common Metals, 17 (1969) 133-149.

[245] D. Rupp, S.M. Weygand, Loading rate dependence of the fracture toughness of polycrystalline tungsten, in, Elsevier, P.O. Box 211, Amsterdam, 1000 AE, Netherlands, 2011, pp. 477-480.

[246] D. Rupp, S.M. Weygand, Anisotropic fracture behaviour and brittle-to-ductile transition of polycrystalline tungsten, Philosophical Magazine, 90 (2010) 4055-4069.

[247] A. Giannattasio, S.G. Roberts, Strain-rate dependence of the brittle-to-ductile transition temperature in tungsten, Philosophical Magazine, 87 (2007) 2589-2598.

[248] T. Zhang, Z. Liu, C. Xu, Influence of size effect on burr formation in micro cutting, International Journal of Advanced Manufacturing Technology, 68 (2013) 1911-1917.

[249] K. Saptaji, S. Subbiah, J.S. Dhupia, Effect of side edge angle and effective rake angle on top burrs in micro-milling, Precision Engineering, 36 (2012) 444-450.

[250] J. Schoop, I.S. Jawahir, T.J. Balk, D. Busbaher, Observations on Cutting Edge Radius Effects in Cryogenic Machining of Porous Tungsten, in: Vacuum Electronics Conference, IEEE International, 2015.

[251] S. Venkatachalam, X. Li, S.Y. Liang, Predictive modeling of transition undeformed chip thickness in ductile-regime micro-machining of single crystal brittle materials, J. Mater. Process. Technol., 209 (2009) 3306-3319.

[252] Z. Fang, M. Hu, W. Zhang, X. Zhang, H. Yang, Thermal conductivity and nanoindentation hardness of as-prepared and oxidized porous silicon layers, Journal of Materials Science: Materials in Electronics, 19 (2008) 1128-1134.

[253] H.A. Bahlyuk, Computational model of the mutual dependence of hardness and strength of porous materials, Mater. Sci., 42 (2006) 566-568.

[254] O.V. Bakun, S.A. Nochevkin, Y.N. Podrezov, S.A. Firstov, Relation of hardness to the yield point of porous iron, Poroshkovaya Metallurgiya, (1993) 96-99.

[255] A.M. Lennon, K.T. Ramesh, The thermoviscoplastic response of polycrystalline tungsten in compression, Materials Science and Engineering: A, 276 (2000) 9-21.

[256] J.R. Stephens, Effect of Interstitial Impurities on the Low-Temperature Tensile Properties of Tungsten, in: NASA TN 1964.

[257] E. Bassett, J. Köhler, B. Denkena, On the honed cutting edge and its side effects during orthogonal turning operations of AISI1045 with coated WC-Co inserts, CIRP Journal of Manufacturing Science and Technology, 5 (2012) 108-126.

[258] D. Grochała, S. Berczyński, Z. Grządziel, Stress in the surface layer of objects burnished after milling, The International Journal of Advanced Manufacturing Technology, 72 (2014) 1655-1663.

[259] R.R. Doradla, M.K.P. Adusumilli, C.S.K. Aduru, Study of Surface Integrity from Ball and Roller Burnishing Processes, International Journal of Applied Engineering Research, 6 (2011).

VITA

Julius Schoop was born in 1989 in Marburg, Germany. After growing up near Hannover, Germany in the town of Burgwedel and graduating high school (Gymnasium), he moved to Danville, KY, USA to pursue a Bachelor of Science in Chemical Physics at Centre College. Following graduation from Centre College in 2011, he joined Dr. T. John Balk's research group to pursue a Ph.D. in Materials Engineering at the University of Kentucky in Lexington, KY, USA. Later in 2011, Julius joined an interdisciplinary research project with the Institute for Sustainable Manufacturing (ISM), co-advised by ISM director Dr. I. S. Jawahir (Mechanical Engineering).

LIST OF PUBLICATIONS

1. J. Schoop, M. Effgen, T.J. Balk, and I.S. Jawahir. "**Improved Product Quality and Resource Efficiency in Porous Tungsten Machining for Dispenser Cathode Application by Elimination of the Infiltration Process**" Paper presented at the *20th CIRP LCE* Singapore, 2013.
2. J. Schoop, M. Effgen, T.J. Balk, and I.S. Jawahir. "**The Effects of Depth of Cut and Precooling on Surface Porosity from Cryogenic Machining of Porous Tungsten.**" Paper presented at the 1*4th CIRP CMMO*, Torino, Italy, 2013.
3. J. Schoop, and T. J. Balk. "**Engineering Defect-Free Nanoporous Pd from Optimized Pd-Ni Precursor Alloy by Understanding Palladium-Hydrogen Interactions During Dealloying**" *Metallurgical and Materials Transactions A* 45, no. 4 (2014): 2309-14.
4. J. Schoop, I. S. Jawahir, T. J. Balk, and D. Busbaher. "**High Performance Infiltrant-Free Cryogenic Machining of 82% Density Porous Tungsten under Computer Numerical Control**" Paper presented at the *Vacuum Electronics Conference, IEEE International*, 22-24, April 2014.
5. Caudill, J., B. Huang, C. Arvin, J. Schoop, K. Meyer, and I. S. Jawahir. "**Enhancing the Surface Integrity of Ti-6Al-4V Alloy through Cryogenic Burnishing**" *Procedia CIRP* 13 (2014): 243-248.
6. J. Schoop, F. Ambrosy, F. Zanger, V. Schulze, I.S. Jawahir and T.J. Balk. "**Increased Surface Integrity in Porous Tungsten from Cryogenic Machining with Cermet Cutting Tool**" *Materials and Manufacturing Processeses*, available online, May 2015.

7. J. Schoop, I. S. Jawahir, T. J. Balk, and D. Busbaher. "**Observations on Cutting Edge Radius Effects in Cryogenic Machining of Porous Tungsten**" *Paper presented at Vacuum Electronics Conference, IEEE International*, Beijing, April 2015.
8. J. Schoop, F. Ambrosy, F. Zanger, V. Schulze, T.J. Balk and I.S. Jawahir "**Cryogenic Machining of Porous Tungsten for Enhanced Surface Integrity**" *Journal of Materials Processing Technology*, *Submitted June 2015*.
9. J. Schoop, T.J. Balk and I.S. Jawahir "**Size Effect in Sustainable Machining of Porous Powdered Metal**" *Precision Engineering, Submitted August 2015*.